# Toward A High Throughput Label-Free Platform for Monitoring Interaction Between Cells and Superparamagnetic Iron Oxide Nanoparticles

SONIA ABAD TAN

A THESIS SUBMITTED
TO THE FACULTY OF GRADUATE STUDIES
IN PARTIAL FULFILLMENT OF THE REQUIREMENTS
FOR THE DEGREE OF
MASTER OF SCIENCE

GRADUATE PROGRAM IN BIOLOGY
YORK UNIVERSITY
TORONTO, ONTARIO

May 2019

# Abstract

This thesis focuses on cytotoxicity examination of superparamagnetic iron oxide nanoparticles (SPIONs) using different methods, including impedance spectroscopy. Despite the significant advances in adapting various biological and chemical methods to assess in-vitro toxicity of SPIONs, less attention has been paid on the development of a high throughput label-free screening platform to study the interaction between the cells and nanoparticles. In this thesis, we have taken the first step by proposing a label-free impedimetric method for monitoring cells treated with SPIONs. This study has demonstrated the effects of SPIONs on the adhesion, growth, proliferation, and viability of neuroblastoma 2A cells using impedance spectroscopy in comparison to other standard microscopic and cell viability testing methods. Results suggest that the change in impedance of electrodes exposed to the mixture of cells and SPIONs offers a wide dynamic range suitable for monitoring the effects of SPIONs with a concentration of less than 100 μg/mL.

*For my family.*

*For Roland and Samantha.*

*For Friends and mentors.*

*For those who are in pursuit of knowledge.*

# Acknowledgments

This thesis was realized through the encouragement and assistance of unselfish mentors. I want to express my profound gratitude to:

My supervisor (Professor Ebrahim Ghafar-Zadeh) for his untiring efforts, indispensable support, constructive suggestions which motivated me to complete my thesis. I sincerely appreciate for letting me do my master project in Biologically Inspired Sensors and Actuator (BioSA) laboratory that made me discover the beauty of merging biological and engineering theories and applications. With his constant encouragement and push, my hesitation at the beginning had blossomed into a deep interest in the electrical and mathematical aspects of my research.

A member of my supervisory committee (Professor Georg Zoidl) for his valuable inputs and critiques during the committee meetings, presentations, and writing and submitting my conference paper extracted from this thesis. Professor Dasantila Golemi-Kotra and Professor Sebastian Magierowski for all the comments and pointers to improve the thesis during the defence.

Medical devices laboratory technologist (Mr. Giancarlo Ayala Charca) for helping me to source out some electrical materials needed in the study. I appreciate his continuous support.

Ms. Christiane Zoidl and Azita Saber for the cell culture training that refreshes my mind with the right protocol and techniques in handling the cells used in the study.

To my BioSA laboratory buddies, Azita Saber, Samal Mundidasa and Parveen Zainab, for being so supportive and believing in me.

To my family, who had been a source of strength, encouragement, and love. I want to thank them for being so understanding every time I work timelessly in the laboratory, where I feel I cannot fulfill my duties as a mother and as a wife.

# Table of Contents

# List of Abbreviations

| | |
|---|---|
| A3 | human T lymphocyte |
| A549 | human lung epithelial cancer cells |
| AminS | Aminosilane |
| AVG | Average |
| BBB | Blood-Brain Barrier |
| bEnd.3 | mouse brain-derived microvessel endothelial cell line |
| C17.2 | neural progenitor cells |
| C | Capacitance |
| Car/A-G | Carboxyl/Amine group |
| CarXR | carboxydextran-coated Resovist |
| CC | Cell Concentrations |
| CCM | Complete Culture Media |
| CV | coefficient of variation |
| DexE | dextran-coated Endorem, |
| DLC | Double Layer Capacitance |
| DMEM | Dulbecco's Modified Eagle Medium |
| DMSA | dimercaptosuccinic acid |
| DOX | doxorubicin |
| ECIS | Electric Cell-substrate Impedance Sensing |
| EDTA | Ethylenediaminetetraacetic acid |
| EIS | electrochemical impedance spectroscopy |

| | |
|---|---|
| f | Frequency |
| FBS | Fetal Bovine Serum |
| hESc-CMs | human embryonic stem cell-derived cardiomyocytes |
| HTSS | high throughput screening systems |
| L929 | mouse fibroblast |
| Max | Maximum |
| MBMEC | mouse brain microvascular Endothelial Cells |
| MCF-7 | Human breast cancer cell |
| Min | Minimum |
| MLs | Magnetoliposomes |
| MNPs | Magnetic nanoparticles |
| MRI | Magnetic Resonance Imaging |
| MVEC | microvascular endothelial cells |
| N2a | Neuroblastoma 2a or Neuro2A cells |
| NIH3T3 | Mouse embryonic fibroblasts, |
| NPs | Nanoparticles |
| OSCC | oral squamous cell carcinoma |
| PBS | Phosphate Buffered Saline |
| PC | Polycarbonate |
| PC12 | Rat pheochromocytoma cells |
| PC12 | rat pheochromocytoma cells |
| PCB | Printed Circuit Board |
| PS | Penicillin-Streptomycin |

| | |
|---|---|
| PVA | polyvinyl alcohol |
| $R_1$ | Resistance - series |
| $R_2$ | Resistance - parallel |
| RCGC | primary rat cerebellar granule cells/neurons |
| S | Surface area or maximum change |
| S1 | primary somatosensory barrel cortex |
| SPIONs | Superparamagnetic Iron Oxide Nanoparticles |
| STD | Standard Deviation |
| TBDE | Trypan Blue Dye Exclusion |
| TE | Type of electrodes |
| TK6 | human lymphoblast cells |
| TP1 | Time Period 1 |
| TP2 | Time Period 2 |
| TP3 | Time Period 3 |
| TR1 | Trial 1 |
| TR2 | Trial 2 |
| TR3 | Trial 3 |
| U87MG | Human glioblastoma cells |
| VSOP | citrate-coated very small iron oxide particles |
| Z | Impedance |

# List of Tables

# List of Figures

# Chapter 1

# Introduction

Superparamagnetic Iron Oxide Nanoparticles (SPIONs) have attracted the attention of researchers for clinical and research purposes due to their structural and magnetic properties suitable for drug delivery, disease diagnostics and treatment purposes [1]-[2]. SPIONs are chemically made up of magnetite ($Fe_3O_4$) and maghemite ($\gamma$-$Fe_2O_3$) [3]. The superparamagnetic property of SPIONs is dependent on its small diameter size in which magnetization is easily affected by temperature, causing a high magnetic moment [4]. By applying a magnetic field, SPIONs are directed as nanoscale carriers to a target organ in the body. For instance, several studies have shown that SPIONs can cross the Blood Brain Barrier (BBB) [5]-[6] and deliver the drug into the brain [7]-[8]. In these studies, the uptake of SPIONs by the astrocytes [9] can be used as an indicator of nanoparticle (NP) delivery through BBB. Other studies have shown that SPIONs lower than a certain concentration level are not toxic compared to other higher saturation magnetic NPs [10]-[11] [12]. The Food and Drug Administration's (FDA) approval [13] of SPIONs as MRI contrast agents has created an intense interest in promoting the use of these nanomaterials in humans [14] for various clinical applications including diagnostic and treatment of brain diseases over the last decade [15]-[16]. Despite significant advances of SPIONs for various life science applications, still many research studies should be conducted to enhance our understanding of the effects of SPIONs with different concentrations on cellular activities. It is in this direction that this thesis delves on specifically by focusing on the interaction of SPIONs and brain cells using various methods, including impedance spectroscopy. Figure 1 illustrates the proposed *in-vitro* method in this thesis to mimic the uptake of SPIONs on brain cells. This method offers great advantages for studying the interaction of SPIONs and the brain cells as described and demonstrated in the next chapters. The remainder of this chapter provides a comprehensive review of the literature to explain the advantages of SPIONs for neuronal studies, and other applications in section 1.1 followed up by section 1.2 that briefly reviews the *in-vitro* studies of the effects of SPIONs on cells. The applications of a label-free high throughput impedance-based method for cellular analysis is discussed in section 1.3.  Several related works are put forward and compared in section 1.4. At the end of this chapter, a summary of the literature review, and organization of research, and thesis are articulated.

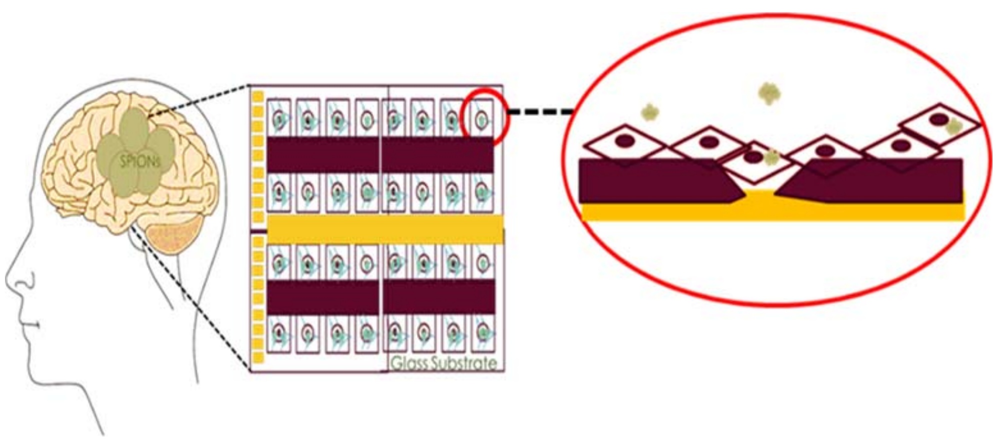


Figure 1| Schematic representation of the interaction of the brain cells with SPIONs when studied in *in-vitro* using an impedance-based assay.

## 1.1. SPIONs applications

SPIONs have demonstrated great advantages for various life science applications including non-invasive Magnetic Resonance Imaging (MRI) [11], diagnosis of ailment, drug delivery and development [17], thermotherapy [17], biological separation [18], cell transfection [19], immunoassays [20], gene delivery [21], tissue engineering [22], and cell tracking in cancer and its treatments [23]. Some important SPIONs' applications are briefly put forward as follows.

- *MRI Contrast Agent*: MRI is used to visualize and track a diseased portion of the brain. The strength of the signal is influenced by the two relaxation times of water protons, the longitudinal ($T_L$) and transverse ($T_T$) [24]-[25]. For the image refinement, contrast agents are utilized to decrease $T_L$ and $T_T$ relaxation times. The SPIONs acts as negative contrast agents producing a negative signal on $T_T$ weighted images and enhancing $T_T$ contrast [26].
- *Tumor Diagnostics and Therapy*: Functionalized SPIONs can play an essential role in the delivery of therapeutic components and subsequently for initiating tumor cell death [27]. A biocompatible coating on SPIONs provides suitable functional groups for conjugating with tumor cells [28]-[29]. For instance, SPIONs can be attached to the anti-IL-1$\beta$ monoclonal antibody to be used for MRI diagnoses and targeted therapy by neutralizing IL-1$\beta$ which is overexpressed in the epileptogenic area of an acute rat model with temporal lobe epilepsy [30], a disease in the brain associated with inflammation [31].
- *Thermotherapy*: To implement a hyperthermia treatment, SPIONs can be introduced in the body through a magnetic delivery system or local injection to the affected area [32]. SPIONs can vibrate and produce heat in an interchanging magnetic field [8]- [9]. The generated heat can be used for thermotherapy purpose.

- *Crossing BBB:* As aforementioned, recent studies have reported that SPIONs can enter the brain without causing damage to the blood-brain barrier [33]. To date, many types of research have been conducted to understand the BBB mechanisms and enhance the BBB permeability using functionalized SPIONs. Among these efforts is an optimized *in-vitro* BBB model, which was recently being reported using mouse brain endothelial cells and astrocytes [34]-[35]. Also, experimental data demonstrated how one could modify SPIONs to deliver drugs to the brain better to treat a wide range of neurological disorders [36].
- *Drug Delivery:* SPIONs are widely used because of their larger surface to mass ratio [37] compared to other NPs, their quantum properties [38] and their ability to adsorb [39] and carry other compounds. The aims for such NP entrapment of drugs are either enhanced delivery to or uptake by, target cells and a reduction in the toxicity of the free drug to non-target organs. Both situations will increase the ratio between the doses resulting in therapeutic efficacy and toxicity to other organ systems. For these reasons, the creation of long-lived and target-specific NPs and accurate toxicity studies should be performed to increase the advantages of these particles for the applications as mentioned earlier. [40]. It is noteworthy that SPIONs are not stable under physiological conditions due to the reduction of electrostatic repulsion, which causes NP aggregation. To re-disperse SPIONs in biological media, further surface modifications are applied in particular on the commercially available SPIONs [41].

## 1.2. Effects of NPs on Cells: *In-Vitro* Studies

To date, many papers have reported the advantage of NPs for drug delivery purposes using *in-vivo* animal models [42]-[43]. In comparison with in-vivo studies of NPs, less attention has been paid to study the effect of NPs using *in-vitro* cell culture models. In general, even though *in-vivo* animal model studies offer exceptional advantages for testing NPs or other drugs in human-like fully functional organs, *in-vitro* cell culture models can also provide unique benefits for various fundamental biological and clinical studies. These advantages include higher environmental control, less variability, low complexity and higher repeatability [44]. It is noteworthy to mention that N2a cells have been used widely for *in-vitro* neuroscience studies due to their capacity to differentiate [45] and respond to electrophysiological stimulation [46]. In this thesis, N2a cells were used as an *in-vitro* cell culture model.

### *1.2.1. Fundamental Effects*

In *in-vitro* models, NPs including SPIONs can directly be added to the cell culture, and they interact with the culture medium [47], aggregate in the intercellular spaces, attach to the cell membrane [48] and affect intracellular parts of the cell [49]. Indeed, the culture medium can change the properties of NPs by forming a protein coat covering the entire NP [50]. This may increase the adhesion properties of NPs for the attachment to the cell membrane. NPs' distinctive physicochemical properties with increased responsiveness and propensity to pass through the cell membrane and other biological barriers cause stress and induce cytotoxicity [11]. Herein, the major effects of NPs on cells are highlighted.

- *Effect on cell membrane*: All type of NPs, including SPIONs, can be assimilated into the cell via different processes and all these passes through the protective barrier of the cell - the cell membrane. As NPs make 'their way through the cell membrane, it affects the major components of the membrane, the proteins [51]-[52] and the lipid bilayer [53].
- *Effect on Lysosomes:* A study using silica (SiO2) NPs on human cervix carcinoma (HeLa) cells, had shown that NPs disrupts normal activities of the lysosomes by causing damage

in its cargo delivery via autophagosomes. Although the autophagy-mediated protein turnover and degradation of internalized epidermal growth factor were affected, it did not induce cell death [54].

- *Effect on cytoplasmic organelles*: Experimental investigation has shown evidence that NPs affect cytoplasmic organelles like the mitochondria [55] and nucleus [56]. Another study had shown that even if using gold nanoparticles (GNPs) do not accumulate within the mitochondria, NPs close to the organelle could still enhance damage due to the delocalization of photoelectrons from the cytosol. Furthermore, the presence of GNPs in the cytosol increases the energy deposition in the mitochondrial volume more than the presence of GNPs within the nuclear volume [57].
- *Effect on the cell activities*: The effect of GNPs on cell differentiation and maturation has been highlighted in another study. It has been observed that the cells developed longer neuronal outgrowth in the presence of GNPs [58]-[59].
- *Other effects*: The exposure of the cell to NPs brings about harmful effects such as damage mitochondrial function, inflammation, the formation of apoptotic bodies, membrane leakage of lactate dehydrogenase, reactive oxygen species (ROS) production, increase in micronuclei, and chromosome condensation [11]. In such cytotoxicity studies, there are various indicators such as micronuclei that are an indicator of gross chromosomal damage that is used to measure genotoxicity.

Despite significant advances in studying of NPs in different types of cells, still, the effects of many kinds of NPs on various parts of cells or different types of cells have not been studied. In this thesis, we only focus on exploring the effects of SPIONs on N2a using three cellular level indicators, namely; cell viability, morphology, and cell adhesion.

### *1.2.2. In-vitro Toxicity Assays*

As aforementioned, NPs can affect many different parts of the cell. Thus, various conventional toxicity assays are required to measure the damage caused by NPs. As per the literature, these assays include MTT assay, cell metabolic activity assay (WST-1), Cell Proliferation 5-Bromo-2´-Deoxyuridine (BrdU) Analysis [60]-[61], lactate dehydrogenase (LDH) leakage, fluorescent propidium iodide (PI), [3H] thymidine, Clonogenic assays, Electron paramagnetic resonance (EPR), Lipid peroxidation Assay, Enzyme-linked immunosorbent assay (ELISA) and Trypan blue dye exclusion (TBDE) test [62].

Most recently, various new sensing methods are used in toxicity studies. Among these new methods, Fritzsche *et al.* reported a cell-based fluorometric sensor system [63]-[64]. This system uses fluorescence data, which is generated by connecting a multi-well culture plate to a fluorescence spectrometer to determine the toxicity level of different drugs. With software, concentration curves are further analyzed. These curves are also used to indicate the concentration of the toxicant. In another effort, impedance spectroscopy [65]-[66] has opened the possibility of a faster, real-time, high-throughput acquisition of results. For instance, an electric cell-substrate impedance sensing (ECIS) device that is connected to a PDMS perfusion system and an impedance spectroscopy system [67] has been used to monitor mammalian cell activities under the presence of a toxicant. Also, the impedance-based method was used to investigate the increase of impedance in macrophage cell line J774, epithelial cell line MDCK and fibroblasts [68]. In this direction, another effort was made by Zhu et al., who presented the lateral flow immunoassay (LFIA) to determine toxicity at the genetic level [69]. In another attempt, a multichannel dissolved oxygen sensor consisting of a 96-well electrodes biosensor introduced by the group of Sadik et al. to detect toxicity. Their measurement setup was used for monitoring the amount of oxygen used by the cell

[70]. Also, the paper authored by Özel et al. provided information on using electrochemical approaches in monitoring the effect of NPs [71].

## 1.3. High Throughput Impedance-Based Cellular Analysis

Impedance-based techniques have been widely reported for the assessment of cellular activities such as adhesion of cells [72]-[73] and cell growth [74]. In these techniques, the cells are cultured on the top of sensing electrodes connected to an impedance spectroscopy system. This system can measure the impedance of the electrode exposed to the biological materials (see Chapter 2). These techniques have been successfully used to monitor the attachment and growth of *vero* and human cells [75] due to the variation of their electrical properties. For instance, the activation of acetylcholine receptors in N2A results in higher conductivity that could be measured using Impedance based techniques.

Many efforts have been made to show the advantages of impedance analysis using 2D or 3D cell culture models [76] for various cellular analysis. It has been highlighted in the work of Seriburi and Meldrum (2008) that impedance can be used to monitor the adhesion and spreading of junctional epidermolysis bullosa gravis (JEBG) cells [77]. In their work, morphological change such as a change in shape and confluence was accompanied by the change of impedance. Also, in another study, the impedance change was correlated to the number of colon cancer cells in culture [78]. Moreover, an impedance-based Electric Cell-substrate Impedance Sensing (ECIS) was used to investigate cell morphology, basal and substratum distance, and capacitance of the cell membrane's anatomical planes of epithelial cells [79]. It is also in this study that the change in impedance and the equivalent circuit elements had been used to examine the change of $Ca^{2+}$ concentration in kidney cells. Meanwhile, According to Wang et al., the impedance can be used to assess cellular processes in terms of cell death with millisecond time resolution [80].

By considering the high demand and urgency of screening and evaluating the effect of different NPs used in the clinical sector, impedance-based high throughput screening systems (HTSS) is the best solution to meet the challenge. A high-throughput is a process that accelerates the rate of screening of a large number of compounds in a day. [81] Thus, this system offers advantages of high speed, real-time assessments of the different effect of NPs simultaneously [82]. Despite significant advances in impedance-based systems, relatively little attention has been paid to use these systems for toxicity assessment of NPs. Among these few, Moe *et al*. reported a microelectronic sensing device consisting of 96 micro-wells capable of measuring the real-time activities [83]. In their work, an impedance-based method was used for demonstrating various assessment methods related to cellular activities. These methods include the assessment of toxicity level, cell death, evaluation of cell membrane integrity, attachment and proliferation.
As aforementioned, to date, many papers have reported the advantages of impedance-based and capacitive techniques [84] for monitoring the growth of living cells. However, this project is the first to demonstrate the advantage of an impedance sensing method for monitoring the effects of SPIONs on the cells in culture. In this work, as a control of the proposed impedance-based results, we also use other standard biological methods as described in chapter II.

Table 1 highlights the uses of impedance-based methods in cellular analysis. For instance, in a study conducted by Williams et al. [85], an impedance-based assay was used in monitoring the distribution and reaction of cells using an implanted electrode. Meanwhile, several types of research were performed by Szulcek et al. [86] and Arias et al. [87] using ECIS to observe adhesion, spreading proliferation, and migration of cells; maturation of a confluent cell barrier wound healing, and apoptosis. Another notable work was conducted by Kuzmanov to study cell integrity and permeability using impedance technique. Additionally, a change in cell shape can be monitored by an impedance-based device as an effect of chlorotoxin [88]. In another attempt made by Peters et al. [89], cytotoxicity monitoring was performed using an impedance-based assay. As per the above discussion, the impedance-based cellular monitoring can be used as a reliable method for cellular analysis as described in the next chapter; we will use this impedance-based method for cytotoxicity study of SPIONs.

**Table 1|** Comparative use of impedance-based for cellular analysis

| **Cells/tissue** | **Types of Impedance-based Assay** | **Cellular Analysis** | **Ref.** |
|---|---|---|---|
| [1]S1barrel cortex | Impedance spectra using HP4284 LCR meter with Implanted electrodes | Identify changes of impedance magnitude at 1kHz. Results suggested that variation in impedance is due to the distribution and reactions of cells around the implanted electrodes. | [85] |
| [2]MVEC | [7]ECIS | Quantify cell behavior such as adhesion, proliferation, cell migration, formation, and maturation of a confluent cell barrier, and wound healing after the application of an electrical wound | [86] |
| [3]OSCC | ECIS | Monitor cell adhesion, spreading, proliferation and apoptosis after the addition of anti-cancer drug-cisplatin. | [87] |
| [4]MBMEC | Impedance spectroscopy using cellZscope | Investigate the integrity and permeability of endothelial cells. | [90] |
| [5]U87MG | Single-cell bioelectrical impedance using single and multi-cell electrodes | Monitor change in shape and impedance after introducing chlorotoxin, an ion channel inhibitor. | [88] |
| [6]hESC-CMs | Cardiomyocytes Impedance Assay using gold film electrodes and MEA | Detection of beating and toxicity of drugs to cardiomyocytes | [89] |

[1]S1, primary somatosensory barrel cortex, [2]microvascular endothelial cells, [3]orals squamous cell carcinoma, [4]mouse brain microvascular Endothelial Cells, [5]Human glioblastoma cells, [6]human embryonic stem cell-derived cardiomyocytes, [7]Electric cell-substrate impedance sensing

## 1.4. Related Works

As the focus of this thesis is placed on iron oxide NPs, in this subsection, a more comprehensive review of related works is provided. To date, several studies have examined the cytotoxic potential of magnetic nanoparticles (MNPs) or SPIONs by employing a range of different surface coatings. In this subsection, we review the toxicity effect of NPs, particularly SPIONs on living cells, as seen in Table 2. This table shows various *in-vitro* toxicity studies using different types of cell lines, NPs, and tools for evaluation purposes. For instance, Marcus *et al*. [91] reported the effect of uncoated and coated MNPs on Rat pheochromocytoma PC12 cells (R-PC12). As seen in table 2, uncoated MNPs did not diffuse in the cells and only aggregated on the cell membrane. Two other types of coated MNPs, namely Starch-magnetite MNPs and Dextran-magnetite MNPs, showed lower and higher viability (or less toxicity) effects respectively in comparing with uncoated MNPs. In their work, in addition to MTT viability assay, Electrophysiological and Morphometric methods were used for fully cytotoxicity analysis. As shown by Mahmoudi et al. [92] both Polyvinyl alcohol (PVA) coated and uncoated SPIONs manifested a decreased viability of L929 mouse fibroblast cells. This effect was also demonstrated in the MTT assay along with ultraviolet-visible spectroscopy and optical microscopy. Moreover, as tested by Jarockyte et al. [93] a second generation tetrazolium dye, Cell Proliferation Kit II (XTT), had been used to assess the viability and proliferation of a mouse embryonic fibroblast (NIH3T3) which manifested a slight decrease of viability within 3-24h of incubation when uncoated SPIONs were introduced.

In a similar study, Magdolenova et al. employed several other viability assays, including trypan blue exclusion, relative growth activity assay, Cytokinesis-block proliferation index (CBPI) [94]. As the results, they had demonstrated a reduction of viability of TK6 human lymphoblast cells exposed to coated and uncoated SPIONs. As revealed by Ying and Hwang [95], in using Fluorescein diacetate uptake-based cytotoxicity assay, toxicity varies depending on the concentration and particles of NPs. Meanwhile, another study indicated that bEnd.3 showed reduced viability when exposed to a coated NPs as revealed by MTT assay [96]. Likewise, an investigation that made use of MTT, TBDE, and a resazurin-based PrestoBlue (PB) assay revealed no death of cells, but proliferation was decreased [97]. In PB assay, the red color can be used as an indicator of A549 viability as a result of the reduction of PrestoBlue to resorufin [98]. It was mentioned by Soenen et al. [99] that modifying NPs' coating such as dextran, carboxydextran, lipid, and citrate can also affect adhesion and proliferation but not the surface area of the C17.2 and PC12 cells as revealed by lactate dehydrogenase (LDH) assay and manual cell counting using Bürker chamber. A similar study [100] using LDH assay, demonstrated high viability of retinal ganglion cell (RGC) cells exposed to a dimercaptosuccinate (DMSA) NPs. It is also worth mentioning that two separate studies [101] and [102], using SPIONs coated with doxorubicin (DOX) and dimercaptosuccinic acid (DMSA) respectively had exhibited different viability results using MTT and TBDE assays as seen in table 1. In both studies, MCF-7 cells were incubated with SPIONs. It seems DMSA-coated SPIONs has enhanced the viability in comparison with DOX-covered SPIONs.

**Table 2**| *In-vitro* toxicity studies of nanoparticles

| Cell | Type | Coat | Size nm | Qualitative Effects | Characterization | Ref. |
|---|---|---|---|---|---|---|
| [1]R- PC12 | MNP | No | 10 | The increase of MNPs does not affect cell viability. MNPs were attached on the outer membrane of the cell and did not penetrate the cells. No cytotoxic effect up to 0.1 mg/ml but at a high concentration of 0.25 mg/ml, 51 % of the PC12 cells remained viable after 72 hours | XTT cell viability assay, Imaging, and morphometric analysis, [2]Elec. | [91] |
| R- PC12 | MNP | Starch | 10 | The slight decrease in cell viability after 72 hours MNPs concentration increased (80 and 70 % viability at 0.02 and 0.1 mg/ml, respectively). At 0.25 mg/ml, MNPs were toxic to PC12 cells. After 24 h no cells remained viable | | |
| R- PC12 | MNP | Dextran | 10 | Cell viability decreased at a MNP concentration of 0.25 mg/ml. | | |
| R- PC12 | MNP | NO | 20 | MNPs penetrated the cell without toxic effect. Morphology patterns of cells are not affected | | |
| [3]L929 | SPION | [4]PVA | 20-30 | 17.8% uncoated & 34.6% modified SPIONs viability, Affects viability, Bubble formation | Ultraviolet visible spectroscopy (UV/vis), | [92] |

| | | | | | | |
|---|---|---|---|---|---|---|
| | | | | | MTT Assay, Optical Microscopy | |
| 5NIH3T3 | SPION | | 10-50 | 95% of the cells were viable within 3–24 h of incubation and a slight decrease in viability was observed after 48 h of incubation. A slight reduction of viability, Localization of SPIONs in the vesicle, No functionalized SPIONs accumulation in cells, nucleus, and none are toxic at a desirable concentration, negative contrast in the MRI | XTT cell viability assay, bright-field microscopy, MR Imaging | [93] |
| 6TK6 | Iron oxide U-Fe3O4 | No | 5-13 | U-Fe3O4 NPs did not show toxic effect, The TBE assay showed slightly reduced cell viability, of TK6 cells at 45mg/cm2 (76% after 0.5h; 66% after 2h) whereas 75mg/cm2 strongly decreased cell viability (42.5% after 0.5h; 48% after 2h) | Trypan blue exclusion Relative Growth Activity Assay using Automated Cell Counter (Invitrogen) CBPI and by incorporation of 3H-TdR into DNA of proliferating blood cells. .Electron Microscopy | [94] |
| 6TK6 | Iron oxide OC-Fe3O4 | Oleate | 5-12 | OC-Fe3O4 NPs were found to be toxic and affected DNA and morphology of the cells, Viability was reduced to 7.5% for those that were exposed to 30mg/cm2 OC-Fe3O4 NPs | | |
| 7A3 | Iron oxide | 19Car/A-G | 10-50 | LC50 of A3 on 1hr-FDA, 24hr FDA, and WST-1 assay, Toxicity vary with the mass concentration, the total number of particles per well, and the total surface area of particles per well | Fluorescein diacetate (FDA) uptake based cytotoxicity assay, WST-1 Assay | [95] |
| 8bEnd.3 | AmS-IONPs | 20AminS | 27 | Toxicity is dependent on surface coating.<br>At concentration above 200 µg/mL reduced neuron viability by 50% in the presence or absence of a magnetic field, 20% reductions in viability were observed with COOH-AmS-IONPs. With an applied magnetic field, AmS-IONPs reduced viability to 75% in astrocyte cultures.<br>COOH-AmS-IONPs caused 65% and 35% viability reduction in the absence and presence of a magnetic field, respectively | MTT Assay, Electron Microscopy | [96] |
| 9A549 | SPIONs | No | 9.3 ± 1.4 | Viability $Fe_3O_4$@COOH is greater than 80% at 1000 µg/mL compared to control cells, while bare $Fe_3O_4$ and $Fe_3O_4$@NH2 displayed viability higher than 80% at a concentration | Trypan Blue Dye Exclusion Assay, MTT Assay, Resazurin based PrestoBlue (PB) assay | [97] |
| 9A549 | SPIONs | @NH2 | 9 ± 1.3 | | | |

| | | | | | | |
|---|---|---|---|---|---|---|
| [9]A549 | SPIONs | @COOH | 10.4 ± 1.6 | of 100 µg/mL and less. No mortality was observed, Decreased cell Proliferation, Effect was dose-dependent | | |
| [10]C17.2/PC12 | iron oxide | [16]DexE | 14 | Endorem uptake= 46.59 ± 4.70 µg Fe/cell. | lactate dehydrogenase assay, CytoTox 96 non-radioactive cytotoxicity assay, manual counting using a Bürker Chamber was used for cell proliferation, No significant changes in cell surface area between control cells and IONP-treated cells could be observed, High intracellular IONP concentrations affect focal adhesions and proliferation, (slows cell cycle progression and decrease proliferation) | [99] |
| [10]C17.2/PC12 | iron oxide | [17]CarXR | 14 | Resovist uptake = 31.99 ± 2.99 µg Fe/cell. | | |
| [10]C17.2/PC12 | iron oxide | lipid-coated [18]MLs and | 14 | Cationic MLs =67.37 ± 5.98 pg Fe/cell | | |
| [10]C17.2/PC12 | iron oxide | [15]VSOP | 14 | VSOPs uptake=18.65 ± 2.07 pg Fe/cell.<br>Control= 100% viability<br>The NPs value being uptaken | | |
| [11]RCGC | MNPs | DMSA | 80/120 | alter the cell morphology<br>nor compromise cell viability, concentration and time-dependent, DMSA-coated IONPs are not acutely toxic to cultured neurons and that a protein corona around the particles strongly affects their interaction with neurons, cell viability indicated by the low extracellular LDH activity (around 20% of total), while 80%<br>of the LDH remained cellular | lactate dehydrogenase (LDH), MTT assay | [100] |
| [12]MCF-7 | SPIONs | [14]DOX | 10 ± 2 | DOX-SPION suspension was significantly<br>more active against MCF-7 cells than DOX solution, DOX in<br>solution = 10% mortality, DOX-SPION suspension cell mortality=nearly 40%, | tetrazolium dye (MTT) assay | [101] |
| [12]MCF-7 | SPIONs | [13]DMSA | 15 | At 24 hours MTT Assay= >96% viability in relation to the control, Trypan Blue Assay = > 90% cell survival, There was no significant effect on cell morphology, cytoskeleton organization, cell cycle distribution, reactive oxygen species generation, and cell viability compared to the control | MTT Assay, Trypan Blue Assay, Bright field, and fluorescence microscopy | [102] |

[1]Rat pheochromocytoma PC12 cells, [2]Electrophysiological measurements, [3]L929 mouse fibroblast, [4]polyvinyl alcohol PVA, [5]Mouse embryonic fibroblasts NIH3T3, [6]TK6 human lymphoblast cells, [7] A3 human T lymphocyte, [8]mouse brain-derived microvessel endothelial cell line, bEnd.3, [9]A549 human lung epithelial cancer cells, [10]C17.2 neural progenitor cells, and PC12 rat pheochromocytoma cells, [11]RCGC primary rat cerebellar granule cells/neurons, [12]Human breast cancer MCF-7 cell, [13]dimercaptosuccinic acid, [14]doxorubicin, [15]citrate-coated very small iron oxide particles, [16]dextran-coated Endorem, [17]carboxydextran-coated Resovist, [18]magnetoliposomes, [19]Carboxyl/Amine group, [20]Aminosil

## 1.5. Summary of Literature Review

This chapter described the applications of SPIONs for various life science applications, then provided a review of general toxicity effects of NPs and more specifically SPIONs on cells. Furthermore, the related toxicity effects such as weakening the integrity of the cell membrane, disrupting activities of the different cytoplasmic organelles like lysosome, mitochondria, and nucleus, were discussed. Additionally, the effects of NPs on various cells activities such as attachment, and growth were taken into considerations. Among various toxicity assays for different types of NPs, this chapter presented a comprehensive review of cytotoxicity studies on Iron Oxide NPs as seen in table 2, using multiple assessment methods including optical microscopy, conventional cell viability test, and MTT, XTT, UV spectroscopy, FDA, LDH, and CytoTox 96 non-radioactive. Furthermore, this chapter presented a brief review of new sensing methods more specifically impedance spectroscopy for cellular applications, including cytotoxicity.

## 1.6. Structure and Goal of Thesis

In this section, the research design, main goals, and organization of this thesis are presented.

### *1.6.1. Research Design*

The study involved the assessment of five different concentrations of SPIONs on a single concentration of N2A cells using TBDE assay, Scepter cell counter, optical microscopy using a motic camera, and impedance-based devices. Aside from the treated groups, both positive and negative control groups were monitored. Three trials were performed for each SPIONs concentration exposed to the cells in culture. In each trial, three replicates were performed as described in chapter 2 and briefly at the beginning of chapter 3. The impedance recording and microscopic image capturing from each experiment were performed in eight different times. The viability test was also performed after 72 hours in each experiment. After running the experiments and recording data, the data were analyzed.

### *1.6.2. Aims of the Thesis*

The central hypothesis of this thesis was to determine the effects of SPIONs on cellular activity, including adhesion, growth, proliferation, the formation of neurites and cell viability. In this work, three different assessment methods, including biological, microscopic and the equivalent circuit of the impedance data obtained, were used. This project aimed to study the advantage of impedance-based toxicity method to open an avenue for developing high throughput real-time, cost-effective impedance based screening array for toxicity studies. Also, this project aimed to run the entire related experiments in order to assess the required time and materials using conventional methods and obtain a large amount of data to validate results. The actual assessment results helped us to take an essential step toward the development of a high throughput impedance-based label-free platform for toxicity studies. This project was designed to generate a large amount of data from an actual toxicity study on SPIONs. The data and images may be further analyzed to give a more profound understanding of image processing and impedance electrical signal in the future for the development of next generation high-throughput device.

### *1.6.3. Organization of Thesis*

Chapter 1 highlights the premise, objectives, and research design of this study. Also, it presents a comprehensive review of several related kinds of literature. Chapter 2 emphasizes the materials used in this study and explains the methods that had been performed to gather the data. Further details of impedance analysis are also included in chapter 2. Meanwhile, the results and related discussions are put forward in chapter 3. Chapter 3 presents the results in the form of graphs, figures, and tables. Each result is explicitly discussed including the integration of impedance spectroscopy results and equivalent circuit model. Then, chapter 4 wraps up this thesis by giving a summary of the content of this thesis, conclusion based on the results, and contributions. It also tackles the future direction of this research after a brief financial and time analysis.

# Chapter 2

# Materials and Methods

In this chapter, the materials and methods used in the study are presented. It also describes the research process and the details of the methods in an operational manner.

## 2.1. Materials

### *2.1.1 Organism*

The Neuroblastoma 2a cells (Neuro2a or N2a cells) are a fast-growing mouse neuroblastoma cell line derived from an albino mouse strain [103]. This cell line was purchased from ATCC®. The maintenance, storage, and manipulation of the cell line used in this study was performed at the Medical Devices Laboratory at the Bergeron Building, York University.

### *2.1.2 Chemicals*

Most of the chemicals and reagents, including DMEM, FBS, PS, PBS, and trypan blue dye. Ethanol (Commercial ALC.), fetal bovine serum (FBS) (Life Technologies) and water (ultrapure type I) were purchased from Sigma-Aldrich (Oakville, Canada). The spherical shape SPIONs were purchased from Skyspring Nanomaterials, Inc (Houston TX, USA). The average size of SPIONs used in this study was ~ 10-15nm.

#### *2.1.2.1 Solutions and Media for Cell Culture*

| | |
|---|---|
| *Phosphate buffered saline (PBS)* | 0.9 % Sodium chloride, 99 % Water, 0.0144 % Potassium dihydrogen orthophosphate, 0.0795 % Sodium monohydrogen phosphate, heptahydrate, pH 7.2, sterile-filtered (Sigma-Aldrich Canada Co.) |
| *Trypsin-EDTA solution* | 0.05% trypsin, 0.02% EDTA (1x) in D-PBS (PAA) |
| *Dulbecco's Modified Eagle Medium (DMEM)* | 4500 mg/L glucose, L-glutamine, and sodium bicarbonate, without sodium pyruvate, liquid, sterile-filtered, suitable for cell culture (Sigma Life Science) |
| *Complete Culture Media (CCM)* | DMEM + 10% Fetal Bovine Serum (FBS) +1% penicillin/streptomycin |
| *Antibiotics - penicillin/streptomycin* | 10,000 units penicillin and 10 mg streptomycin/mL, sterile-filtered, Bio-Reagent, suitable for cell culture (Sigma) |

#### 2.1.2.2. Nanoparticle solution

| | |
|---|---|
| *SPIONs* | $Fe_3O_4$, 10~15nm, 98+%; black dispersion in water; super-paramagnetic property, spherical shape with the size of 10-15nm. |

### *2.1.3. Consumables*

Most of the non-chemical consumables as listed below were purchased from Fisher Scientific, and the electrodes for impedance measurements were purchased from Applied Biophysics Inc.

#### *2.1.3.1 Consumables for Biological Sample Preparation and Test*

| | |
|---|---|
| *Serological pipettes* | Sarstedt *(5ml, 10ml, 25ml) Sarstedt AG & Co. KG* |
| *Culture dishes* | *TC-Schale (100x20mm, 60x15mm) Standard* Sarstedt AG & Co. KG |
| *Culture Plates* | *(12-well, 6-well) Standard* Sarstedt AG & Co. KG |
| *Conical centrifuge tubes* | Thermo Scientific™ Nunc 15mL & 50mL Conical Sterile Polypropylene Centrifuge Tubes Thermo Scientific |
| *Petri dish* | Sarstedt, Fisher Scientific |
| *Plastic consumables (Universal Fit pipette tips and microtubes)* | Sarstedt, Corning Inc. and Sarsted Inc. |
| *Cell counter sensors* | 40 uM sensor, Scepter™ 2.0 Millipore Sigma |

#### *2.1.3.2. Consumable for Impedance Analysis*

| | |
|---|---|
| *Electrode Array ( type 1)* | ECIS (Applied Biophysics Inc, NY, USA), PC (Clear polycarbonate substrate)1E, Diameter of the electrode ( central hole), 250um |

| | |
|---|---|
| *Electrode Array (type 2)* (Figure 2) | ECIS (Applied Biophysics Inc, NY, USA), PCB (Non-transparent Printed Circuit Board) IE Diameter of the electrode ( central hole), 250um |

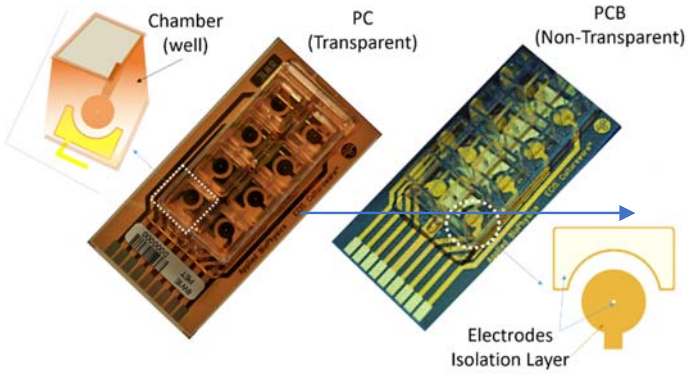


**Figure 2|** The electrode Type. Both clear polycarbonate substrate or PC and the non-transparent Printed Circuit Board or PCB have a single circular electrode that measures 250µm with an area of 0.049mm$^2$ in each well. An isolation layer surrounds the electrode.

### *2.1.4. Equipment*

All equipment used in this project for biological sample preparation and analysis, impedance measurement and analysis and microscopic analysis are listed below.

#### *2.1.4.1 Required Equipment for Biological Sample Preparation and Test*

| **Equipment** | **Model and Company name** |
|---|---|
| Incubator | Heracell 150i, Thermo Fisher Scientific |
| Refrigerator | Forma, Thermo Scientific |
| Freezer | Forma 900 series, Thermo Scientific |
| Laminar Flow Unit | 1300 Series A2, Thermo Scientific |
| Vacuum Aspirator Collection System- | HiFlow, F19917-0250, SP Scienceware |

| | |
|---|---|
| Lab Centrifuge | Sorvall ST 8, Thermo Scientific |
| Water Bath | Isotemp Digital 2320 Water Bath, Fisher Scientific |
| Analog Vortex Mixer | Fisherbrand™**,** Fisher Scientific |
| Analytical Balance | Quintix® 220 g x 0.1 mg, Sartorius |
| pH Meter | Hanna Checker®, Sigma Aldrich |
| Handheld Cell Counter | Scepter™ 2.0, Millipore Sigma |

#### *2.1.4.2 Required Equipment and Accessories for Microscopic Analysis*

| | |
|---|---|
| *Inverted and phase contract Microscope* | Fisherbrand™ Inverted Infinity, Phase contrast 10x and 20x, light splitter (100% or 20/80%), Fishers Scientific |
| *Microscopy Camera* | Education™ Motic D-Moticam 1080 Digital HDMI, 2MP, Fishers Scientific |
| *Hemocytometer* | BLAUBRAND® Neubauer, Millipore Sigma |

#### *2.1.4.3. Required Equipment for Impedance Analysis*

| | |
|---|---|
| *Impedance Measurement System* | Autolab PGSTAT101, FRA32M electrochemical impedance spectroscopy (EIS) module, Metrohm (see Figure 3b). |

### *2.1.5 Software*

The following software was utilized in obtaining data and for analysis purposes.

| | |
|---|---|
| *Cell counting Analysis* | Scepter™ 2.0 Software Pro User Interface (see Figure 3a) MilliporeSigma, Canada |

| | |
|---|---|
| *Microscopy image recording* | Motic 2.0 software, Fishers Scientific |
| *Impedance recording and analysis* | NOVA 2.0 software, Metrohm (Canada) |
| *Data analysis and display* | Excel, Microsoft |

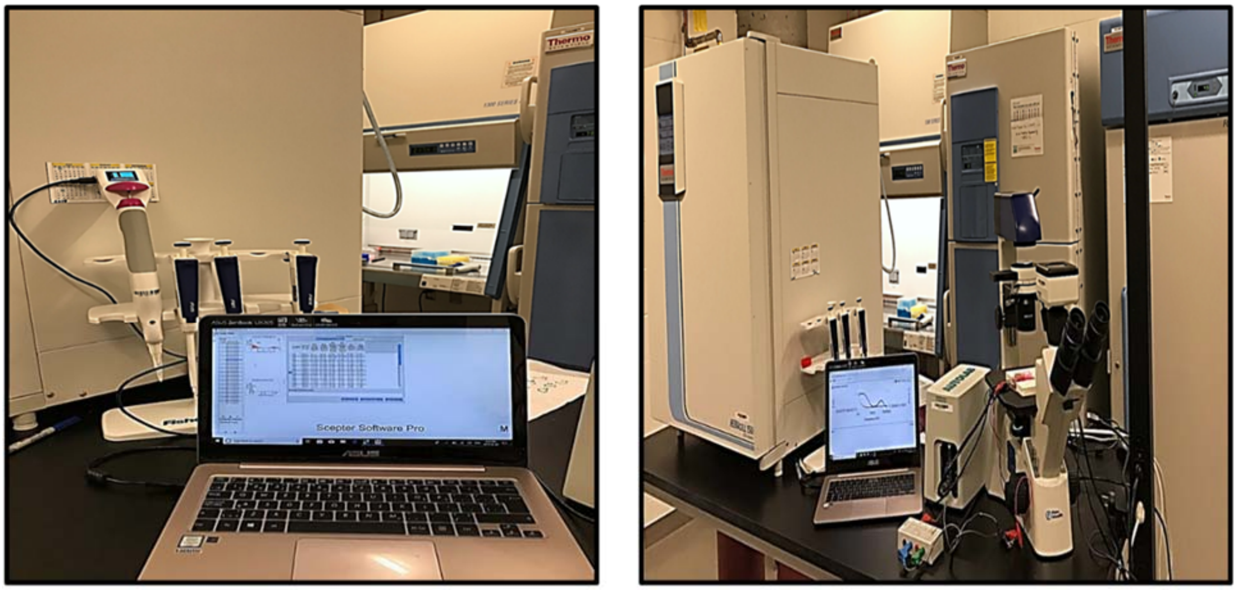


(a) (b)

**Figure 3|** Equipment for (a) scepter cell counting and (b) impedance analysis. A 40uM sensor was attached to the scepter cell counter where 50 uL of the cell suspension was drawn. Autolab PGSTAT101, FRA32M electrochemical impedance spectroscopy (EIS) module, Metrohm was used to generate and record impedance data.

## 2.2 Methods

In this work, the cells were cultured with different concentration of SPIONs (0, 25, 50, 100, 200 and 300 µg/mL) in the traditional Petri dish and the ECIS electrode array as seen in Figure 4. The cell viability, cell morphology analysis, and the impedance-based cell–surface attachment in the presence of SPIONs were measured using various methods. The details of the measurement results are shown in the next section.

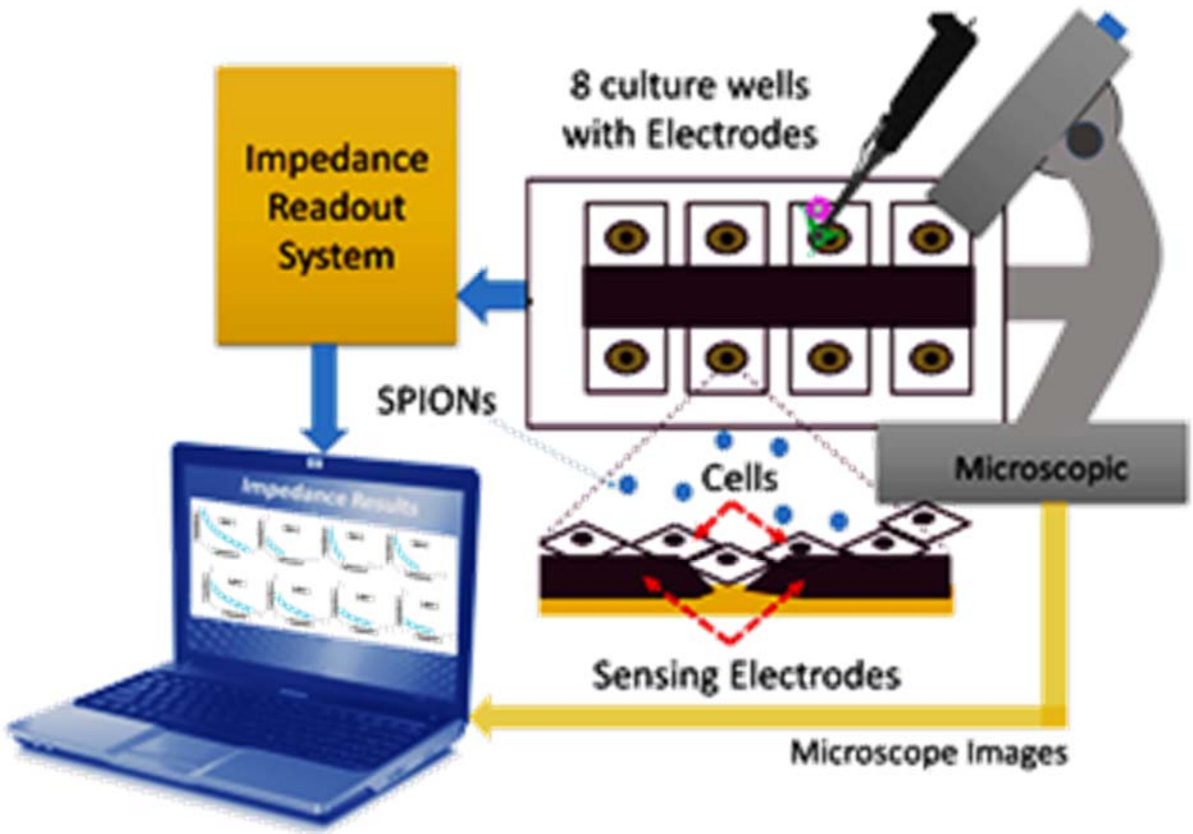


**Figure 4|** Scheme of the proposed experimental setup, including an array of 8 sensors incorporated with cell culture wells. These electrodes are connected to a computer through an impedance readout system. The cells are loaded by a standard pipette and observed under a microscope.

### *2.2.1 Sample preparation and biological test*

In this subsection, the protocols related to the preparation of samples, including biological cells, SPIONs, and related biological assays, are put forward.

#### *2.2.1.1. Preparation of SPIONs with different Concentration*

After thorough calculations, the 300µg/mL, 200 µg/mL, 100 µg/mL, 50 µg/mL, and 25 µg/mL concentrations of SPIONs were prepared by weighing 6, 4, 2, 1, 0.5 mg of SPIONs respectively using the Sartorius Quintix®and dissolved in the cell culture medium (CCM) to reach a total volume of 20 mL of the mixture. Then, SPION solutions were transferred into a conical tube containing a small amount of the CCM. A vortex mixer with a dimension of 20.3 x 14 x 12.2cm was set at the speed knob 9 with a speed of 3200 rpm to disperse the SPIONs for 15 minutes. After that, CCM was added to reach the desired volume used for the test.

#### *2.2.1.2 Cell Culture and Maintenance*

N2a cells were grown in complete culture medium (CCM) containing Dulbecco's Modified Eagle's Media (DMEM) with 10% Fetal Bovine Serum (FBS) and 1% antibiotic solution Penicillin-Streptomycin (PS). The cells were maintained in a Heracell $CO_2$ incubator with 5% CO2/37°C temperature.

As a part of maintenance, the cells were passaged twice a week. Once 90-100% confluency was reached, the cells were washed twice with 5ml pre-warmed PBS, treated with 1 ml pre-warmed trypsin-EDTA and incubated for 1-5 minutes for the cells to detach from the substrate. To ensure the detachment, cells were viewed under the microscope. A 1mL CCM was added and transferred to a 15 mL conical centrifuge tube containing 1mL CCM. The mixture was put in the centrifuge with a speed of 2500 rpm in 2 minutes. After which, the supernatant was removed, and the cells were resuspended with pre-warmed CCM in a culture Petri dish.

#### *2.2.1.3 Cell Concentration Preparation and Inoculation*

After counting the cells using hemocytometer, the concentration of $2.5x10^5$ cells/ml was prepared by diluting N2a cells with CCM an/or SPIONs mixture. The cells were seeded in both non-transparent (PCB model) and transparent (PC model) 8-well ECIS array. It is noteworthy that a single concentration of cell was prepared and used for all the test.

#### *2.2.1.4 Preparation for Trypan Blue Dye Exclusion Test Mixture*

Trypan Blue Dye Exclusion (TBDE) was used to determine the number of alive and dead cells after 72 hours of exposure into the different concentrations of SPIONs. When the cell is alive, its membrane does not allow penetration of the dye leaving the cells to appear rounded, clear and shiny under the microscope which distinguishes it from a dead cell that enables penetration of the blue dye. A 100 μL of the cell samples were diluted and gently mixed with an equal volume of trypan blue in a microtube, and it was set aside in room temperature for 3-5 minutes.

#### *2.2.1.5 Cell Counting and Cell Viability Test*

After 72h cell culture, the cells were collected using the standard trypsinization method. A randomized, double-blind method was carried out for the preparation of the dilution of the trypan blue dye and cell suspension to avoid bias. Each Eppendorf tube was labelled and covered with tape. Three biological replicates were prepared for every concentration. BLAUBRAND® Neubauer Hemocytometer (Millipore Sigma) was used to count the number of dead and live cells. The coverslip was slightly moistened with ultrapure water and slid it into the hemocytometer, gently avoiding the formation of bubbles. A 10µL mixture of cells and trypan blue dye was loaded under the coverslip. The hemocytometer was placed under the inverted microscope using a 10X objective lens. The number of live (unstained cells) and dead (stained) cells were counted in all the five areas with 16 squares.

The Scepter™ 2.0 Handheld Cell Counter (Millipore Sigma) was also used to measure the concentration of cells. A cell suspension diluted with PBS reaching to a total volume of 100µL. The mixture was put in a 2.0 mL microcentrifuge tube. For using the Scepter cell counter, a 40µm sensor was attached and submerged into the mixture. After a 50uL sample was drawn into the channels of the sensor, the cell concentration was displayed on the screen, and the files were transferred into the computer for analysis.

### *2.2.2 Microscopic methods*

An inverted microscope equipped with a camera (motic 2.0) and various (e.g., 4X, 10X and 20X) objectives was used to capture microscopic images in eight different times. This microscopic images were used to monitor cellular morphological changes and likely their adhesion, growth, and differentiation, in the presence of different concentrations of SPIONs.

### *2.2.3 Electrical methods*

#### *2.2.3.1. The principle of Impedance Spectroscopy Technique for Cellular Analysis*

Impedance spectroscopy is a technique that measures the electrical impedance between two adjacent electrodes exposed to the chemical or biological materials. Impedance is a combination of resistive and capacitive properties of the material. The equivalent circuit of the electrode exposed to the cells in culture can be represented with the schematic shown in Figure 5.

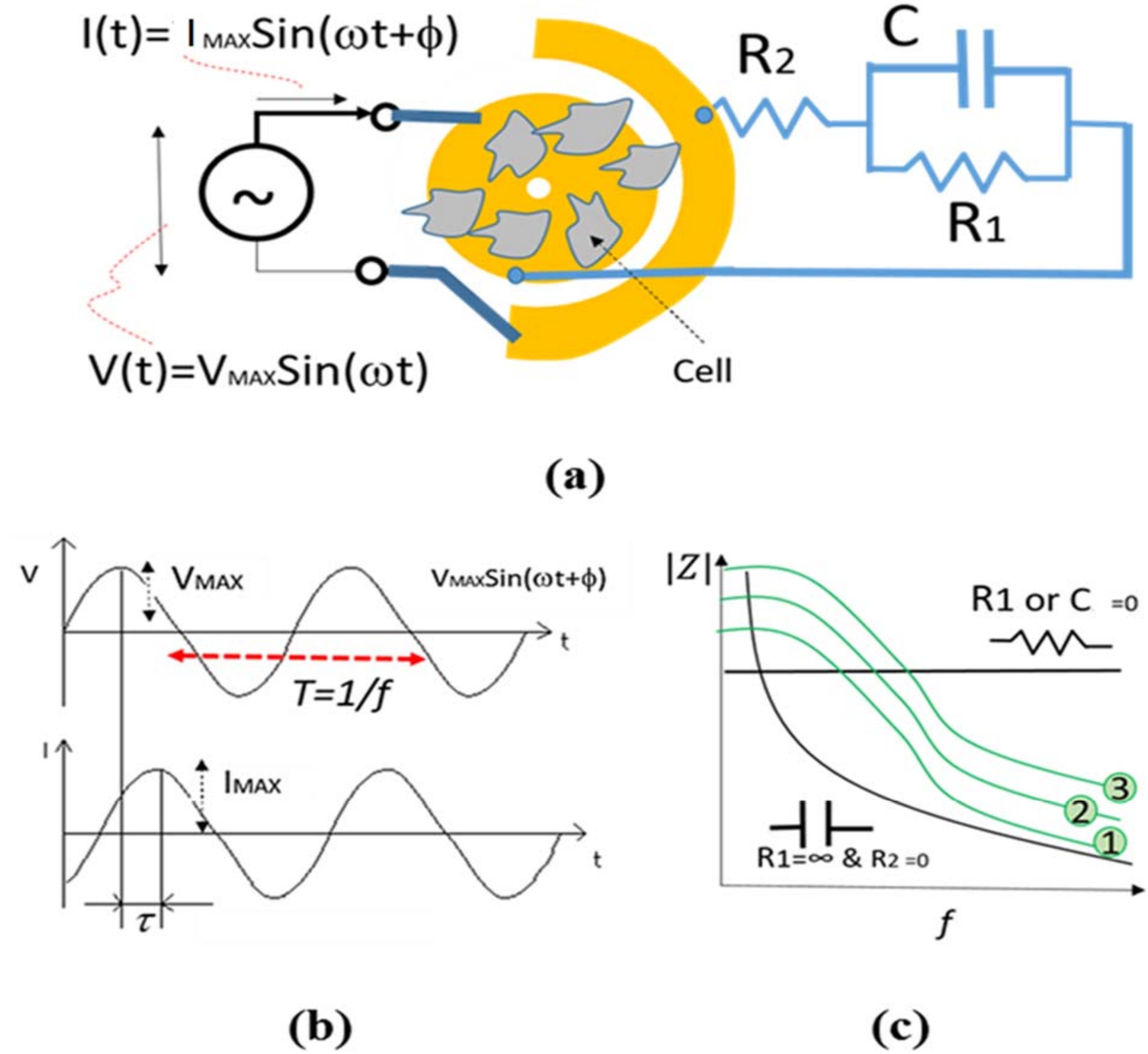


**Figure 5|** Principle of impedance measurement. The equivalent circuit model R-R-C of the electrode exposed to the medium with different SPIONs concentrations and cells. VMAX is the amplitude of the electrical voltage and IMAX is the amplitude of the current signals. Frequency (f) is inversely proportional to time (T). The green curves represent the change of impedance.

The magnitude of impedance between the electrodes can be represented by equation (1).

$$|Z| = \sqrt{\frac{(R_1+R_2)^2+(\omega C_1 R_2 R_1)^2}{1+(\omega C_1 R_1)^2}} \quad (1)$$

Where $R_1$ and C represent the resistance and capacitance properties of cells attached to the electrodes, respectively. Also, $R_2$ represents the resistance of connectors as well as medium. Omega (ω) is equal to 2π *f* where *f* is the frequency of sine shape electrical voltage applied to the sample and resulted in an electrical current with the same frequency (see Figure 5b). *f* is equal to the inverse of the time period T. Indeed; the impedance is equal to the magnitude of $V_{MAX}/I_{MAX}$ where both $V_{MAX}$ and $I_{MAX}$ are the amplitude of electrical voltage and current signals as seen in Figure 5.

As seen in Figure 5c, depending on the medium and biological material, the equivalent circuit can be a simple resistor or capacitor. However, the equivalent impedance magnitude is very similar to the green curves shown in Figure 5c so that by increasing the impedance the curve 1 moves to curve 2 and then 3. In other words, the attachment and confluence of cells on electrodes and in between the electrodes result in higher impedance. It is noteworthy that φ and τ are the time and phase difference, respectively, as seen in Figure 5b so that $\varphi = 2\pi\tau/T = 2\pi f\tau$. In this project, we only use the magnitude of impedance. Therefore, the phase differences are not taken in our calculations**.**

### *2.3.2. Impedance-based Cellular Analysis*

The cell attachment and growth above the electrodes can be monitored by measuring the impedance in between the electrodes [104]- [74]. The attachment of cells above electrodes can increase the dielectric properties and decrease the conductivity; therefore, the amount of impedance in all frequencies is increased as seen in Figure 6a. This figure showed the increase of impedance of electrodes underneath of cells in culture over time.

#### *2.2.3.2.1. Maximum Surface Area*

As the first impedance analysis method, we used the maximum variation of impedance as a healthy state of cells in the presence of SPIONs. As seen in Figure 6b, the surface area S represents the maximum change and calculated by equation (2.)

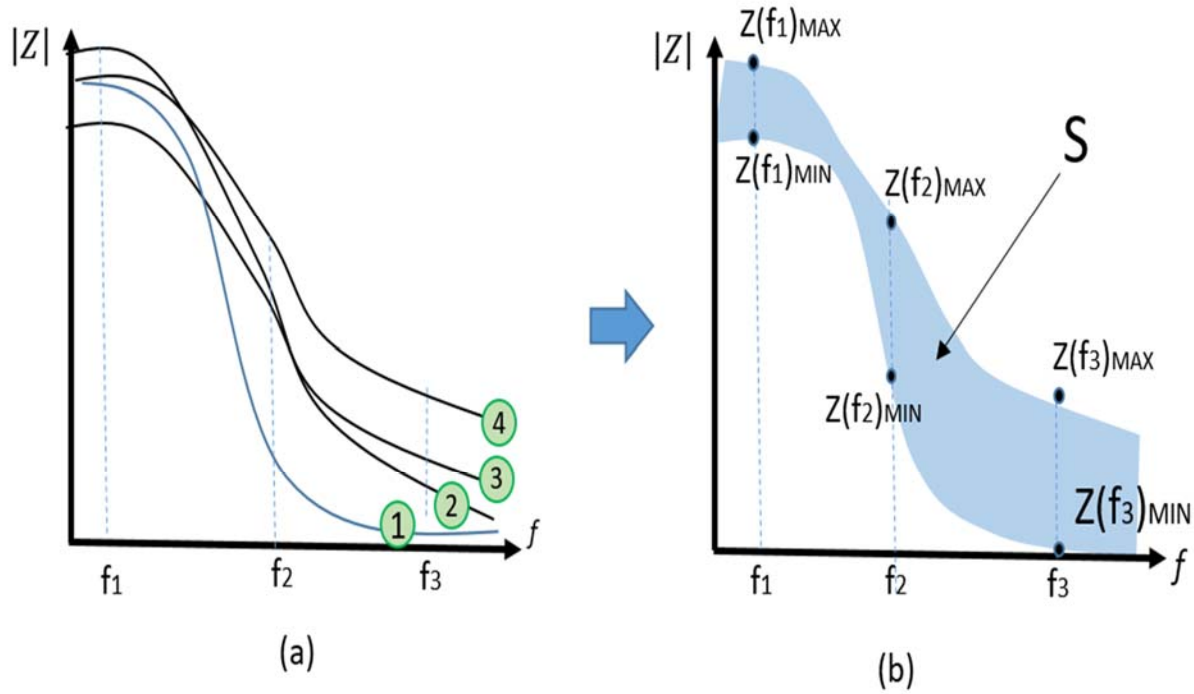


**Figure 6|** Illustration of (a) multi-curves impedance spectroscopy results and (b) the covered surface area S. S represents the change of impedance, /Z/, in each frequency point.

$$S = \sum_{f_{MIN}}^{f_{MAX}} \frac{(Z(f)_{MAX} - Z(f)_{MIN}) \cdot \Delta f}{f_{MAX} - f_{MIN}} \quad \textbf{(2)}$$

By knowing $\Delta f$ is the minimum frequency change and $f_{MAX}$ -$f_{MIN}$ refers to the range of scanned frequencies, ($f_{MAX}$ -$f_{MIN}$)/$\Delta f$ is equal to the number (N) of different frequencies that the impedance was measured. In other words, S was obtained from using the following equation.

$$S = \sum_{1}^{N} \frac{(Z(f)_{MAX} - Z(f)_{MIN})}{N} \qquad \textbf{(3)}$$

As an example, table 3 shows the parametric impedances measured in different frequencies and times. It is assumed that the cells were mixed with an arbitrary concentration of SPIONs. The maximum and minimum values of impedances were obtained and used to calculate the impedance change $\Delta Z=Z(f)_{MAX}-Z(f)_{MIN}$ in different times and frequencies as shown in the table. As a result, a column of various $\Delta Z$ was obtained. Based on equation (3), the average of all numbers in this column is equal to S, and consequently, it shows the maximum variation of impedance.

**Table 3**| Impedance measurement in a range of frequencies ($f_1$-$f_N$) at different times (T1-T8)

| f | T1 | T2 | … | T8 | $Z_{MAX}(f)$ | $Z_{MIN}(f)$ | $Z_{MAX}$-$Z_{MIN}(f)$ |
|---|---|---|---|---|---|---|---|
| $f_1$ | $Z_0(f_1)$ | $Z_1(f_1)$ | … | $Z_{72}(f_1)$ | Max ($Z_0(f_1)$… $Z_{72}(f_1)$) | Min ($Z_0(f_1)$… $Z_{72}(f_1)$) | $Z_{Max}$-$Z_{MIN}(f_1)$ |
| $f_2$ | $Z_0(f_2)$ | $Z_1(f_2)$ | … | $Z_{72}(f_2)$ | Max ($Z_0(f_2)$… $Z_{72}(f_2)$) | Min ($Z_0(f_1)$… $Z_{72}(f_1)$) | $Z_{Max}$-$Z_{MIN}(f_2)$ |
| … | … | … | … | … | … | … | … |
| $f_N$ | $Z_0(f_N)$ | $Z_1(f_N)$ | … | $Z_{72}(f_N)$ | Max ($Z_0(f_N)$… $Z_{72}(f_N)$) | Min ($Z_0(f_1)$… $Z_{72}(f_1)$) | $Z_{maz}$-$Z_{MIN}(f_N)$ |

As aforementioned, S is equal to the average of $Z_{MAX}$-$Z_{MIN}$ in various frequencies. In the next section, we also obtained the variance and standard deviation of $Z_{MAX}$-$Z_{MIN}$. Additionally, one may argue the normalized values of S can be related to the concentration of SPIONs. For this, we also calculated the average or standard deviation of all impedances measured in each frequency ($f_1$-$f_N$) as seen in Table 3, which is continued in Table 4. In this situation, instead of $Z_{MAX}$-$Z_{MIN}(f)$, $Z_{MAX}$-$Z_{MIN}(f)$ /AVG(f) and STD(f) should be calculated and shown in a column. Finally, the average, variance, and STD of this column can be calculated to obtain a kind of normalized S. It is noteworthy that using these calculations methods, we try to quantify the effects of SPIONs on cells in culture.

**Table 4|** Continuation of Table 1, AVG and STD analysis

| F | AVG (f) | STD(f) | $Z_{MAX}$-$Z_{MIN}(f)$/AVG(f) |
|---|---|---|---|
| $f_1$ | AVG ($Z_0(f_1)$… $Z_{72}(f_1)$) | STD ($Z_0(f_1)$… $Z_{72}(f_1)$) | $Z_{Max}$-$Z_{MIN}(f_1)$/AVG($f_1$) |
| $f_2$ | AVG ($Z_0(f_2)$… $Z_{72}(f_2)$) | STD ($Z_0(f_1)$… $Z_{72}(f_1)$) | $Z_{Max}$-$Z_{MIN}(f_2)$ /AVG($f_2$) |
| … | … | … | … |
| $f_N$ | AVG ($Z_0(f_N)$… $Z_{72}(f_N)$) | STD ($Z_0(f_1)$… $Z_{72}(f_N)$) | $Z_{maz}$-$Z_{MIN}(f_N)$ )/AVG($f_N$) |

#### *2.2.3.2.2. Electrical Model*

As per equation (1) and as seen in Table 5, an equivalent circuit with specific values of $R_1$, C and $R_2$ can be fitted with the impedances measured in each time (T1-T8) in a range of frequency, within a particular value of SPIONs. In this method, a software called NOVA 2.0 was used to find the optimum values of an equivalent circuit for each range of frequencies. In this method, various values of C, $R_1$, and $R_2$ for different concentrations of SPIONs were obtained at different times to study the effects of SPIONs on the cell culture over time.

**Table 5|** Electric equivalent circuit for each range of frequencies

| F | T1 | T2 | … | T8 |
|---|---|---|---|---|
| $f_1$ | $Z_0(f_1)$ | $Z_1(f_1)$ | … | $Z_{72}(f_1)$ |
| $f_2$ | $Z_0(f_2)$ | $Z_1(f_2)$ | … | $Z_{72}(f_2)$ |
| … | … | … | … | … |
| $f_N$ | $Z_0(f_N)$ | $Z_1(f_N)$ | … | $Z_{72}(f_N)$ |
| $f1-f_N$ | $C_{1,0}$, $R_{1,0}$, $R_{2,0}$ | $C_{1,1}$, $R_{1,1}$, $R_{2,1}$ | … | $C_{1,8}$, $R_{1,8}$, $R_{1,8}$ |

#### *2.2.3.3. Impedance Measurement Assay*

Using Metrohm Autolab, the impedance spectroscopy of the eight wells were measured in different times (0, 2, 4, 6, 8, 24, 48 and 72 hours). The impedance was monitored using a frequency ranging from 0.1 Hertz (Hz) to 100,000Hz with an alternating current (AC) 100 mV voltage. The electrode array was interconnected into the impedance system using copper wires. The impedance measurement results were saved into excel files for further analysis and display.

Before loading the ECIS array with cells, it was cleaned with PBS, rinsed with ultrapure water and electrodes were pre-conditioned by flooding each well with 200 μL of cysteine solution for 10 minutes and equilibrate with DMEM. In some circumstances, the electrodes were also further cleaned and treated in an oxygen plasma for 60 seconds.

After calibration, a monodisperse $2.5x10^5$ cells/ml concentration of cell was inoculated separately in each of the six wells. During the inoculation, the cell suspensions were agitated to prevent settling of cells from the bottom of the tube. Meanwhile, the remaining wells were filled with the CCM and different concentrations of SPIONs without cells. After each test, the ECIS device was put back in the incubator.

## 2.3. Summary

In this section, the details of materials and methods were elaborated. The main methods, including biological, microscopic and impedance, were used to study the effects of SPIONs on the cells. These methods were applied to a large number of samples, as demonstrated and discussed in the next section. This study brings us a step closer to assess the need for high throughput cellular analysis for various applications for toxicity studies.

# Chapter 3

# Results and Discussions

In this chapter, the experimental results related to biological, microscopic and impedance methods are separately demonstrated and discussed in sections 3.1, 3.2 and 3.3 as summarized below.

- Biological method: The cell viability tests were performed using the trypan blue exclusion assay. This technique was used to count the number of viable cells after 72 hours (T8) exposure.
- Morphological method: The microscopic images of the N2a cells were captured to compare the treated and untreated cells. The treated cells were the cells mixed with the different concentrations (C2-C6) of SPIONs. The N2a cells were cultured in an incubator.
- Electrical method: The attachment of cells and SPIONs above electrodes can change the impedance as described in chapter.2 The impedance spectroscopy of cells in the control (C1) and with the presence of SPIONs (C2-C6) were measured at different times (T1-T8) by hypothesizing that the effect of SPIONs on cells can be tracked using the recorded impedances.

Figure 7 provides an illustrative summary of the experiments performed in this thesis. In these experiments, two series of cell culture experiments were performed using PC and PCB electrode arrays, as mentioned in chapter 2. Each series of the experiment includes three different trials performed in three different time periods (TP1, TP2, and TP3). In each trial, each experiment was replicated three times (G1-G3). By knowing that the initial cell concentration, which is $2.5 \times 10^5$ cell/mL the cell viability (V) is measured after 72 hours.  A seen in Figure 7, in each group (G1, G2 and G3), six different concentrations (C1-C6) of SPIONs were mixed with cells and cultured in the incubator for 72 hours. The microscopic images (M) and impedance measurements (I) were obtained in eight different times (T1-T8). All experiments were repeated without cells in order to control the results.

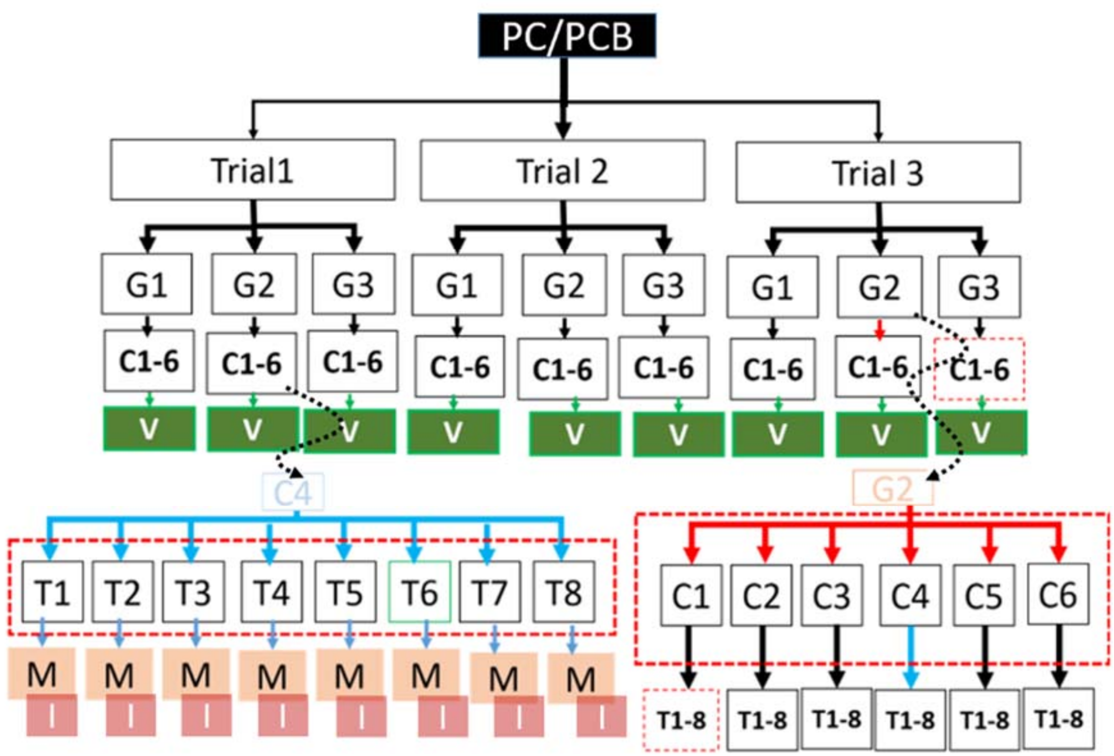


**Figure 7|** An illustrative summary of experiments performed in this thesis. There are three different trials (Trial 1, 2 and 3), each trial includes three groups (G1-G3), and each group includes six different concentrations (C1-C6) of SPIONs measured in 8 different times. All tests were performed using PC and PCB electrode arrays. Viability (V) and Impedance measurement (I) were recorded. Microscopic images (M) were captured.

Based on table 6, the number of experiments per chamber is $TR \cdot CC \cdot T \cdot C \cdot G = 864$. The number of experiments using PC and PCB electrode reaches to 1728. By knowing that the microscopic images of experiments related to PCB electrodes were performed on Petri dish, the total number of an experiment should be added with about TR*G*C=54 petri-dishes.

**Table 6|** Facts about the experiment

| Fact | Quantity |
|---|---|
| Trials (TR1-TR3) | TR=3 |
| Group (Replications) | G=3, G1-G3 |
| Types of electrodes (PC, PCB) | TE=2 |
| Cell Concentrations | CC=2, CC1=2.5x$10^5$ cells/mL, CC2=0 |
| SPIONs concentration (C1-C6) | C=6, C1-C6=0, 25, 50, 100, 200, 300 ug/mL |
| Control (Positive and Negative) | C1= N2a cells only (positive control), CCM, SPIONs concentrations only (negative control) |
| Measurement times (T1-T8) | T1=0, T2= 2, T3=4, T4=6, T5=8, T6=24, T7=48, T8=72 hours. |

| | |
|---|---|
| Time period of each trials ( TP1-TP3) | PCB:<br>TP1=12/6/2017-12/30/2017,<br>TP2=05/27/2018-06/20/2018,<br>TP3=08/03/2018-08/25/2018<br>PC:<br>TP1=07/13/2018-07/10/2018,<br>TP2=08/03/2018-09/10/2018,<br>TP3=09/13/2018-09/20/2018 |

## 3.1 Biological Effects

This section demonstrates the effect of SPIONs on the viability of cells. Figure 8 shows the percentages of alive and dead cells in the presence of six different concentrations of SPIONs (0, 25, 50, 100, 200 and 300 µg/mL) in the cell culture.

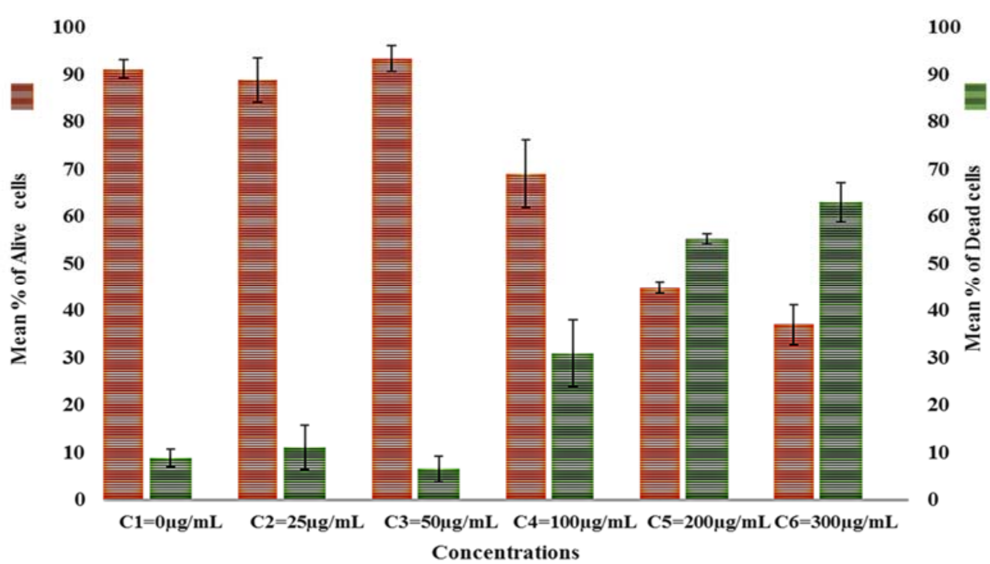

(a)

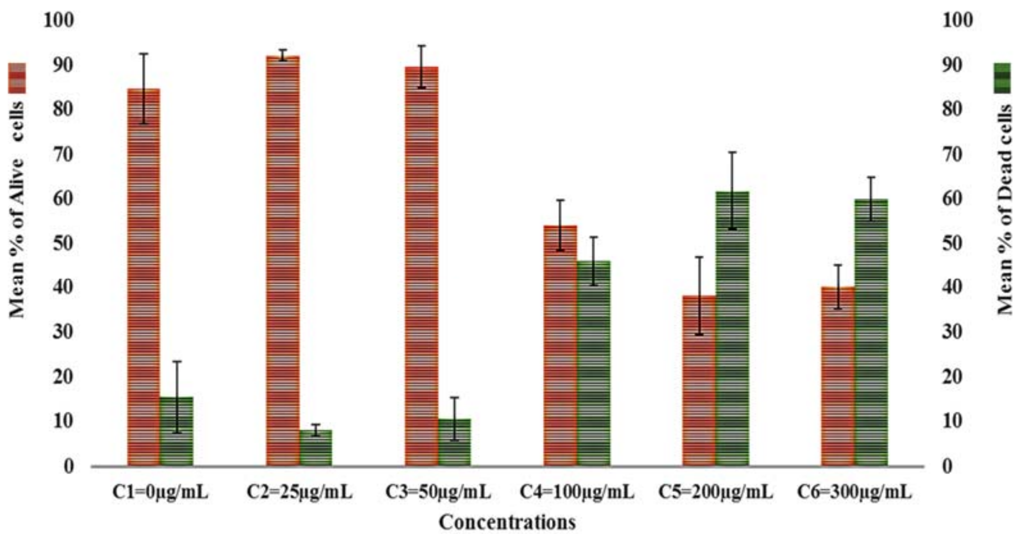


(b)

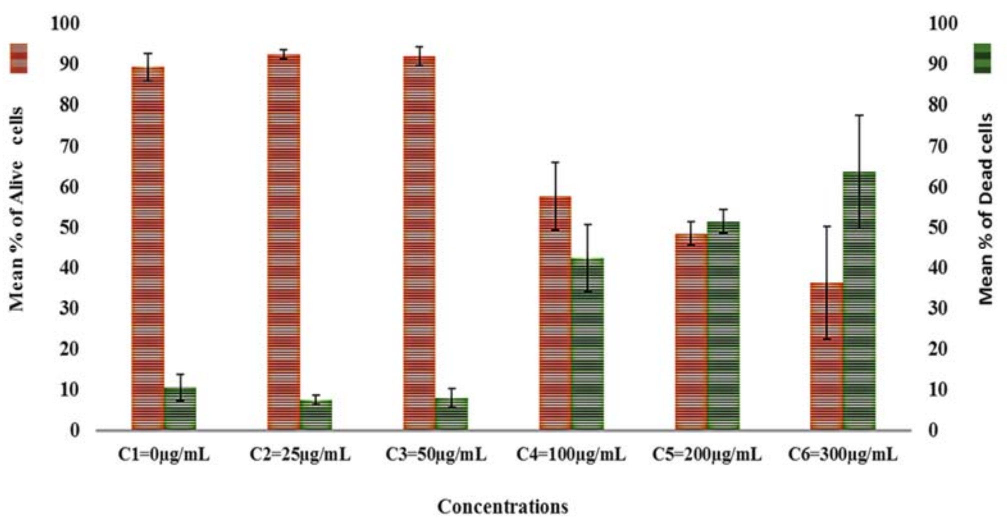


(c)

**Figure 8|** Viability Results. The mean percentages of both alive and dead N2a cells in the three groups (a) group 1, (b) group 2 and (c) group 3 were graphed with respect to six different concentrations of SPIONs, 0µg/mL, 25µg/mL, 50µg/mL, 100µg/mL, 200µg/mL, and 300µg/mL. Each bar represents the mean percentage of cells counted using TBDE. The error bars represent the standard error of the mean.

.

In each group, the mean value of the three replicates was calculated for both alive and dead cells.

Consistent with the results shown above, an inverse relationship between the concentration of SPIONs and cell viability was found. As seen in Figure 8, for C1<50 µg/mL, the cell viability was high and almost invariant. On the other hand, the cells exposed to C ≥ 300µg/ml SPIONs show the highest percentages of cell mortality. The same trend was observed using the PC array device. Low cell viability with percentages of 59, 47, 40% in higher concentrations of SPIONs, 100µg/mL, 200µg/mL, 300µg/mL, respectively, was observed in PCB array device. All three trials on PCB and PC are presented in Appendix A. As shown in this appendix, increasing the concentrations of SPIONs, results to lower cell viability which may be due to the increased toxicity effect of SPIONs on cells. These results are in agreement with the results observed by Naqvi et al. [104] and [102] where higher doses of NPs amplify toxicity.

Besides, from the 2.50E+05 initial cell concentration at T1, all N2a cells in the control with no SPIONS (C1) and those that were treated with different concentrations of SPIONs (C2-C6) manifested an increased cell concentration after 72 hours (T8). However, C4, C5, C6 showed lower cell concentration growth compared to C1. Relative to C1, the percent difference of cultured cells using C4, C5, C6, was 59, 44 and 53% respectively when these differences are 24 and 16% using C2 and C3 respectively. Higher concentrations of SPIONs showed higher difference relative to the control, as shown in Appendix A.2.

Although viability test was mainly determined using the Trypan Blue Dye Exclusion (TBDE), the number of cells were also counted using a Scepter™ 2.0 Handheld Cell Counter (see Appendix C). Figure 9 shows the mean values of counted cells using TBDE and Scepter counter. Additionally, this figure illustrates a higher number of cells measured by Scepter cell counter compared to the one obtained in TBDE. The difference might be due to the presence of SPIONs' aggregates along with the cells being detected, considering that Figure 9 shows the concentration for the total event, not the gated concentrations. Moreover, the calculated percent coefficient of variation (% CV) of the cell concentration in all concentrations (C1-C6) using TBDE is 8.85, 6.05, 8.69, 4.75, 6.32, 10.80, respectively. Relative to TBDE, using the scepter cell counter, % CV of in C1-C6 are 40.48, 27.13, 20.04, 30.65, 40.38, and 56.88 respectively. Comparing %CV results obtained using two different techniques, TBDE results shows less variation and consequently high accuracy, relative to scepter cell counter's results. Appendix C reveals the complete cell counter results using the scepter handheld cell counter tool.

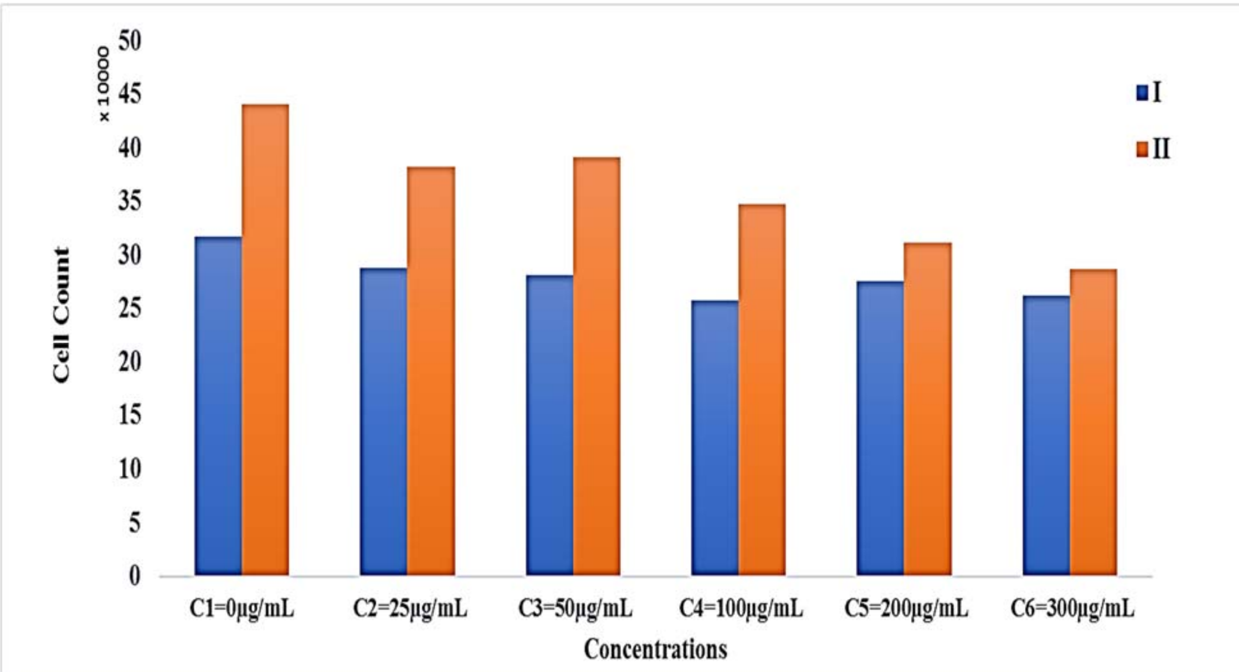


**Figure 9|** Comparison of TBDE and cell counter. The trypan blue dye exclusion (I) showing a lower number of cells counted in all the concentrations of SPIONs (C1=0µg/mL, C2=25µg/mL, C3=50µg/mL, C4=100µg/mL, C5=200 µg/mL, C6=300µg/mL) compared to the Scepter Handheld Cell counter (II). C1=0 µg/mL showed the highest number of cells counted for both I and II.

## 3.2 Morphological Effects

In this section, the adhesion, confluence and morphological changes of cells are evaluated using microscopic images. The microscopic changes of cells cultured on transparent electrodes and Petri dishes were captured by a camera (motic 2.0) at different times (T1-T8). The images were captured from the same location of electrodes or Petri dishes and the same magnification (20 x

10 = 200X). Figures 10a-10f show the N2a cells treated with C1-C6 concentrations of SPIONs respectively at T1 while Figures 10g-10l show the same cells incubated with the same concentrations of SPIONs at T8. These microscopic images were used to observe the growth, proliferation, and formation of neurite extensions of the N2a in the presence of various concentrations of SPIONs. In general, based on the results shown in Figure 10 and other images shown in Appendix C, the growth and proliferation of N2a are faster in the absence of SPIONS. A similar observation was pointed out in the study presented by Eustaquio and Leary (2012) where proliferation and differentiation of cells are affected by their exposure to nanoparticles [12]. Similarly, the decreased proliferation brought about by increasing the amount of SPIONs was also observed in the study performed by Lindemann et al. [105]. In addition, Chen et al. (1997) pointed out that modifying the environment of cells such as cell substrate including the medium may alter cell behavior and shape which lead to decrease adhesion and increase cell death [106].

In this experiment, each Petri dish and PCB/PC culture array were seeded with the same concentration of cells. As shown in Figures 10a-10f, the cells had a round shaped at T1. At T8, the cells were adhered entirely, differentiated and somehow developed neurites as seen in Figures 10g-10l. As manifested in Figures 10g-10h, the surfaces of Petri dishes were completely covered with cells where the concentrations of SPIONS were C1 and C2, respectively. This shows the highest cell confluence in the Petri dishes. However, Figures 10j-10l show less cell confluence on the surfaces of Petri dishes, thus it seems that longer neurites were generated to connect the nearby cells. Additionally, by increasing the SPIONs, the size of SPIONs clusters is also increased as seen in Figure 10j-10l. Similarly, Figures 11a-11l show the growth of N2a cells on the surface of the electrode at T1 and T8 in different concentrations of SPIONs. Figures

11g and Figures 11h show 95 to 100% cell confluence after 72 hours of cell culture in the incubator. It is noteworthy that the optically transparent electrode array or so-called PC electrode array allowed us to count the number of cells using an optical microscope and measure the electrical impedance. The morphological changes as a result of the interaction of N2a to the different of SPIONs from T1-T8 are shown in Appendix B.

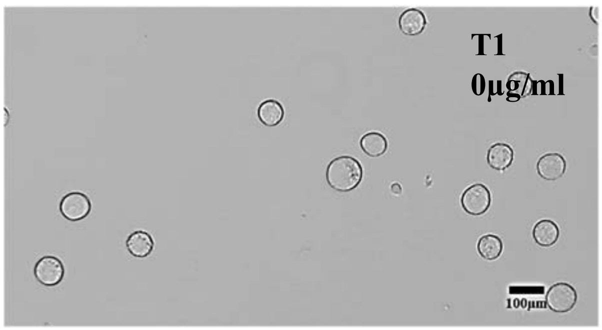


(a)

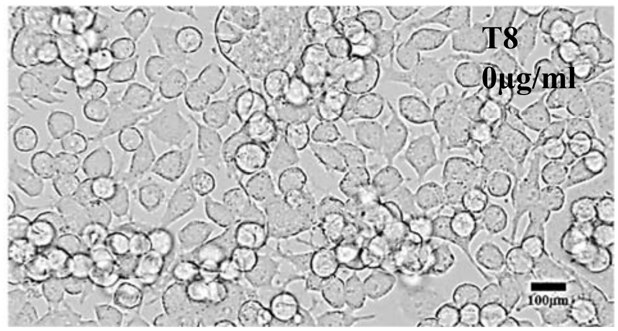


(g)

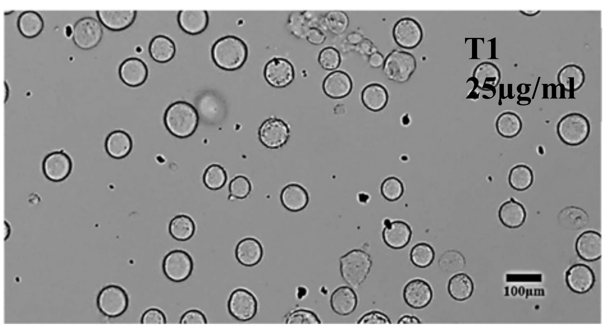


(b)

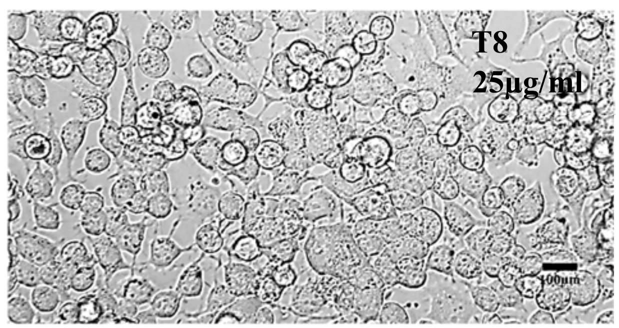


(h)

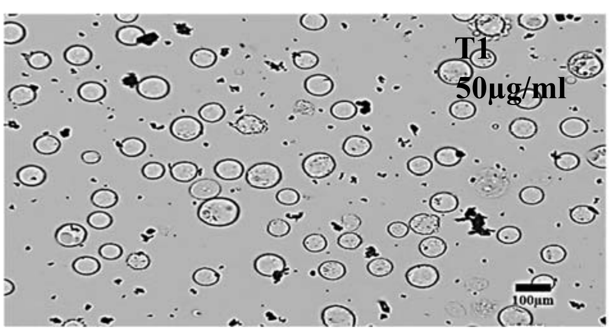


(c)

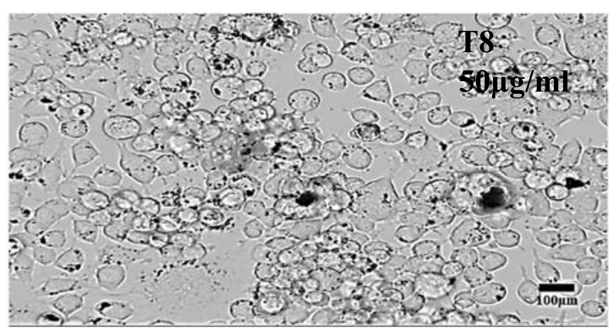


(i)

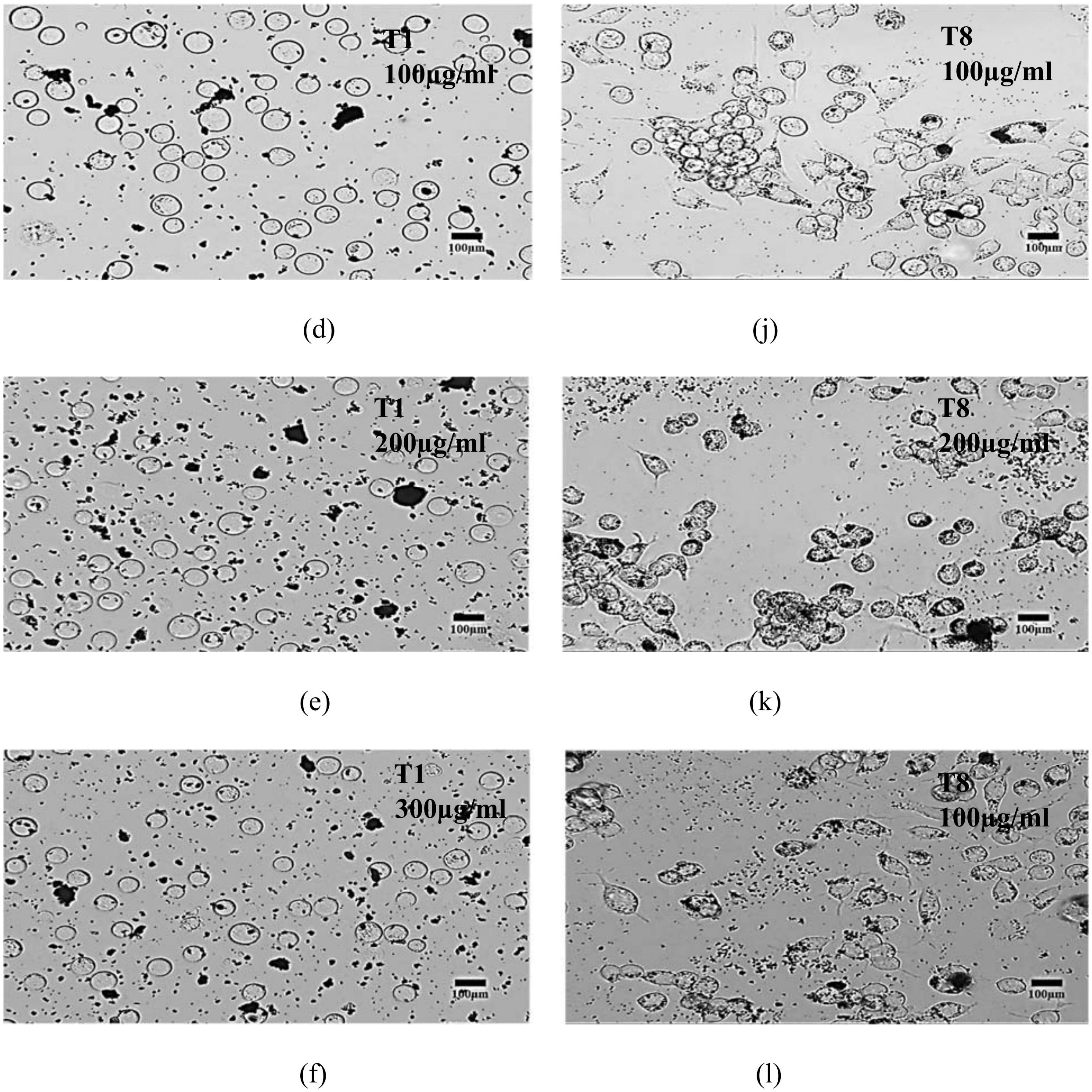


**Figure 10|** Photomicrographs of untreated and treated N2a cells at the initial time (T1) and after 72 hours' (T8) incubation. Images in a, b, c, d, e, and f were taken at T1 while g, h, i, j, k, and l at T8. a, g= 0µg/ml (untreated N2a); b, h=treated with 25µg/ml; c, i =50µg/ml; d, j=100µg/ml; e, k =100µg/ml; f, l=100µg/ml SPIONs concentrations. The confluence of cells is higher at g, h, and i. Scale bar 100µm.

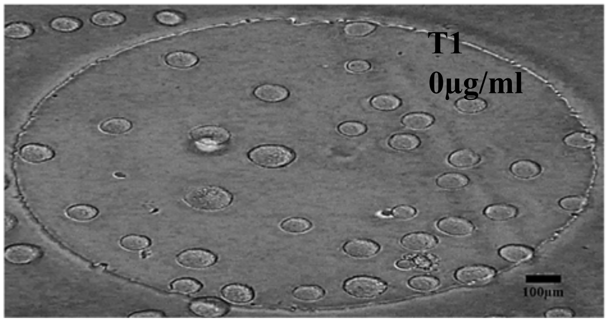
T1
0µg/ml
100µm

(a)

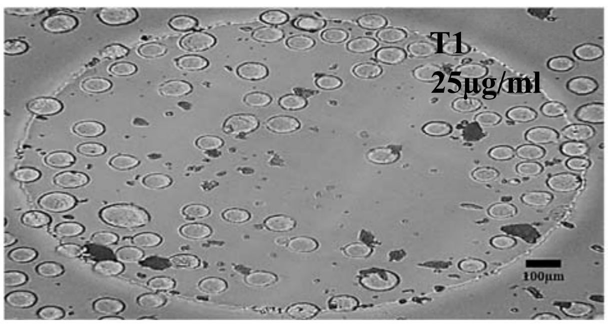
T1
25µg/ml
100µm

(b)

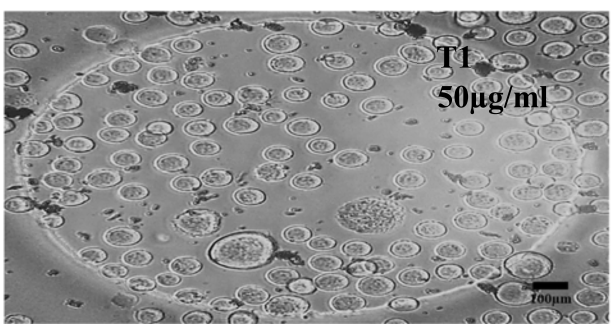
T1
50µg/ml

(c)

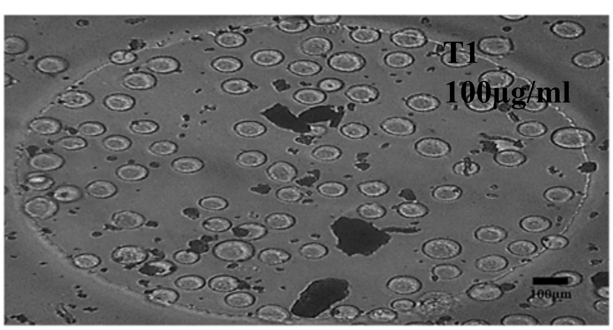
T1
100µg/ml

(d)

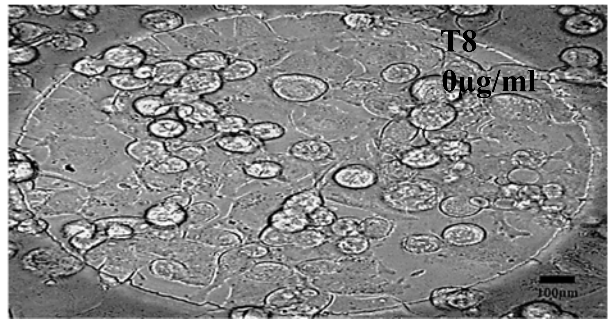
T8
0µg/ml

(g)

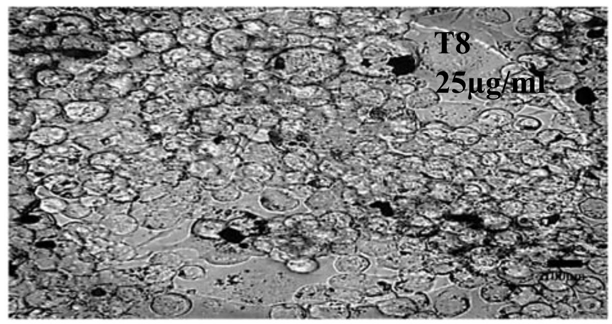
T8
25µg/ml

(h)


T8
50µg/ml

(i)

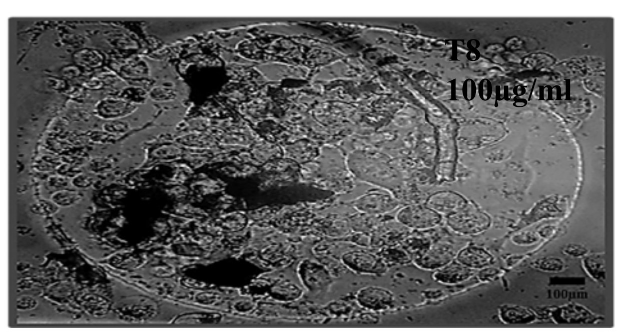
T8
100µg/ml

(j)

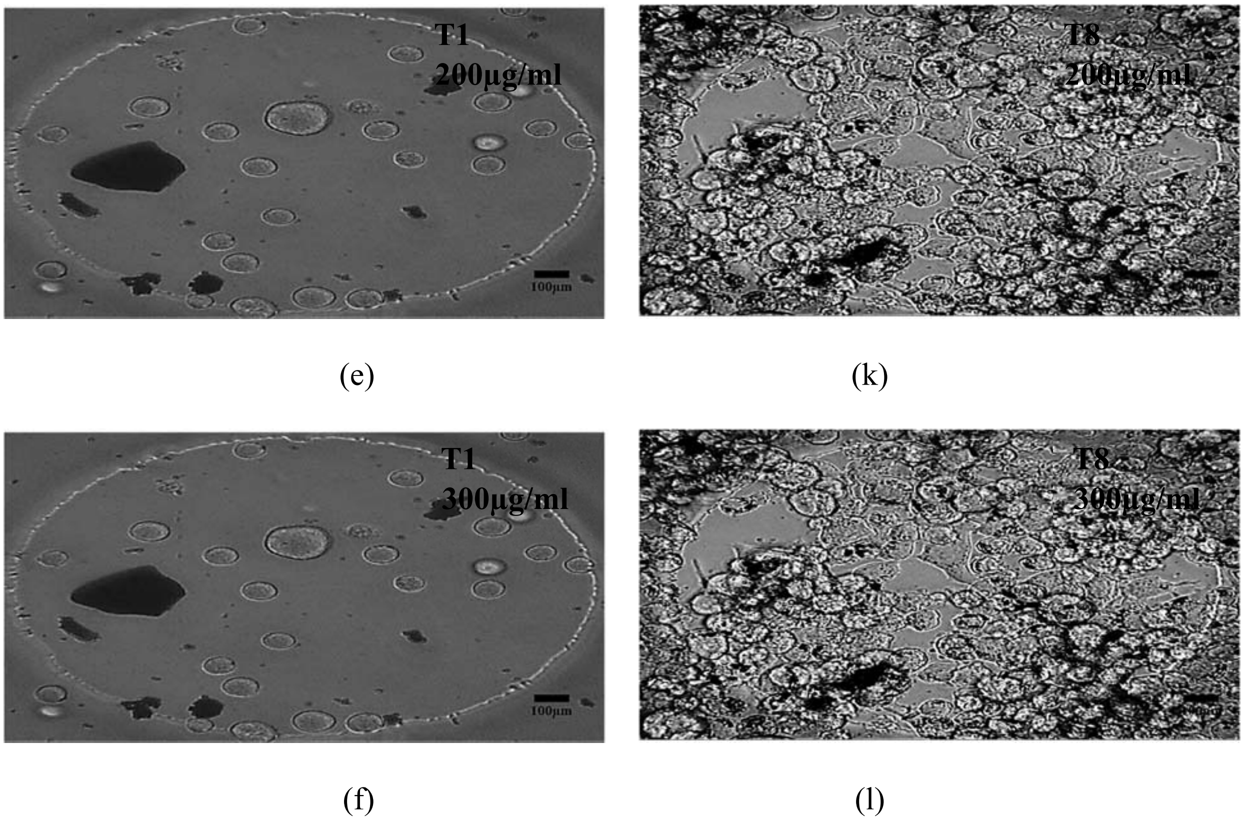


**Figure 11|** Photomicrograph of N2a cells exposed to the different concentrations of SPIONs on the surface of a 250µm diameter electrode on a clear polycarbonate substrate. Images in a, b, c, d, e, and f were taken at T1 while g, h, i, j, k, and l at T8. a, g= 0µg/ml (untreated N2a); b, h=treated with 25µg/ml; c, i =50µg/ml; d, j=100µg/ml; e, k=100µg/ml; f, l =100µg/ml SPIONs concentrations. The confluence of cells is higher at g, h, and i. Scale bar 100µm.

Figure 12 highlights the time the cells started to uptake SPIONs. Each inset shows the morphology and shape of a single cell at T2. The internalization of SPIONs by the cells was indicated by the presence of dark spots in the cytoplasm. From T2, the number of cells with internalized SPIONs and the amount of SPIONs in the cytoplasm had increased over time. Regardless of the concentration of SPIONs, cells had started to internalize the nanoparticles at 2 hours of incubation.

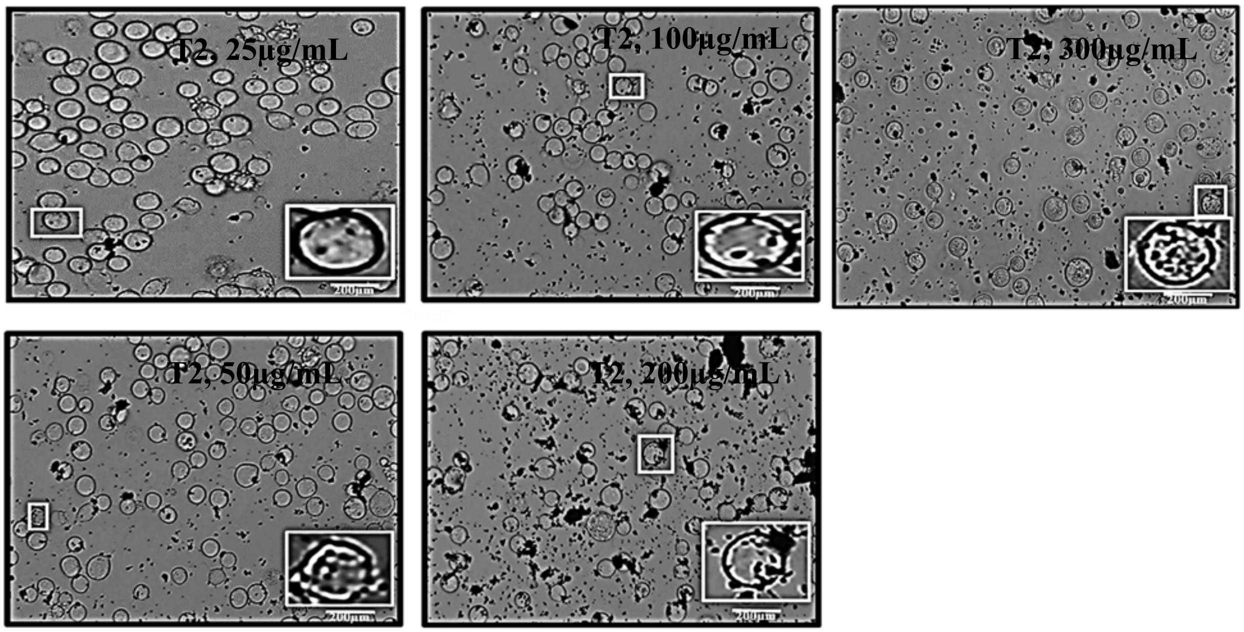


**Figure 12**| Cellular uptake. The images are N2a cells incubated with different concentrations of SPIONs (0μg/mL, 25μg/mL, 50μg/mL, 100μg/mL, 200μg/mL and 300μg/mL. The inset shows individual cells observed at T2, where cells were observed initially uptake the SPIONs. Morphology and shape of the individual cells from each SPIONs concentrations are represented. The scale bar of the inset is 200μm.

## 3.3 Electrical Effects

As aforementioned, in this thesis, 1728 experiments were performed using PC and PCB electrodes. In each experiment, eight impedance measurements were performed at T1to T8. Therefore, the number of the recorded complex impedance $Z_R+jZ_I$ values in 60 different frequencies is about 103,680, where $Z_R$, $Z_I$ are real and imaginary values of impedance in each frequency, as seen in table 7. In this table the magnitude of impedances ($\sqrt{Z_R^2 + Z_I^2}$ ) was shown in different times (T1-T8). In this section, the results were demonstrated and discussed in three different forms – impedance spectroscopy, time-averaged impedance spectroscopy and integration methods as described in chapter 2.

### *3.3.1. Impedance Spectroscopy*

This subsection includes the direct measurement of impedance spectroscopy at different times and different concentrations of SPIONs. Table 7 partially shows the magnitude of impedances at T1-T8 in various frequencies ranging from 0.1 Hz to 100,000 Hz.

**Table 7|** A sample of impedance measurement in eight different times, with the frequency range of 0.1-100KHz at C1.

| Frequency | T1 | T2 | T3 | T4 | T5 | T6 | T7 | T8 |
|---|---|---|---|---|---|---|---|---|
| 0.1 | 1591311 | 1788090 | 1845433 | 1905271 | 1936466 | 2551464 | 2646480 | 2483508 |
| 0.12589 | 1392229 | 1613690 | 1654271 | 1705281 | 1740582 | 2358748 | 2393614 | 2261709 |
| 0.15849 | 1229815 | 1444350 | 1489574 | 1552677 | 1580039 | 2194239 | 2242218 | 2077649 |
| 0.19953 | 1100665 | 1306554 | 1349952 | 1402120 | 1420733 | 2052875 | 2064253 | 1917803 |
| 0.25119 | 986997.7 | 1195129 | 1236538 | 1279733 | 1300714 | 1897634 | 1919006 | 1770034 |
| 0.31623 | 895652.1 | 1091249 | 1135028 | 1172615 | 1195926 | 1761568 | 1799637 | 1629005 |
| 0.39811 | 822172.1 | 1018880 | 1057300 | 1087263 | 1113011 | 1680547 | 1677912 | 1525727 |
| 0.50119 | 751371.5 | 952111 | 990455.9 | 1019149 | 1046336 | 1594401 | 1576466 | 1419292 |
| 0.63096 | 712562.2 | 900056 | 938485.5 | 977048.7 | 990141.5 | 1478979 | 1491643 | 1323400 |
| 0.79433 | 664134.2 | 856963.1 | 892184.2 | 915849.7 | 946656.1 | 1457470 | 1394427 | 1232235 |
| 1 | 627103.2 | 818777.4 | 853829.3 | 883702.3 | 904551.5 | 1357505 | 1305211 | 1147258 |
| … | … | … | … | … | … | … | … | … |
| 25119 | 2644.421 | 2698.195 | 2725.695 | 2741.836 | 2736.834 | 3013.611 | 3282.717 | 3493.791 |
| 31623 | 2424.111 | 2486.919 | 2519.135 | 2537.534 | 2534.271 | 2838.178 | 3113.052 | 3330.472 |
| 39811 | 2247.619 | 2316.085 | 2352.01 | 2371.349 | 2370.603 | 2688.499 | 2965.835 | 3184.751 |
| 50119 | 2103.743 | 2173.723 | 2209.435 | 2232.546 | 2232.609 | 2555.514 | 2826.027 | 3048.819 |
| 63096 | 1984.099 | 2052.586 | 2089.326 | 2112.155 | 2113.513 | 2429.64 | 2689.563 | 2913.769 |
| 79433 | 1881.111 | 1947.183 | 1981.887 | 2004.221 | 2006.622 | 2307.667 | 2551.561 | 2773.715 |
| 100000 | 1789.252 | 1848.986 | 1882.076 | 1903.488 | 1906.164 | 2183.312 | 2401.9 | 2619.237 |

Figure 13a shows the impedance spectroscopy results at different times (T1-T8) using the same concentration of SPIONs (C1). Similarly, Figure 13b-13f show the impedance spectroscopy results at C2-C6, respectively.

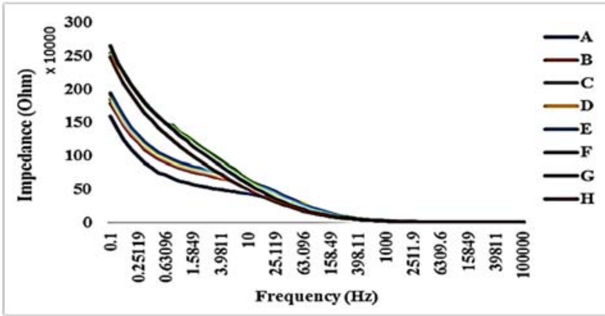


(a)

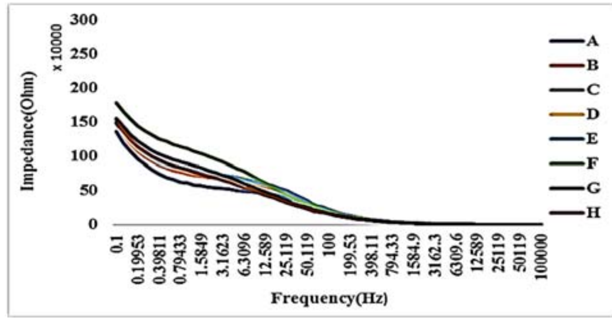


(d)

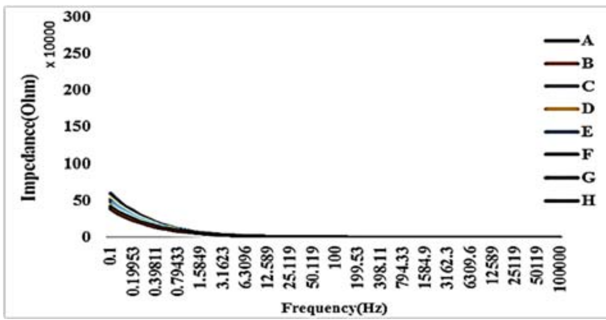


(b)

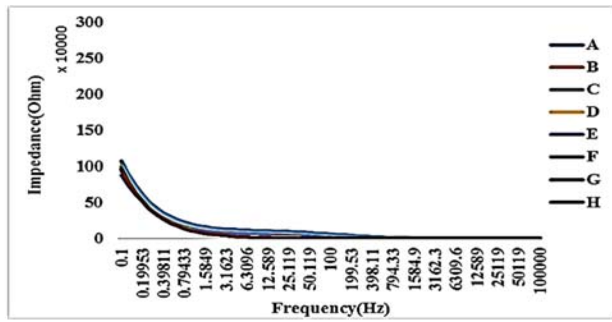


(e)

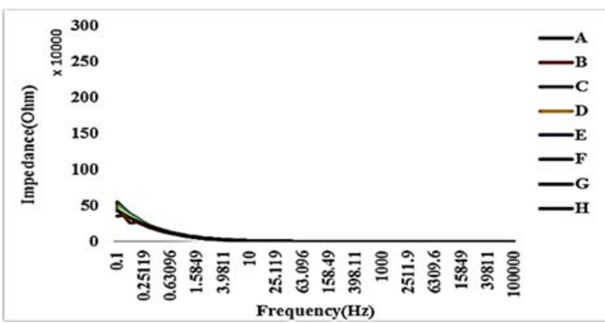


(c)

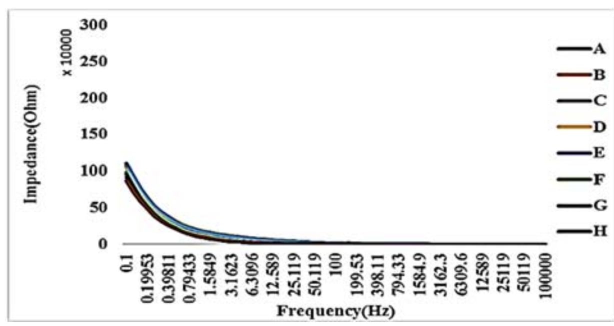


(f)

**Figure 13|** Impedance spectroscopy at different times T1=A, T2=B, T3=C, T4=D, T5=E, T6=F, T7=G and T8=H at different SPIONS concentrations (a) 0µg/mL, (b) 25µg/mL, (c) 50µg/mL, (d) 100µg/mL, (e)20 0µg/mL and (f) 300µg/mL. The curves at 0 µg/ml and 100 µg/ml manifested the lowest impedance at T1 (A), while 25 µg/ml,50 µg/ml, 200 µg/ml and 300 µg/ml showed the lowest impedance at T8 (H).

### *3.3.2. Time-Averaged Impedance Spectroscopy*

Figure 14 shows the time-average of impedance spectroscopy in each frequency where A=N2a (control, C1), B=C2 with cells, C=C3 with cells, D=C4 with cells, E=C5 with cells, F=C6 with cells, G=CCM (Control, C1, without cell), and H=C2 without cells, I=C3 without cells, J=C4 without cells, K=C5 without cells and L=C6 without cells. Each curve in the groups 1, 2 or 3 (e.g., orange color, B) display the mean value of 8 impedance curves related to the same samples, in 8 different times. Therefore, Figure 14 shows the time-average effect of various samples on the impedance. The measurements were categorized into three different groups 1-3 (from the beginning to seventy-two hours of incubation). The highest impedance was manifested by the positive control group (N2a, with cells) while the lowest impedance value was observed from the negative control group (CCM, without cells). Based on the results shown in all groups in Figure 14, the presence of cells with or without SPIONs increase the impedance. This might be due to adhesion between the cell and electrodes. In the other hand, the lower the SPIONs concentration, the lower the impedance was expected in the sensing electrodes without the cells. This might be due to the fact that the lower the SPIONs concentration, the lower dielectric property can be expected. Another interesting outcome in the curves shown in Figure 14a was that the maximum impedance change was about 0.48-0.75 MΩ for SPIONs with concentrations ranging from 0 to 300 µg/mL. Therefore, the resolution of this measurement was about 0.9 kΩ impedance change due to 1 µg/mL SPIONs change. The resolution for Figures 14b-14c was calculated in a similar manner. The mean value of resolutions calculated in all three groups was about 520 Ω.mL/µg. The highest impedance was manifested among the lowest concentrations of SPIONs, C B and A mixed and cultured with cells. Meanwhile, the lowest impedance values were observed in the negative control, CCM (G) and CCM-SPIONs mixtures without cells (H-L).

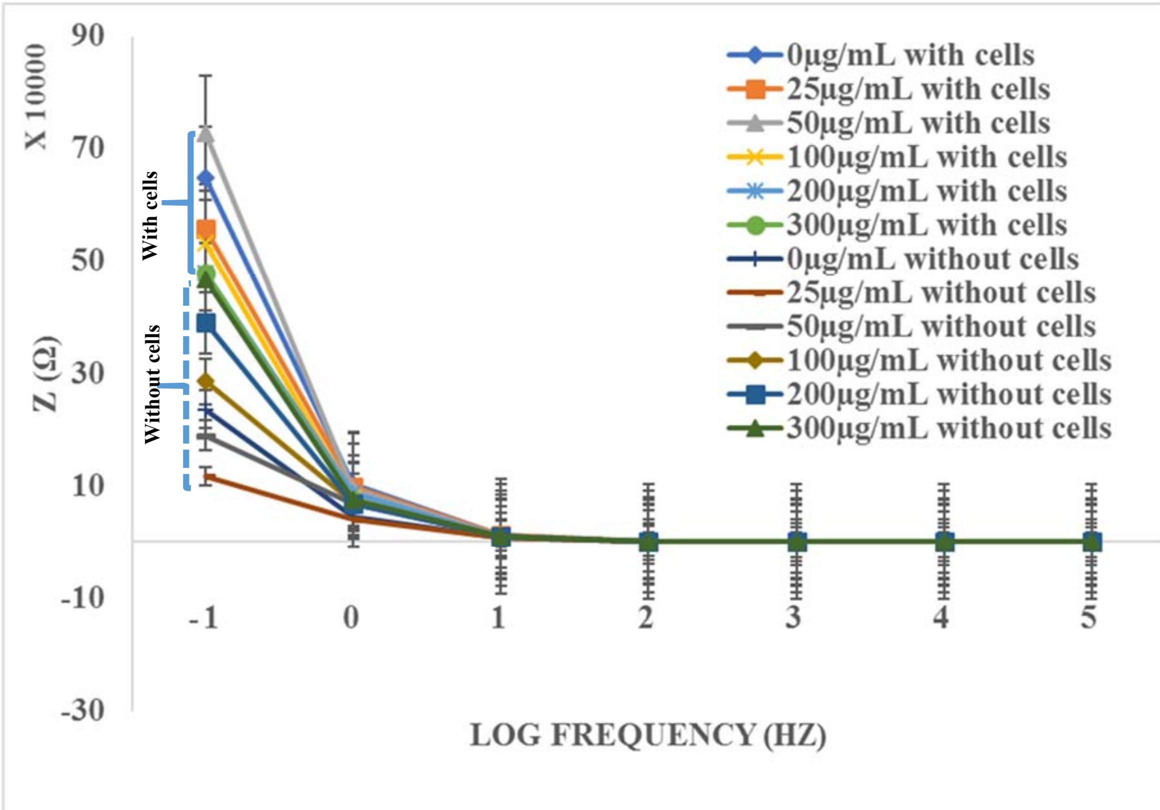

90
70
50
30
10
-10
-30
X 10000
Z (Ω)
With cells
Without cells
-1
0
1
2
3
4
5
LOG FREQUENCY (HZ)
0µg/mL with cells
25µg/mL with cells
50µg/mL with cells
100µg/mL with cells
200µg/mL with cells
300µg/mL with cells
0µg/mL without cells
25µg/mL without cells
50µg/mL without cells
100µg/mL without cells
200µg/mL without cells
300µg/mL without cells


(a)

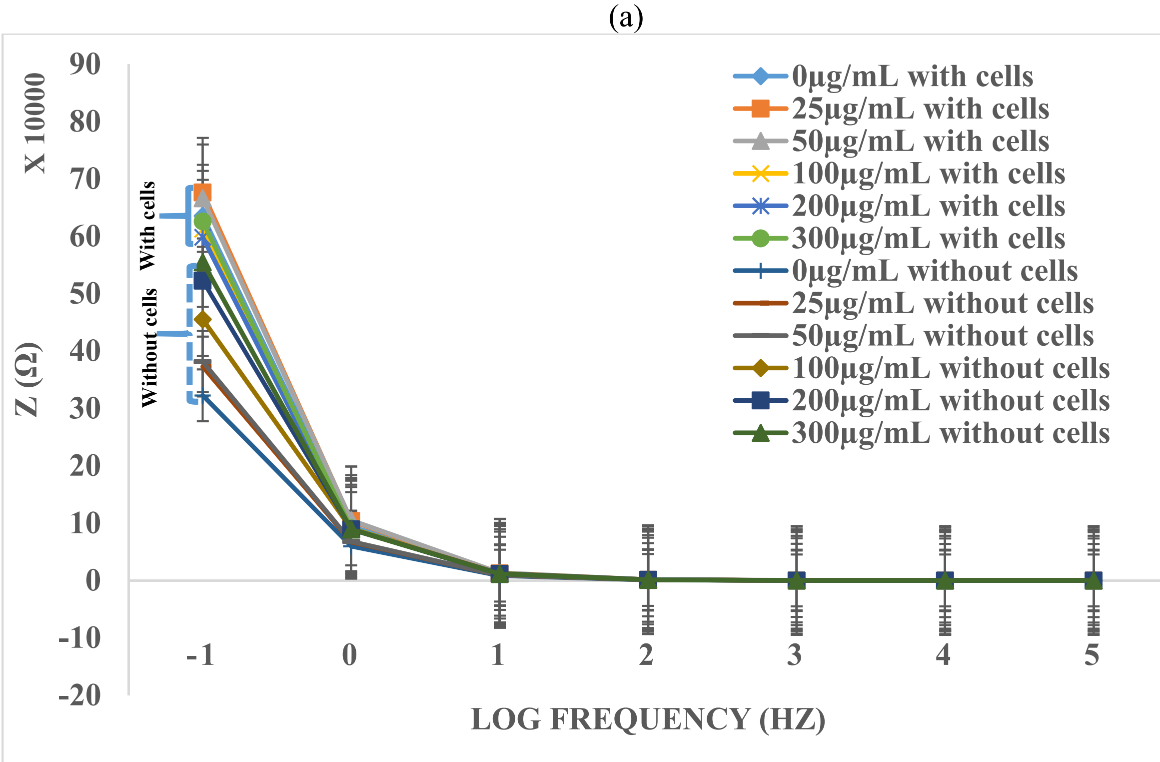

90
80
70
60
50
40
30
20
10
0
-10
-20
X 10000
Z (Ω)
With cells
Without cells
-1
0
1
2
3
4
5
LOG FREQUENCY (HZ)
0µg/mL with cells
25µg/mL with cells
50µg/mL with cells
100µg/mL with cells
200µg/mL with cells
300µg/mL with cells
0µg/mL without cells
25µg/mL without cells
50µg/mL without cells
100µg/mL without cells
200µg/mL without cells
300µg/mL without cells


(b)

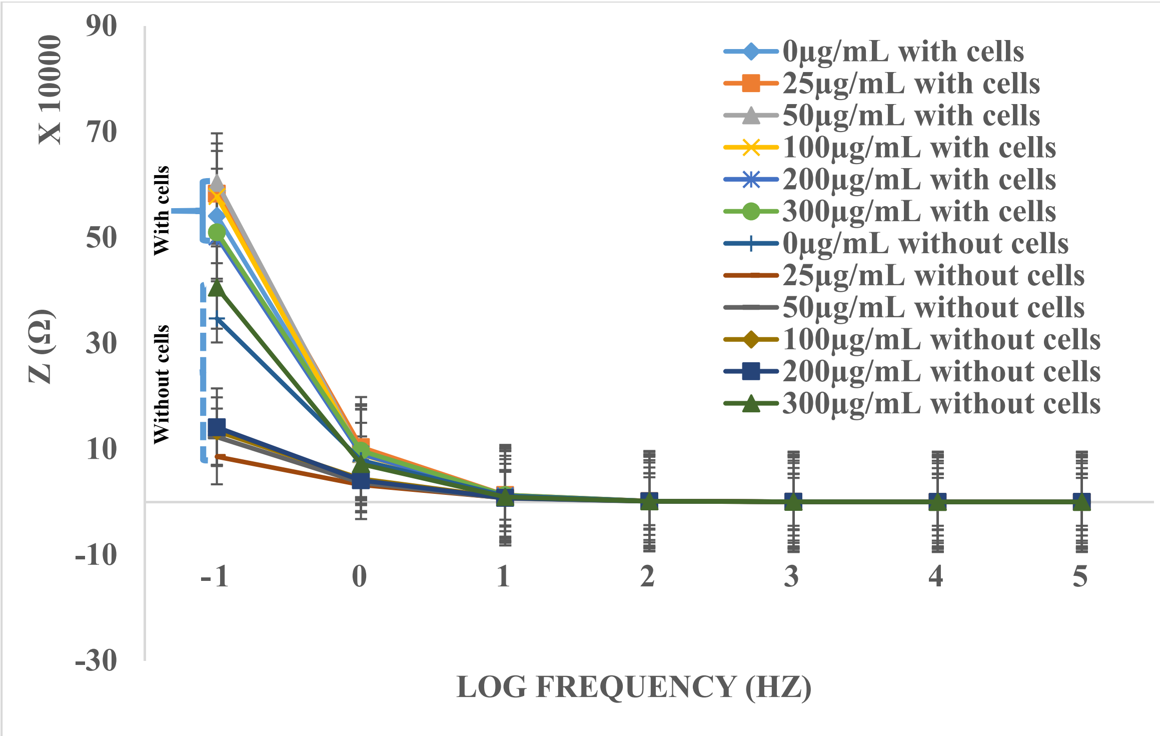


(c)

**Figure 14|**The Impedance Spectroscopy Readings of the control and different concentrations of N2a-SPIONs using a range of frequency from a log -1 to 5 (0.1 to 100000Hz). A $2.5x10^5$ cells/mL concentration was used for the three groups((a) group 1, (b) group 2 and (c) group 3). Legend shows the different concentrations of SPIONs and the control groups (0µg/ml with cells (control), 25µg/ml with cells, 50µg/ml with cells, 100µg/ml with cells, 200µg/ml cells, 300µg/ml with cells, 0µg/ml with cells (control), 25µg/ml without cells, 50 µg/ml without cells, 100µg/ml without cells, 200µg/ml without cells and 300µg/ml without cells. Error bars represent the standard error of the mean of impedance from T1 to T8 of each SPIONs concentrations with or without cells.

### *3.3.3. Integration Methods*

As described in chapter 2, the variation of surface area (ΔS) under the impedance spectroscopy curves was used as a factor to study the attributes of cultured cells in the presence and absence of SPIONs. Figure 15a shows the calculated ΔS from the impedance spectroscopy results at six different SPIONs concentrations (C1-C6) at three different repeats (G1-G3), where the equation $Z_{MAX}$-$Z_{MIN}$ was used. Similarly, Figures 15b and 15c show the calculated ΔS using the equations ZMAX-$Z_{MIN}$(f) /AVG(f) and STD ($Z_0(f_1)$ … $Z_{72}(f_N)$), respectively.

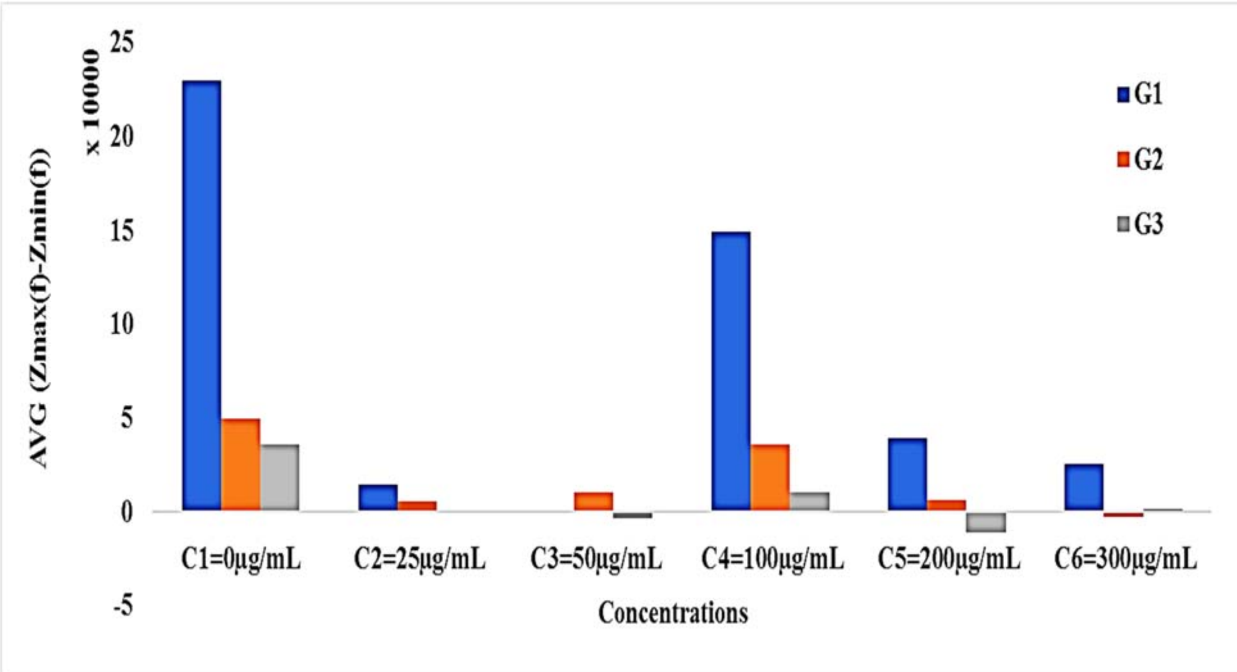

25
20
15
10
5
0
-5
AVG (Zmax(f)-Zmin(f))
x 10000
G1
G2
G3
C1=0µg/mL
C2=25µg/mL
C3=50µg/mL
C4=100µg/mL
C5=200µg/mL
C6=300µg/mL
Concentrations


(a)

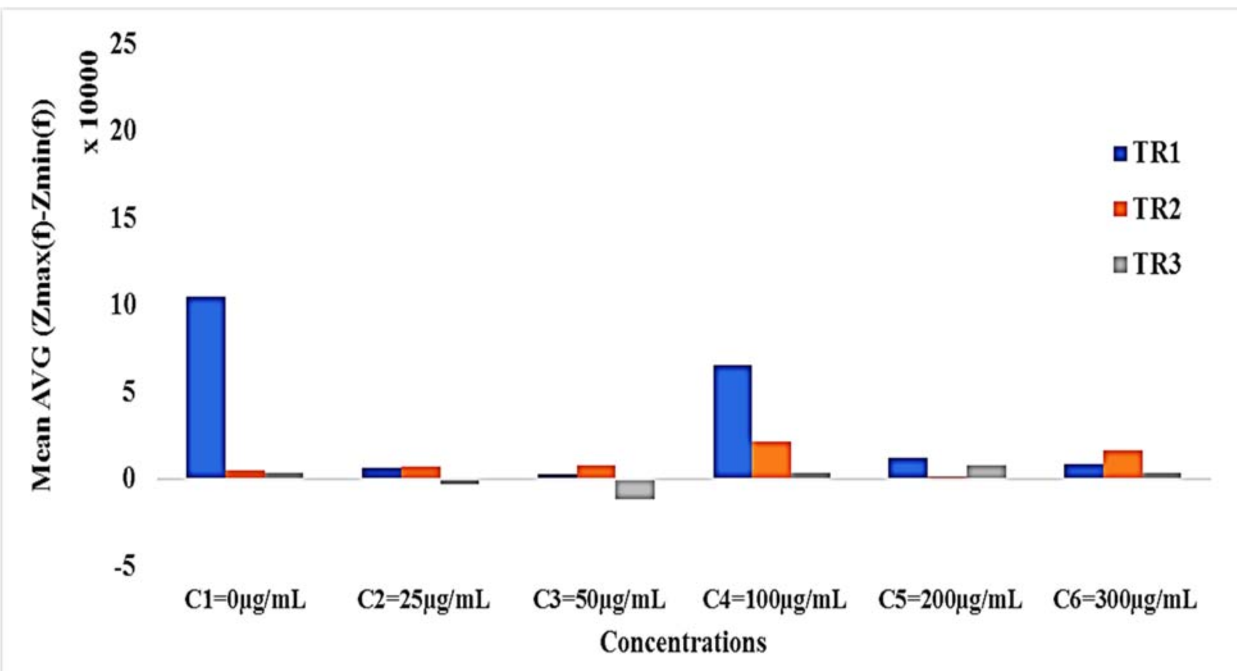

25
20
15
10
5
0
-5
Mean AVG (Zmax(f)-Zmin(f))
x 10000
TR1
TR2
TR3
C1=0µg/mL
C2=25µg/mL
C3=50µg/mL
C4=100µg/mL
C5=200µg/mL
C6=300µg/mL
Concentrations


(b)

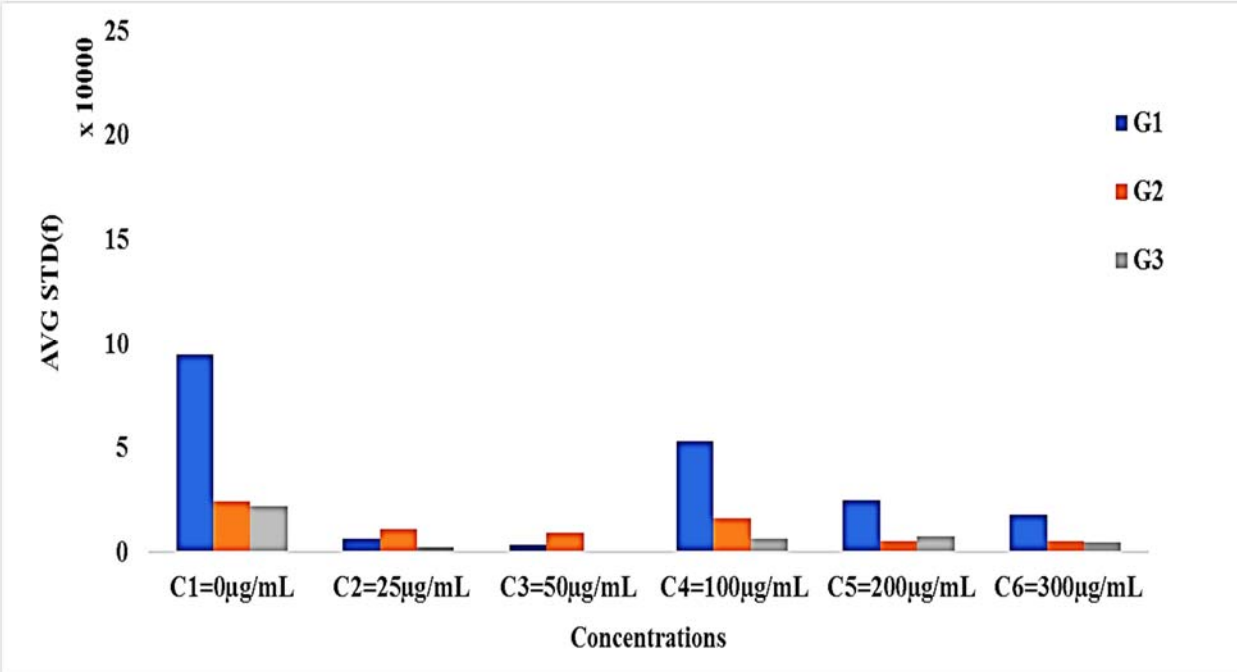


(c)

**Figure 15|** Integrated Impedance Spectroscopy results using equations (a), (b) and (c) at different concentration of SPIONs (C1-C6) and three different groups (G1-G3). A significant increase of ΔS in C1 and C4 was observed.

Based on the results shown in Figure 15, the higher the concentration of SPIONs, the lower ΔS was observed. Figures 15a-15c shows a significant increase of ΔS at C4. While increasing the SPIONs concentration (C5, C6), ΔS was decreased. Interestingly, the same spike at C4 was observed in Trials 2 and 3 as shown in Appendix E. It is noteworthy, despite the fact that in Figures 15a-15c, three different equations were used, the spike at C4 can still be observed. One may argue that the shape and dimensions of electrodes, the material, size and concentration of nanoparticles can be considered as the main factors in the electrical models that have resulted in the creation of a spike at C4. Indeed, there may be many other factors, such as culture medium and viable cells that could affect the results shown in Figures 15a-15c. A general justification can be provided using Figures 10j, 10k and 10l. As seen in Figure 10j, the presence of SPIONs with a high concentration (C4) has significantly resulted in decreasing the cell confluence. Instead of cells, the surface of the electrodes was coated with SPIONs. Therefore, it is expected the charged SPIONs are bonded with the surface of electrodes and significantly increase the double layer capacitance and consequently increase the impedance in low frequencies. This change of impedance can justify the spike at C4. In the other hand, assuming that the SPIONs fully covers the surface of electrodes at C4, the increase of SPIONs concentration may result in creating larger aggregates and affecting the cell attachment or cell growth as seen in Figures 10k and 10l.

### *3.3.4. Equivalent Electrical Circuit's Method*

Figure 16 shows the variation of capacitance, the series, and parallel resistances as a function of SPIONs concentration at T1, T2, T3, T4, T5, T6, T7, and T8 (also see chapter 2). As seen in these Figures, the capacitance (C), series resistance (R1), and parallel resistance (R2) are in the range of 0.5-2.5 μF, 65-110Ω, and 25-225KΩ, respectively. Based on these results, the variation of SPIONs concentration or time do not significantly affect R1 and C. This is because R1 is proportional to the resistance of bulky medium that is highly conductive and the variation of SPIONs concentrations do not significantly change this conductivity. In the other hand, C is proportional to the double layer capacitance (DLC). DLC was affected by the attachment of cells or the distribution of SPIONs on the surface of electrodes. DLC was almost constant because of the higher attachment of cells, the lower surface area coated by SPIONs and vice versa. R2 in parallel with C changes over timeT1-T8. Similarly, R2 changes over the concentration of SPIONs (C1-C6). This might be due to the attachment or the deposition of molecules in the culture medium above the electrodes.

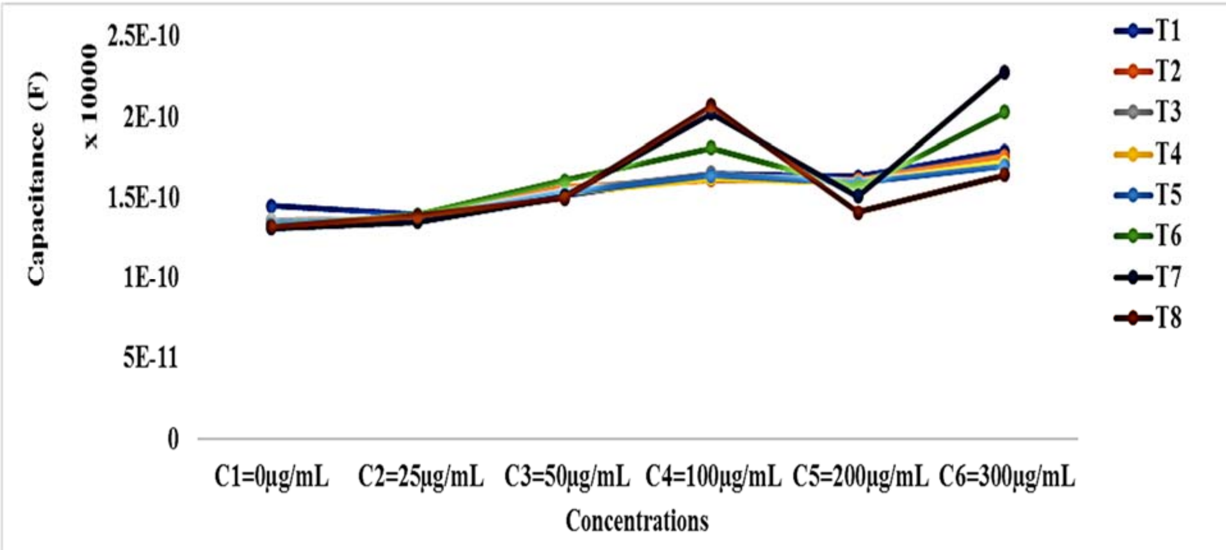
2.5E-10
2E-10
1.5E-10
1E-10
5E-11
0
Capacitance (F) x 10000
C1=0µg/mL
C2=25µg/mL
C3=50µg/mL
C4=100µg/mL
C5=200µg/mL
C6=300µg/mL
Concentrations
T1
T2
T3
T4
T5
T6
T7
T8

(a)

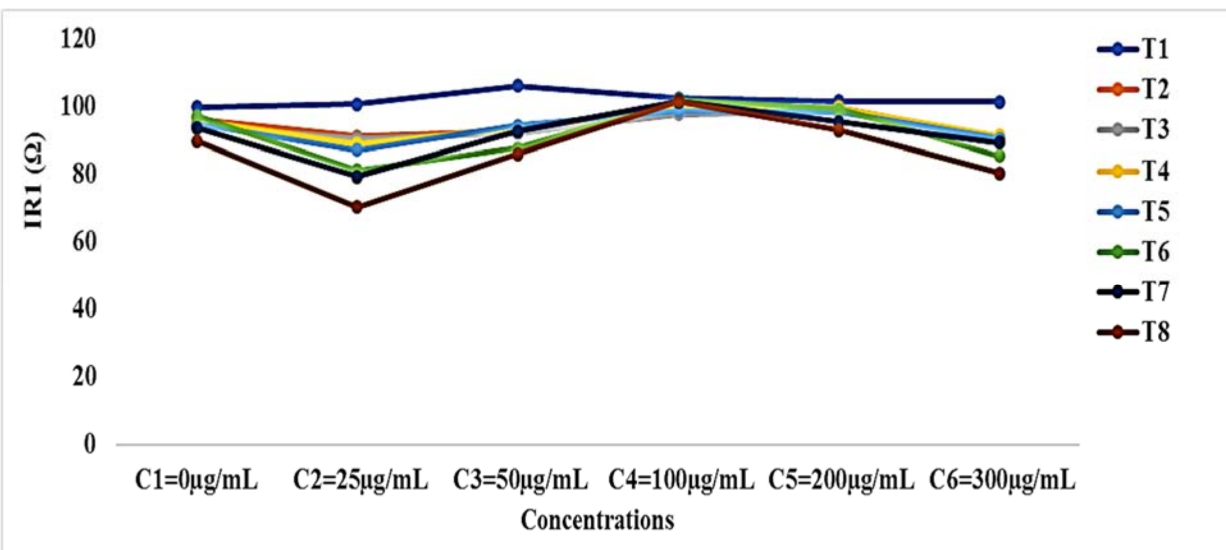
120
100
80
60
40
20
0
IR1 (Ω)
C1=0µg/mL
C2=25µg/mL
C3=50µg/mL
C4=100µg/mL
C5=200µg/mL
C6=300µg/mL
Concentrations
T1
T2
T3
T4
T5
T6
T7
T8

(b)

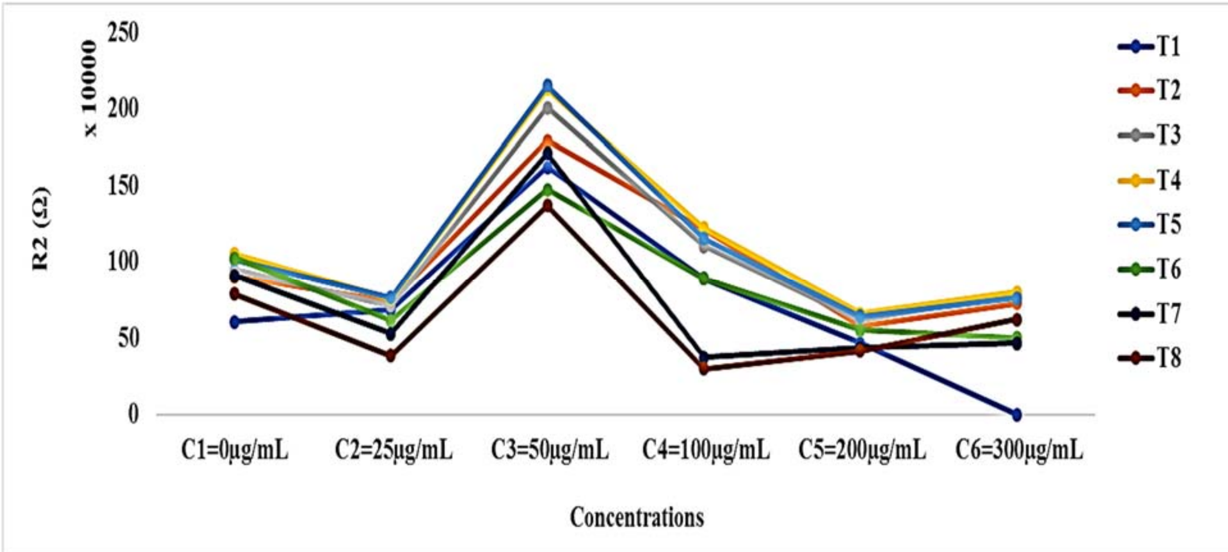


(c)

**Figure 16**| Equivalent electrical circuit including (a) capacitance, (b) series resistance and (c) parallel resistance/impedance. Variation of SPIONs concentrations and time do not significantly affect R1, and C. R2 changes over time and with different SPIONs concentrations.

## 3.4. Summary

In this chapter, we demonstrated and discussed the viability test results using TBDE and Scepter cell counter. Also, the results of microscopy and impedance spectroscopy used to study the toxicity of SPIONs were elaborated.

- Based on the viability test results, there were higher chances for the N2a cells to be susceptible to higher concentrations of SPIONs, and consequently, this results in less viability at C4, C5 and C6.
- Microscopic images showed that attachment and confluence of cells were significantly affected by the presence of SPIONs in the mixture. As per results are shown in this chapter, the exposure of cells to different concentrations of SPIONs affect the proliferation of cells, so that the maximum proliferation was observed when the concentration of SPIONs was

minimum (C1). The number of N2A cells normally increases over time; however, the presence of SPIONs around the cells appeared to restrict the multiplication of cells

- Based on the impedance spectroscopy results, the variation of impedance was influenced by the concentration of both cells and SPIONs. However, the relationship between the changes of impedance or the related electrical components such as R1, R2, and C depends on various parameters such as the specification of electrodes in addition to other biological factors. The impedance spectroscopy offers great advantages as a label-free and low-cost method for the assessment of the effects of SPIONs on cells.

# Chapter 4

# Conclusion

This chapter provides a summary of the thesis and contributions. Also, it describes the future direction of this research after a brief financial and time analysis.

### 4.1.Summary and conclusion

This investigation reported the effects of SPIONs on the cell viability of N2a cells using impedance spectroscopy, microscopy, and viability test assay. These methods were performed in part in multi-well settings, providing proof that this approach is scalable, with potential for high throughput and high content analysis. Based on the results shown in this thesis, a correlation between the impedance of sensing electrodes exposed to the cells treated with different SPIONs was demonstrated. The concentration of SPIONs is a critical factor for cell viability with increasing concentration correlated to increased toxicity. Based on our TBDE results, the viability was reduced to 47% and 40% in 200 and 300 μg/mL SPION concentrations respectively. The microscopic imaging technology used revealed that at higher SPIONs concentration cell density was compromised. Arguably, high-precision toxicity tests require a collection of large numbers of data points from multiple experiments. A high throughput impedance-based cell monitoring platform as reported in this study can be the efficient alternative to more traditional approaches, allowing to perform a large number of experiments simultaneously with lower sample consumption and in a time effective manner. We had demonstrated that high throughput impedance-based label-free platform offers great advantages to study SPIONs in a cell-based context, opening a window of opportunity to design and test the next generation of SPIONs with reduced toxicity for biomedical or medical applications.

### 4.2 Contribution

This study served as a stepping stone towards developing a high throughput system for a wide range of application. This further provides a comprehensive first-hand assessment on the interaction of N2a cells and SPIONs in a label-free non-invasive method which may open a new venue for more efficient cytotoxic screening.

This study also displayed a high volume of images captured exhibiting cell behavior from the time of adding the SPIONs to 72 hours' incubation. Although further analysis of these images needs to be done in the future, this draws us closer in understanding how SPIONs affects the cell to cell interaction and reducing their ability to spread as they start to agglomerate at higher concentrations.

Moreover, with a large number of impedance-based data generated, this study preeminent previous studies on the electrical activities of cells and SPIONs-cell interaction.

This is the first to perform a parallel assessment using trypan blue dye exclusion, scepter handheld cell counter, and impedance-based to count the number of cells. Assessing the viability of cells in three different methods is one of the major strengths of this study. Based on the results obtained from this thesis, we have published/presented the following papers or posters, respectively.

- S Abad Tan *et al.*, Towards Label-Free Platform for Monitoring Interaction Between Cells and Superparamagnetic Iron Oxide Nanoparticles, IEEE LSC, Montreal, October 2018.
- S Abad Tan *et al.* "High-throughput Cell Screening for Spions Studies using Impedance Spectroscopy" Biophysical Journal (Abstract, BPS2018), Vol. 114, Issue 3, p671a, 2018.
- S. Abad Tan. *et al*. A Simulation of in vivo electrophysiological study using a microfluidic device. Poster. Ontario-on-a-Chip May 2017.
- S. Abad Tan. *et al.* Towards High Throughput *In-Vitro* Cytotoxicity Analysis of Super-Paramagnetic Nanoparticles, Bioengineering Journal, Invited, will be submitted.

## 4.3 Future works

A laborious method in carrying out the experiments of this study had been a tough endeavour. The execution of the experimental techniques for a full assessment is accompanied by the challenge in terms of the financial aspect and the time frame. Thus, automation of high throughput screening should be the main focus of any further studies Although several control groups were included in the study, the use of non-live cells as a control group can be considered for future screening.

### *4.3.1 Economic Estimates*

This subsection provides an estimated cost of the materials and chemicals used in the study. Table 8 shows the details of consumable materials and chemicals, including the estimated price for each item. Based on this table, the estimated cost for performing 1728 experiments is about $2300. In a clinically relevant cytotoxicity study, by assuming C=24 different concentrations of SPIONs with more than G=12 times replicates and CC=5 different cell concentrations, the number of experiments will approximately be equal to $184,000. The amount would prove a financial challenge in performing experiments to obtain sufficient data to validate results and conclusions about toxicity studies. The high throughput platform containing a large number of micro-scale chambers enables parallel analysis that significantly decreases cost and the required time, as described in the *next subsection.*

### 4.3.2. *Time Assessment*

The experimental portion of this study involves different trials and replications that are time-consuming.

**Table 8|** The estimated cost of chemicals and materials to perform an assay

| ITEM | Quantity | Price per mL, pc, g, pack) | Total Amount **C$** |
|---|---|---|---|
| Phosphate buffered saline | 270 mL | 0.59 | 159.3 |
| Trypsin-EDTA solution | 54 mL | 0.12 | 6.48 |
| Dulbecco's Modified Eagle Medium (DMEM) | 2700 mL | 0.058 | 156.6 |
| Fetal Bovine Serum | 270 mL | 1.812 | 489.24 |
| Antibiotics - penicillin/streptomycin | 13.5 mL | 0.301 | 4.0635 |
| Superparamagnetic Nanoparticles (SPIONs) | 0.279 g | 703.8 | 196.36 |
| Serological pipettes (5 mL) | 54 pcs | 0.892 | 48.168 |
| Serological pipettes (25 mL) | 54 pcs | 1.836 | 99.144 |
| Culture dishes | 36 pcs | 0.82 | 29.52 |
| Culture Plates | 36 pcs | 4.02 | 144.72 |
| Conical centrifuge tubes | 324 pcs | 0.816 | 264.384 |
| Petri dish | 18 pcs | 2.35 | 42.3 |
| Plastic consumables ( Universal Fit pipette tips and micro tubes) | | | |
| Universal Fit pipette tips ( 100-1000 µL) | 216 pcs | 0.0934 | 20.1744 |
| Universal Fit pipette tips ( 1-200 µL) | 216 pcs | 0.0973 | 21.0168 |
| Pipette tips ( 0.1 - 10µL) | 216 pcs | 0.0495 | 10.692 |
| micro tubes | 486 pcs | 0.202 | 98.172 |
| Cell counter sensors | 42 pcs | 228 | 228 |
| | | | |
| Electrode Array ( type 1) | 2 pcs | 39.95 | 39.95 |
| Electrode Array ( type 2) | 6 pcs | 269.6 | 269.6 |
| **TOTAL** | | | **C$2327.7** |

In this thesis, in addition to biological and microscopic methods, a label-free impedance spectroscopy method was used as s new alternative technique for cellular analysis. The impedance readouts were recorded from eight different times (T1-T8) in each six different (C1-C6) SPIONs concentrations with and without cells. As aforementioned in chapter 3, this generates 1728 curves in almost 60 frequencies. In other words, this approximately counts up 100,000 impedance magnitude numbers. By assuming each number takes 5 seconds, the experiments can be completed after 6-days continues work. The required time for the aforementioned clinically relevant cytotoxicity study (see section 4.3.1) will be 80x6=480 days. In other words, it takes more than 16 months to complete the experiments. A high throughput platform containing at least 100 chambers in parallel for cell culture and impedance analysis, can decrease the required time to less than 480/100~5 days.

### *4.3.3. High Throughput Analysis Device for the Future*

Based on a large number of data generated to establish the interaction of SPIONs to the N2a cells, we anticipate that an automated high throughput screening system will be developed with highly sensitive electrodes to capture more complex activities of the cells. The high throughput analysis device can generate data faster. Since this study focused on the effect of SPIONs to a single type and concentration of cell, this can be further repeated using other types and concentrations of cells. Images depicting the morphology of the cells should be further examined to see potential pathological significant.

# Appendices

## Appendix A

## Bar Graphs of Viability Results in different Trials

### A.1 Bar graphs of the percentages of alive and dead cell count in the different trials

The following figures display the percent difference in the number of alive and dead cells in different concentrations of SPIONs (C1-C6). Each trial (TR1, TR2 and TR3) was replicated (a, b, c) to observed variability of data.

A.1.1 PCB TR 1

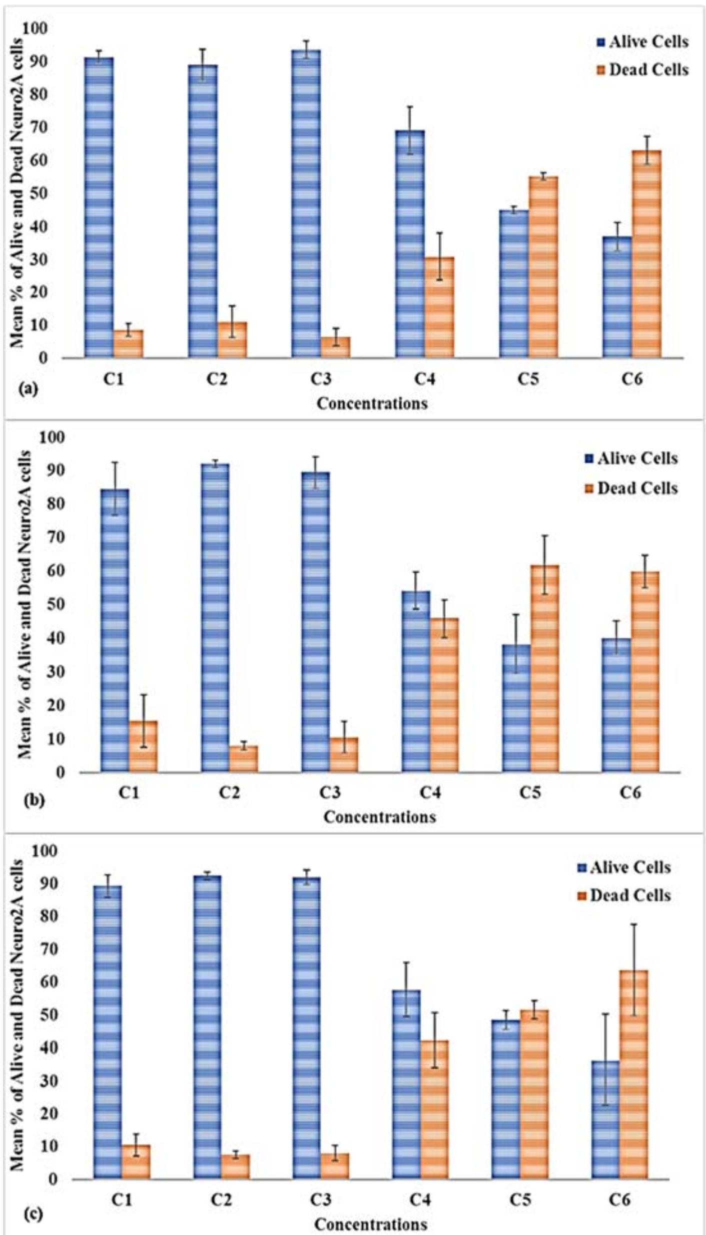

A.1.2 PCB TR 2

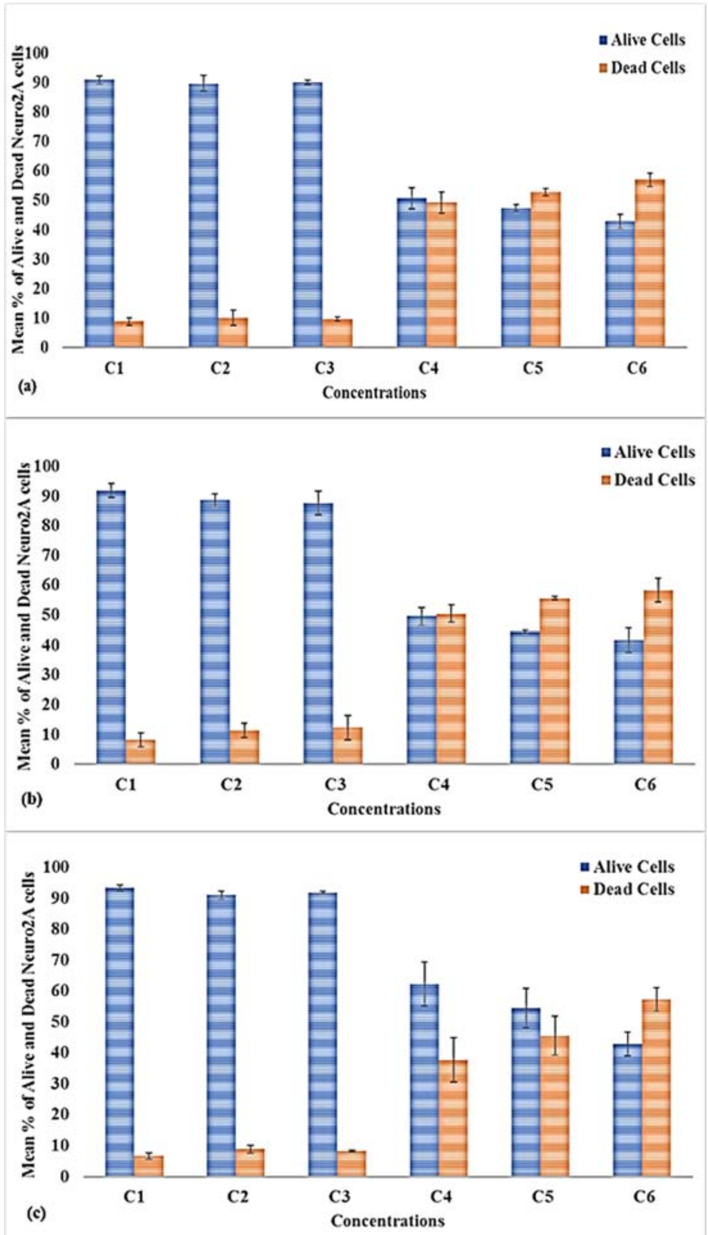
Alive Cells
Dead Cells
Mean % of Alive and Dead Neuro2A cells
100
90
80
70
60
50
40
30
20
10
0
C1
C2
C3
C4
C5
C6
(a)
Concentrations
Alive Cells
Dead Cells
Mean % of Alive and Dead Neuro2A cells
C1
C2
C3
C4
C5
C6
(b)
Concentrations
Alive Cells
Dead Cells
Mean % of Alive and Dead Neuro2A cells
C1
C2
C3
C4
C5
C6
(c)
Concentrations

‘

A.1.3 PCB TR 3

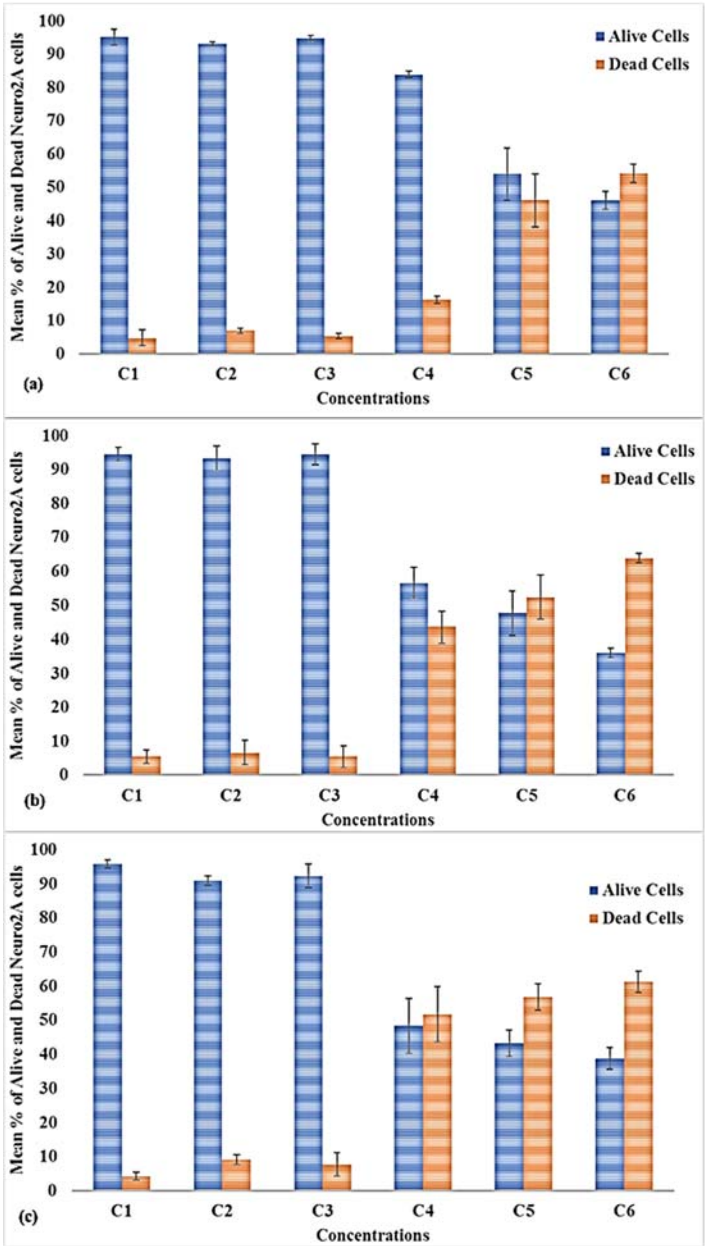

Mean % of Alive and Dead Neuro2A cells
Alive Cells
Dead Cells
C1
C2
C3
C4
C5
C6
(a)
Concentrations
(b)
Concentrations
(c)
Concentrations

A.1.4 PC TR1

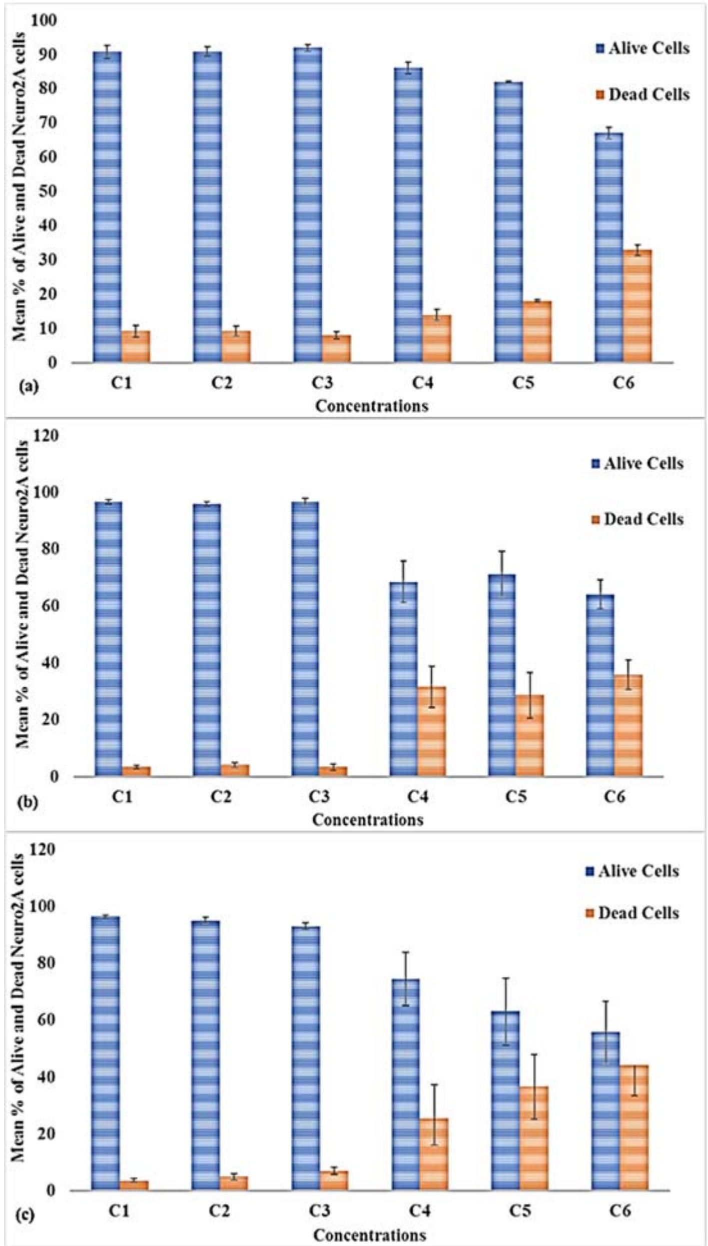

Mean % of Alive and Dead Neuro2A cells
Alive Cells
Dead Cells
(a)
C1
C2
C3
C4
C5
C6
Concentrations
Mean % of Alive and Dead Neuro2A cells
Alive Cells
Dead Cells
(b)
C1
C2
C3
C4
C5
C6
Concentrations
Mean % of Alive and Dead Neuro2A cells
Alive Cells
Dead Cells
(c)
C1
C2
C3
C4
C5
C6
Concentrations

A.1.5 PC TR2

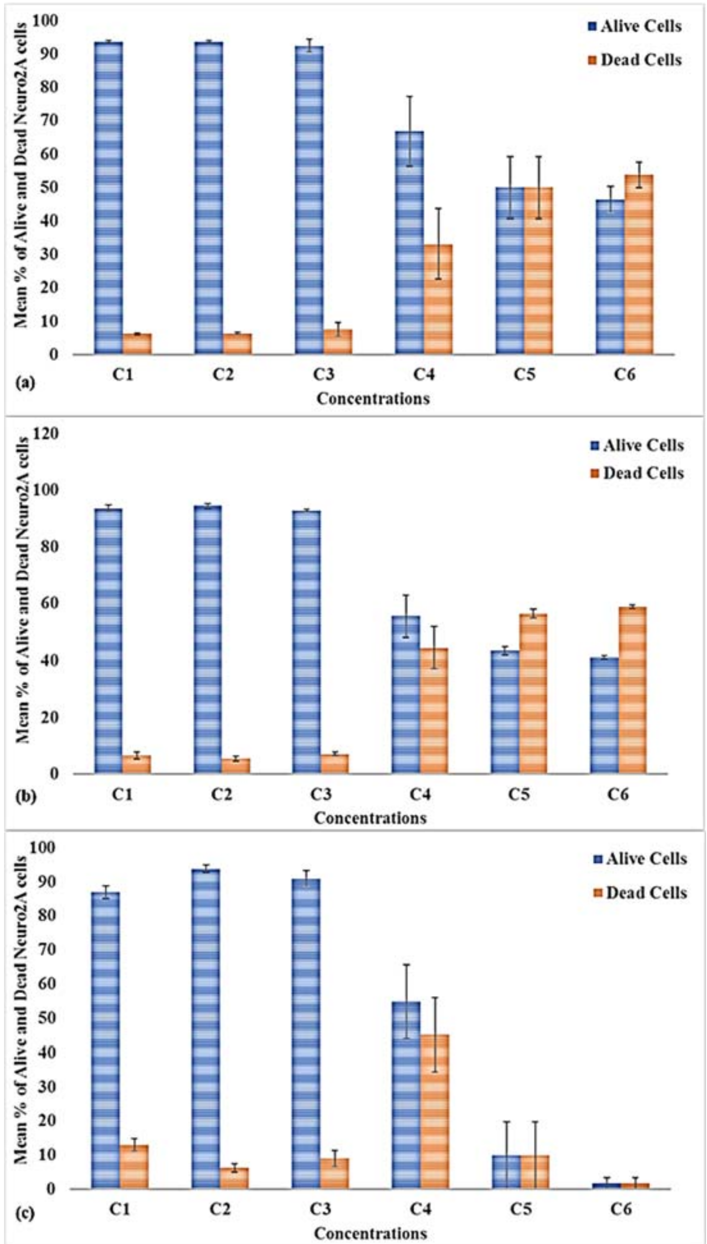

Mean % of Alive and Dead Neuro2A cells
Alive Cells
Dead Cells
(a)
C1
C2
C3
C4
C5
C6
Concentrations
Mean % of Alive and Dead Neuro2A cells
Alive Cells
Dead Cells
(b)
C1
C2
C3
C4
C5
C6
Concentrations
Mean % of Alive and Dead Neuro2A cells
Alive Cells
Dead Cells
(c)
C1
C2
C3
C4
C5
C6
Concentrations

A.1.6 PC TR3

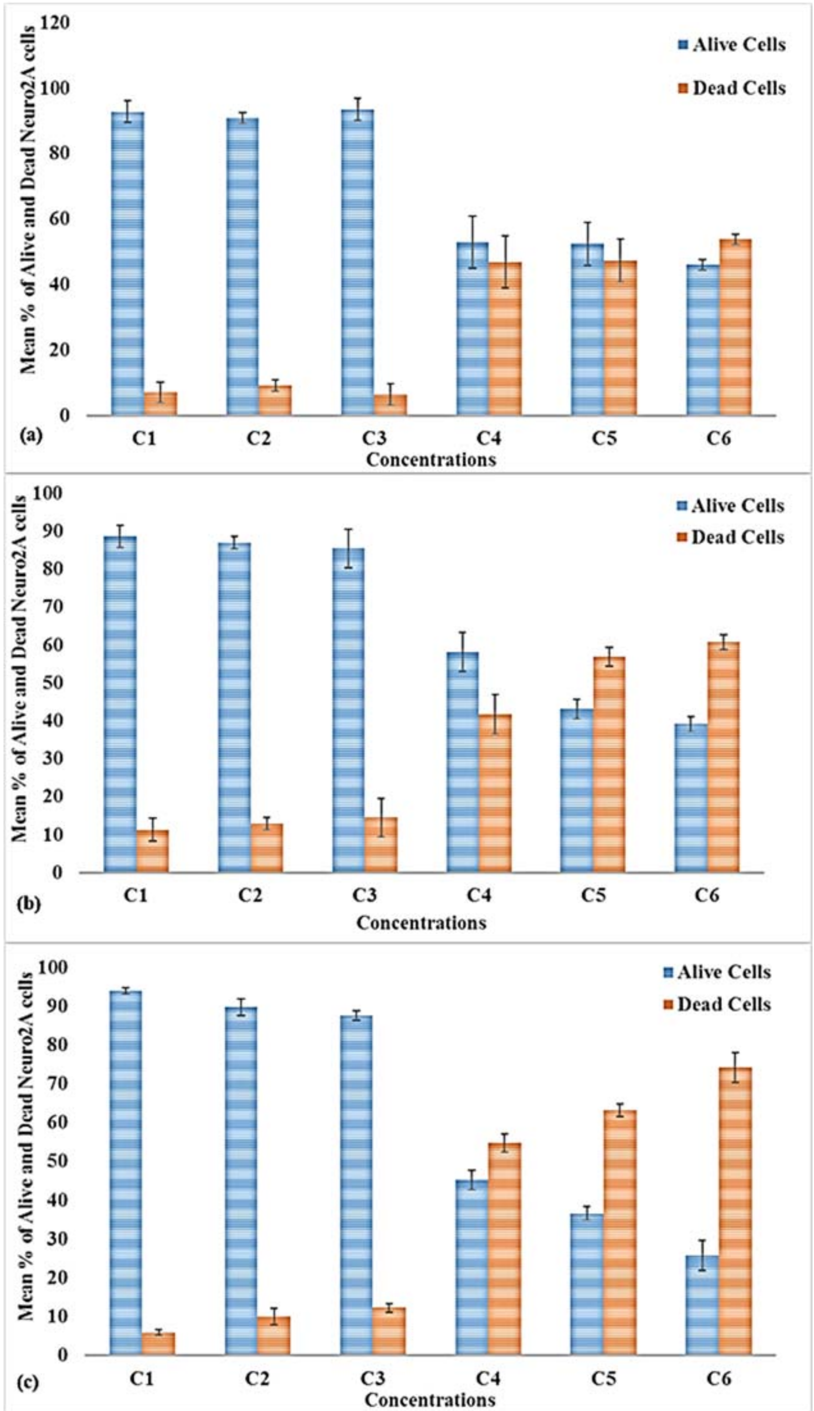

Alive Cells
Dead Cells
Mean % of Alive and Dead Neuro2A cells
(a)
C1
C2
C3
C4
C5
C6
Concentrations
(b)
(c)

### A.2 Comparative Analysis of the growth of cell concentration from C1 to C6

The table compares the cell concentrations from the initial time (T1) to 72 hours (T8) of the different SPIONs concentrations (C1-C6) in terms of the change (Δ growth), comparative differences with reference to the control (C1).

| Concentrations | T1* | T8* | Change | Difference from C1 (control) | % Difference |
|---|---|---|---|---|---|
| **N2A** | 2.50E+05 | 3.26E+05 | 7.59E+04 | | |
| **25µg/mL** | 2.50E+05 | 3.07E+05 | 5.74E+04 | 1.85E+04 | 24 |
| **50µg/mL** | 2.50E+05 | 3.14E+05 | 6.38E+04 | 1.21E+04 | 16 |
| **100µg/mL** | 2.50E+05 | 2.81E+05 | 3.10E+04 | 4.49E+04 | 59 |
| **200µg/mL** | 2.50E+05 | 2.93E+05 | 4.27E+04 | 3.32E+04 | 44 |
| **300µg/mL** | 2.50E+05 | 2.86E+05 | 3.59E+04 | 4.00E+04 | 53 |

*p=0.000812751, significant at 0.05 level of significance

# Appendix B

## Photomicrograph of N2a cells at specific Time intervals

The images depict cell activities from the time of seeding to 72 hours of exposure to SPIONs. Images were captured at the time of seeding (a), at 2hours (b), 4 hours (c), 6 hours (d), 8 hours (e), 24 hours (f), 48 hours (g), and 72 hours (h) in all the different concentrations of SPIONs used in the study. The images were grouped according to the device (I, II) that were used.

B.1 PCB substrate impedance-based device - N2a

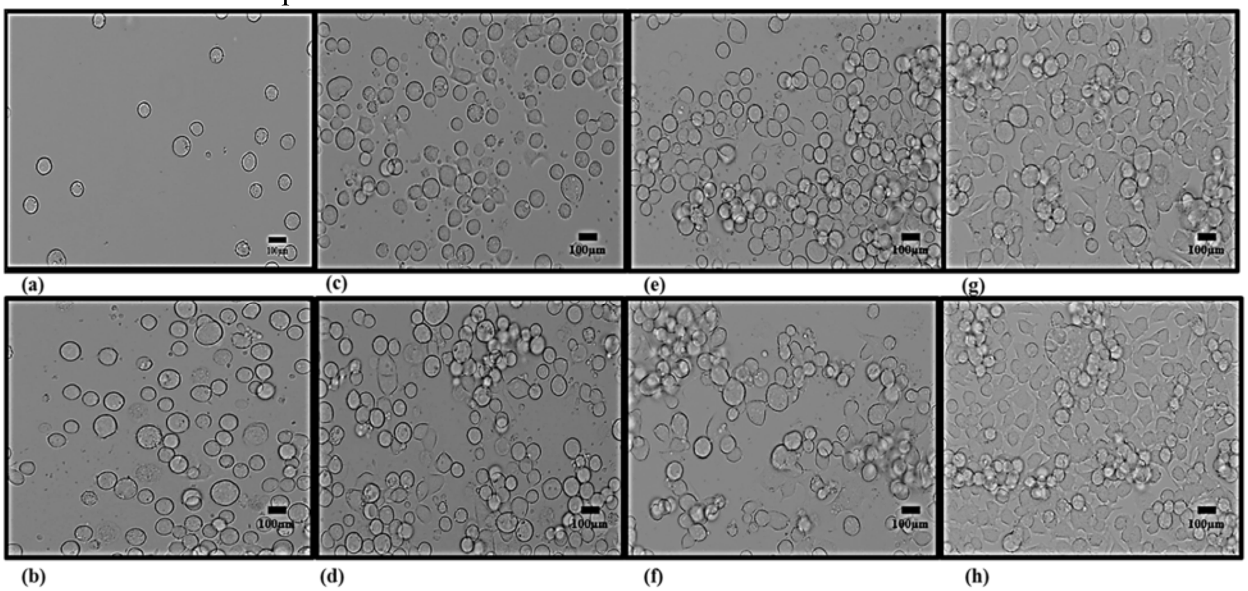


B.2 PCB substrate impedance-based device -  25µg/mL

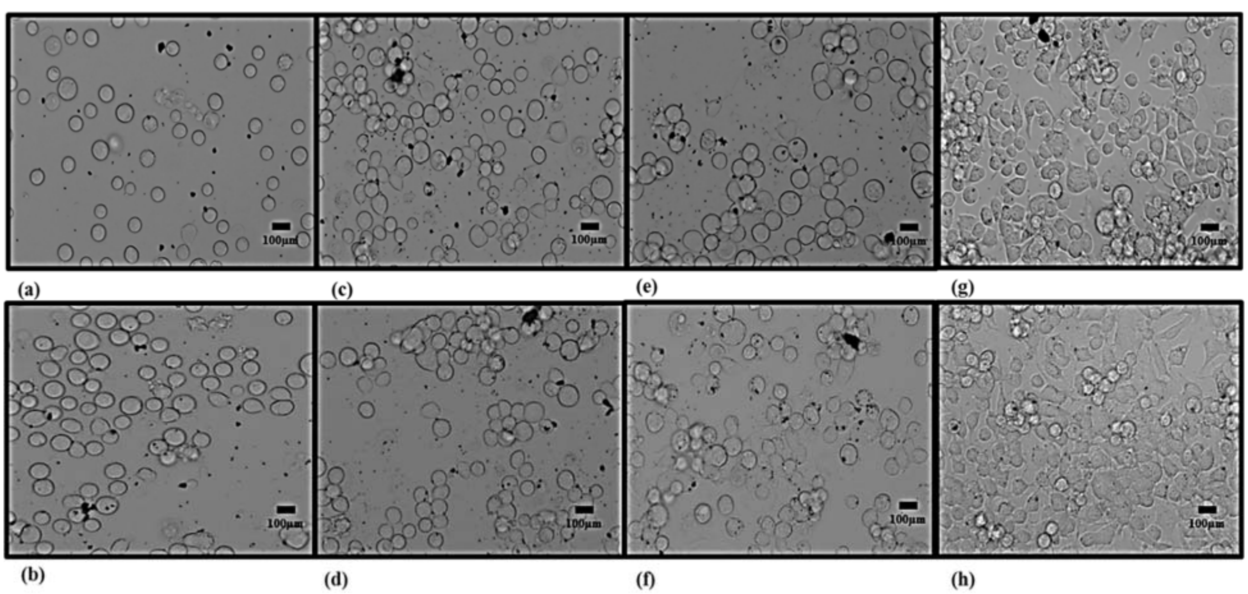

B.3 PCB substrate impedance-based device - 50µg/mL

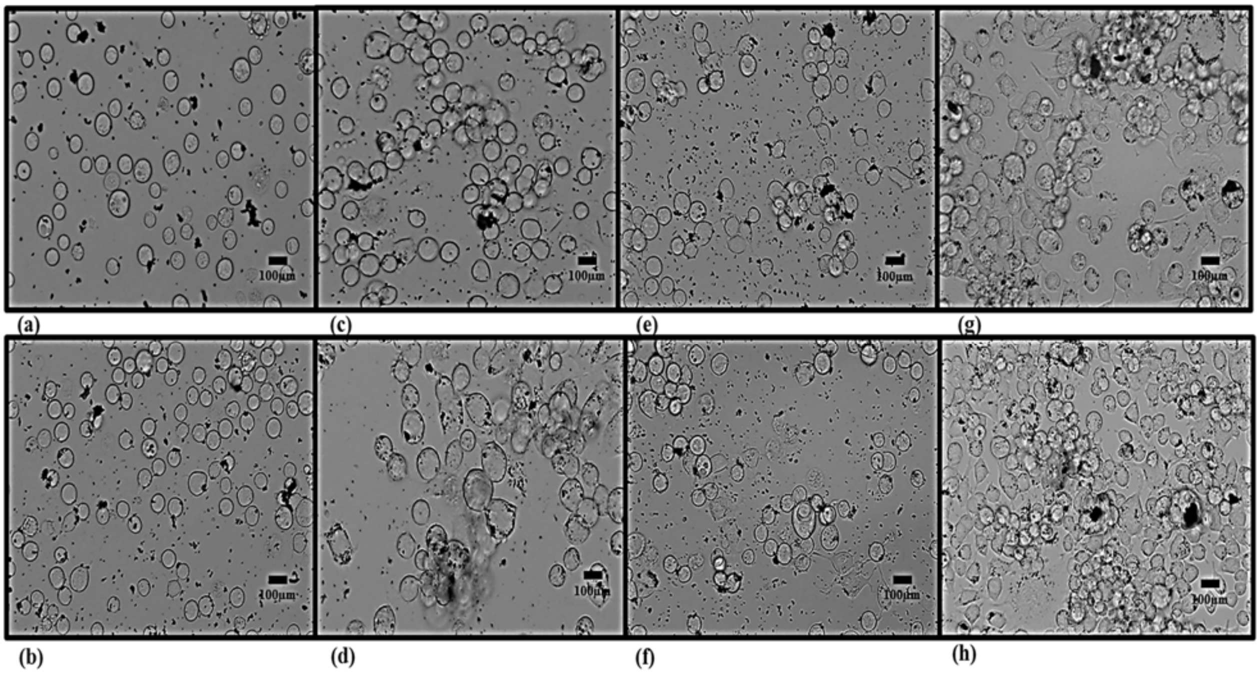


B.4 PCB substrate impedance-based device - 100µg/mL

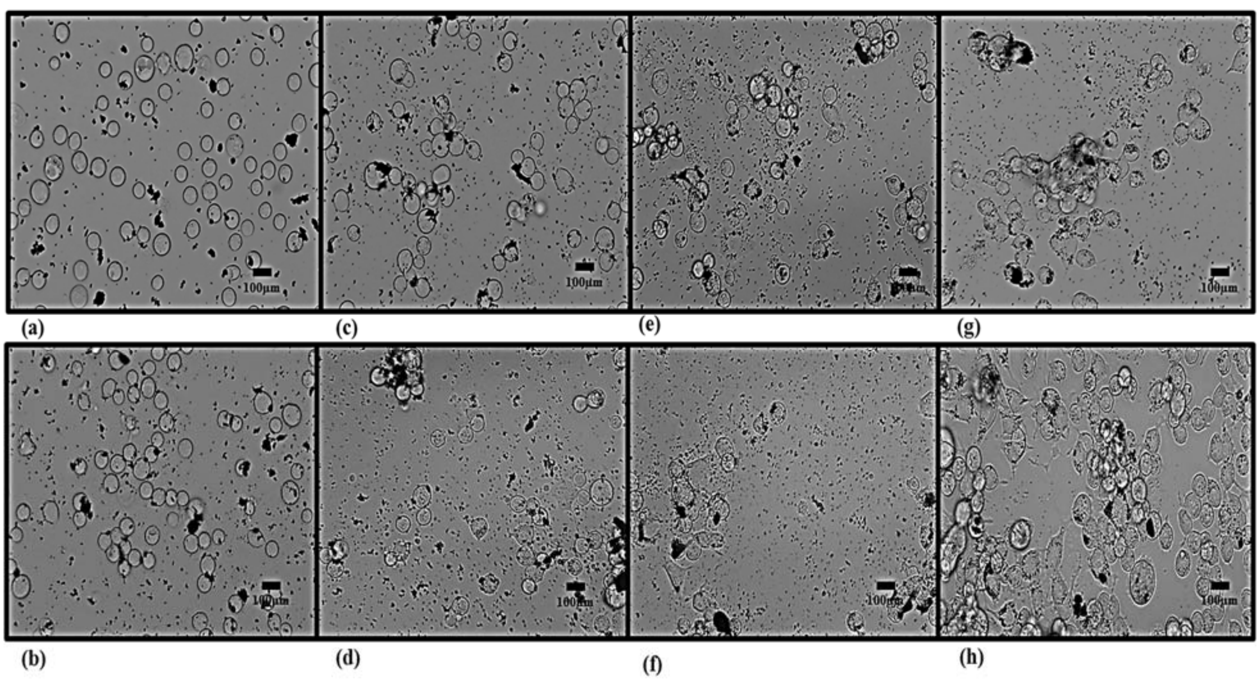

B.5 PCB substrate impedance-based device - 200µg/mL

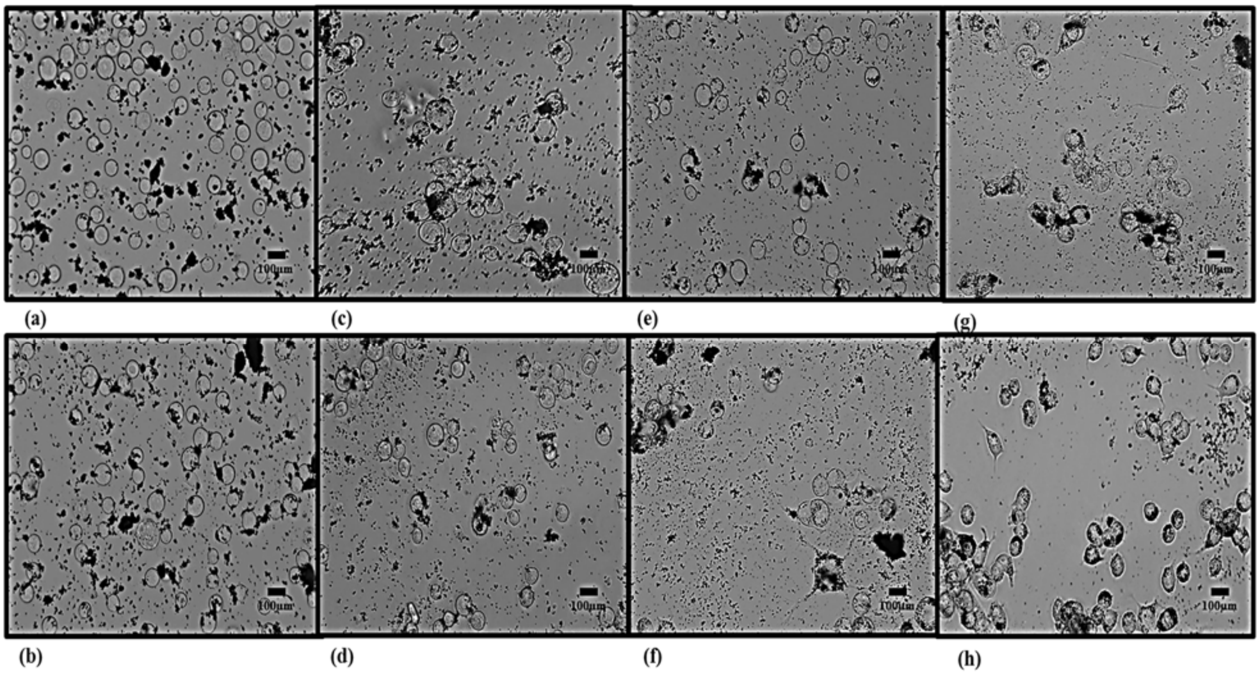


B.6 PCB substrate impedance-based device - 300µg/mL

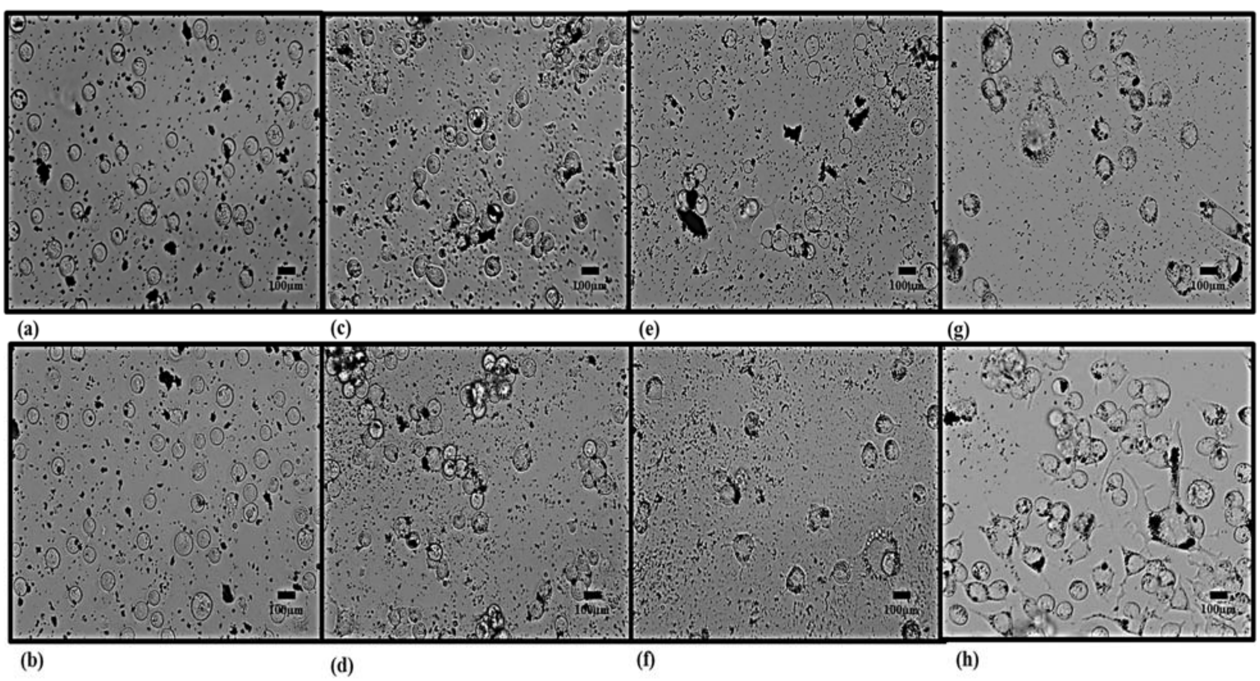

B.7 PC substrate Impedance-based device - N2a

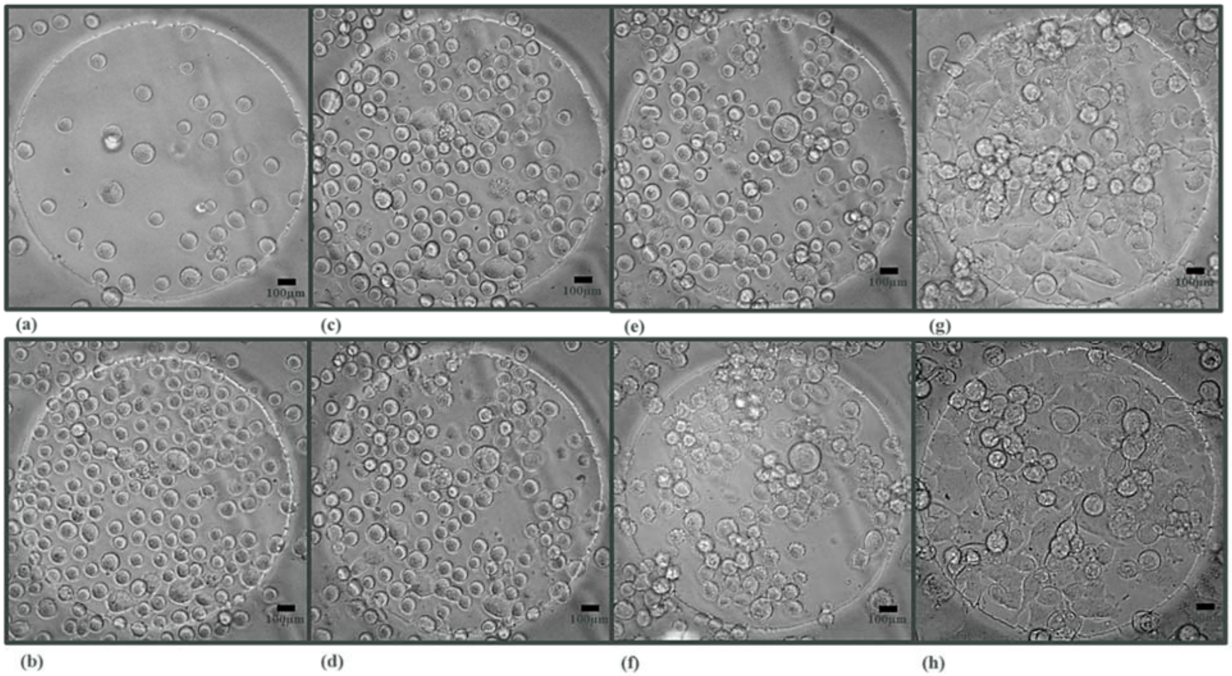


B.8 PC substrate Impedance-based device - 25µg/mL

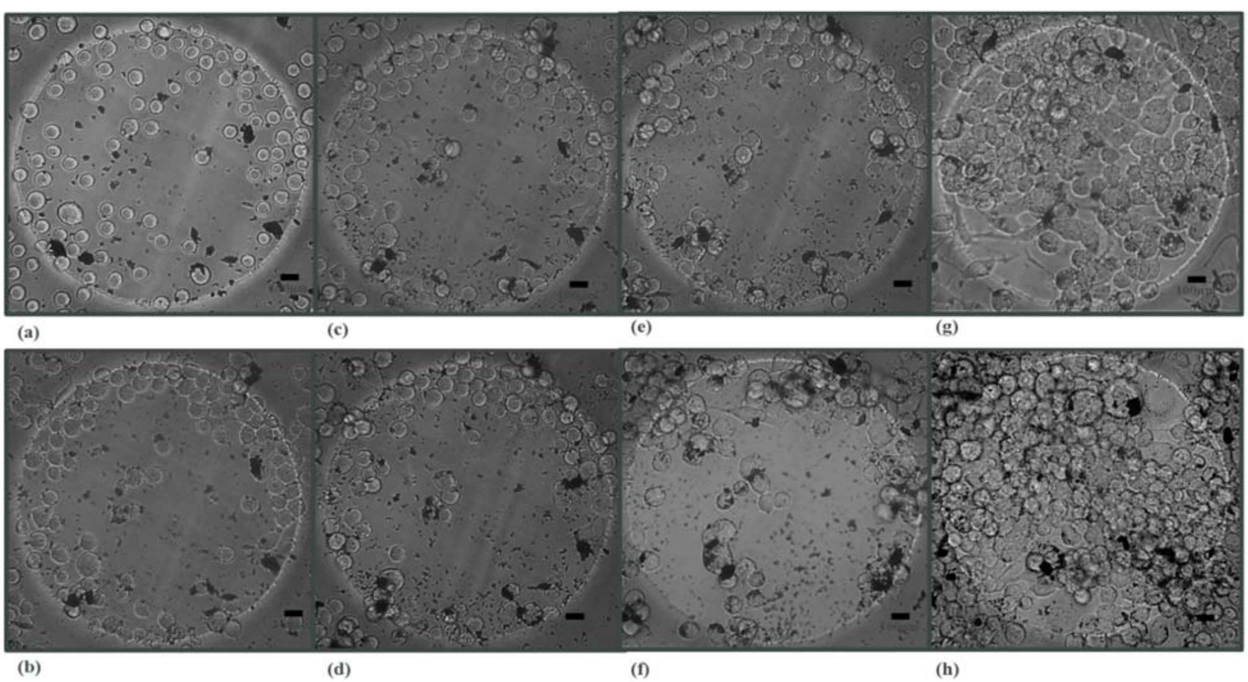

B.9 PC substrate Impedance-based device - 50µg/mL

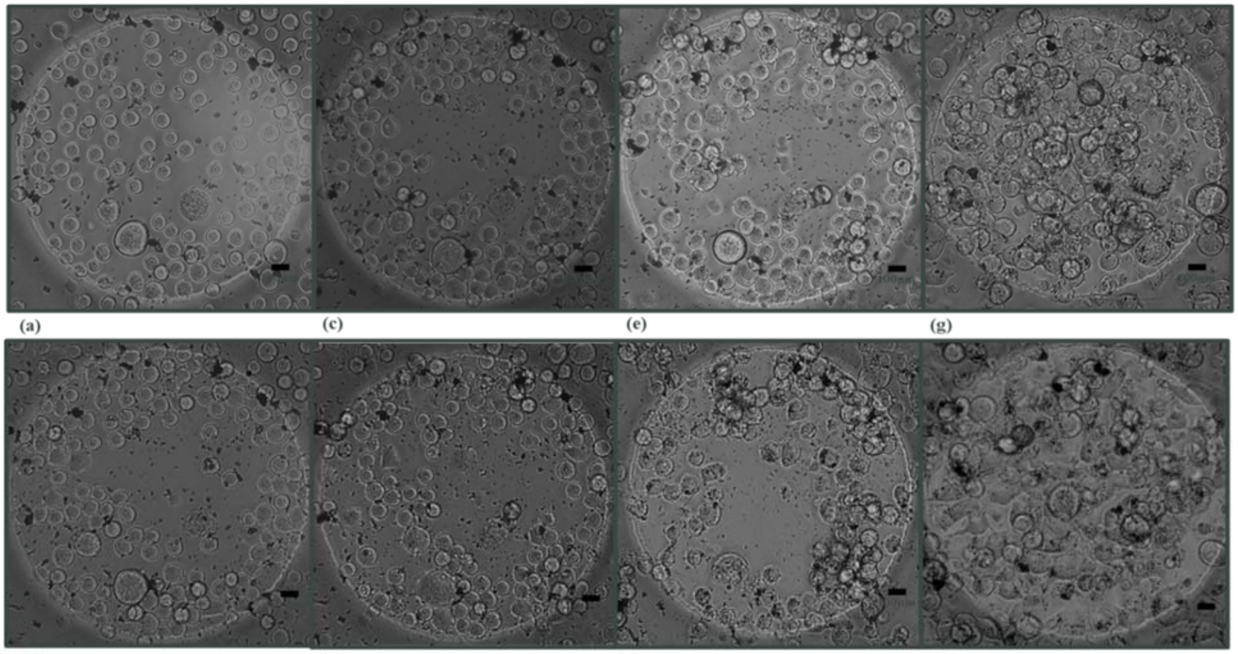

(a) (c) (e) (g)

(b) (d) (f) (h)

B.10 PC substrate Impedance-based device - 100µg/mL

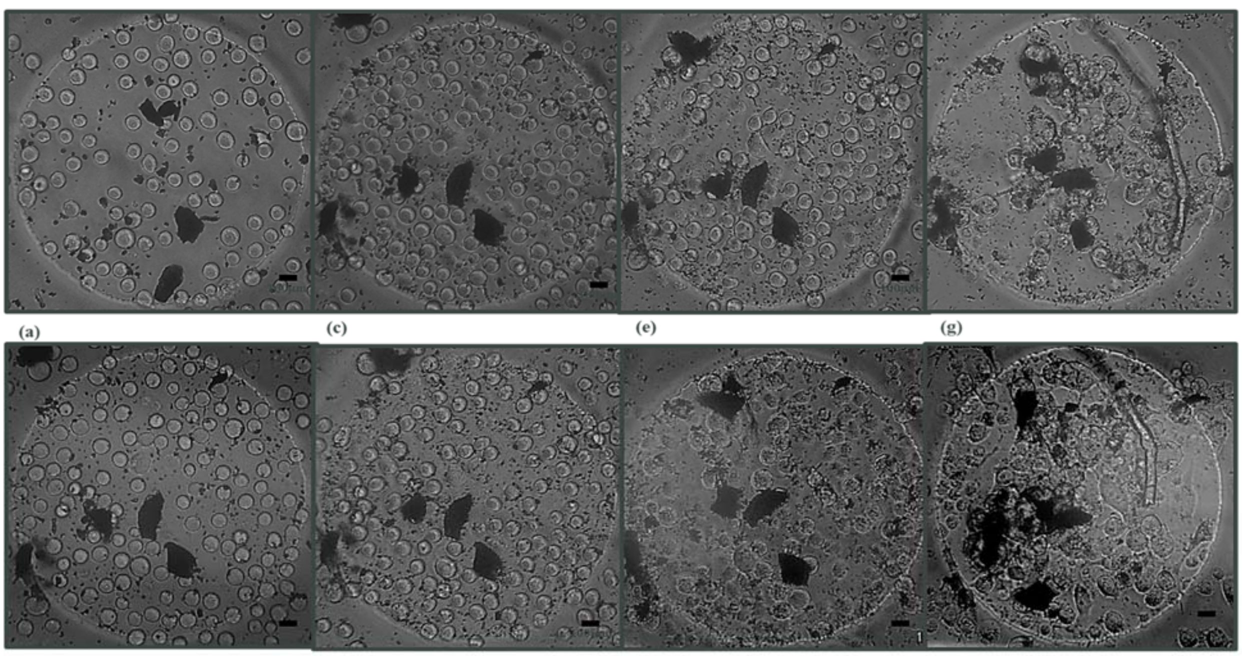

(a) (c) (e) (g)

(b) (d) (f) (h)

B.11 PC substrate Impedance-based device - 200µg/mL

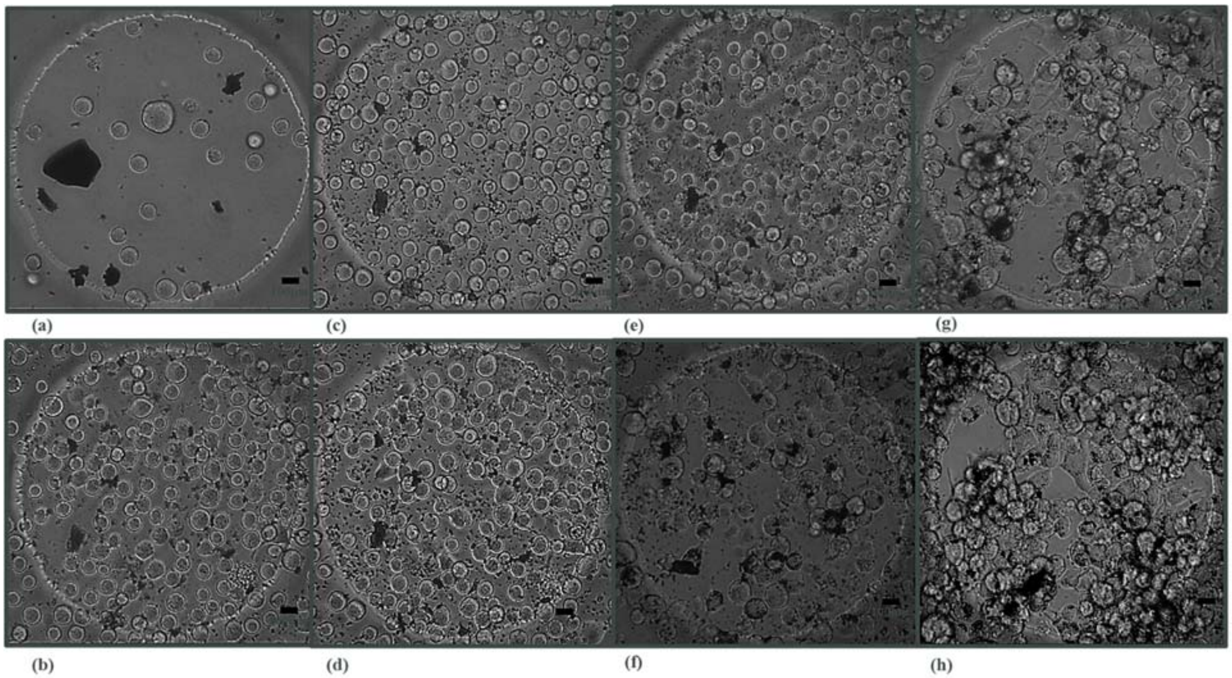


B.12 PC substrate Impedance-based device - 300µg/mL

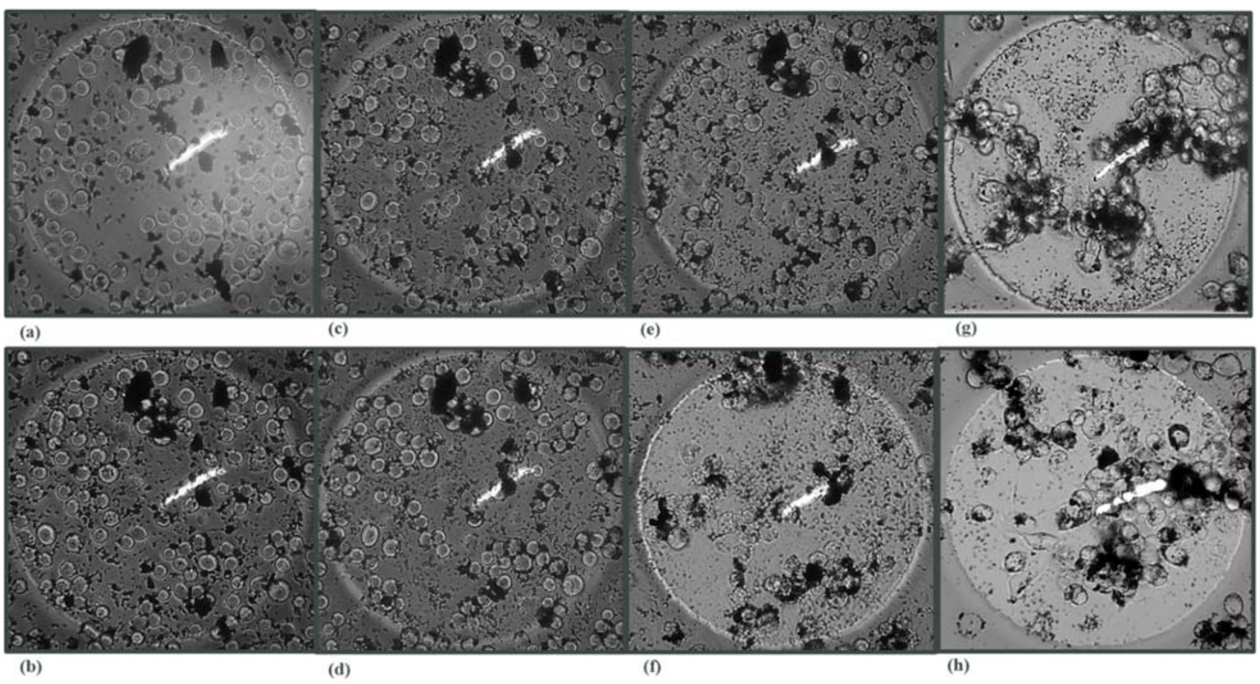

# Appendix C

## Scepter Cell Counter Readings

Assessment on cell viability was also performed using the Scepter™ 2.0 Handheld Cell Counter. After 72 hours' exposure to the different SPIONs concentrations, cells were counted in both impedance-based devices (C.1 and C.2) in three different groups/replicates (G1-G3). In the following measurement results, for each SPIONs concentration C1-C6, the cell concentration CC, and the diameter of cells are measured. The diagrams of cell count versus diameters and cell count versus volume of the sample are also shown.

### C.1 PCB Substrate

### G1

| C1 | Concentration | Diameter | Volume |
|---|---|---|---|
| N2a | 4.01e+05 | 10.69 | 0.64 |

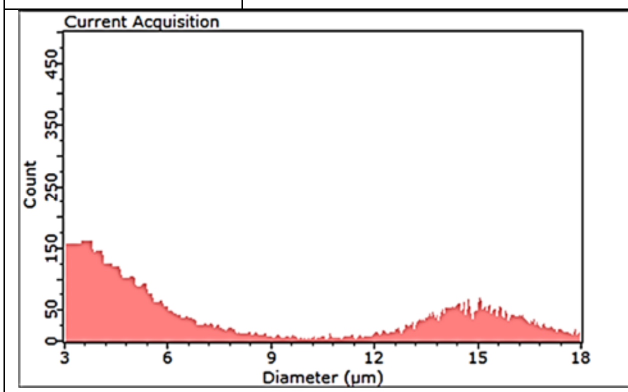


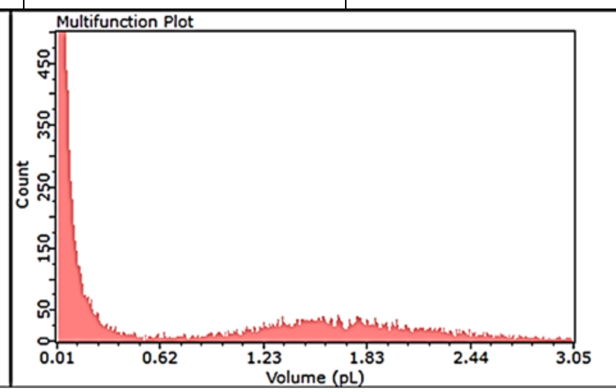


| C2 | Concentration | Diameter | Volume |
|---|---|---|---|
| 25µg/mL | 3.54e+05 | 10.24 | 0.56 |

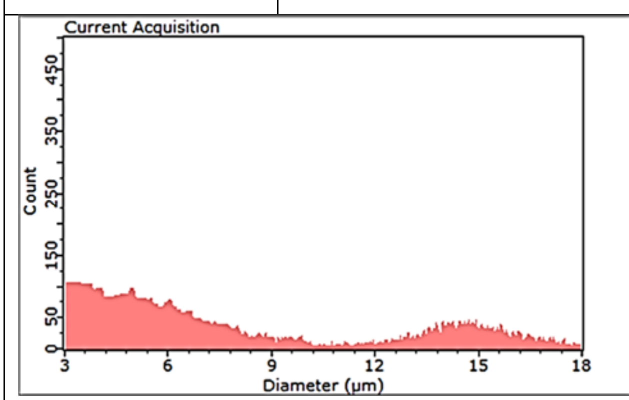


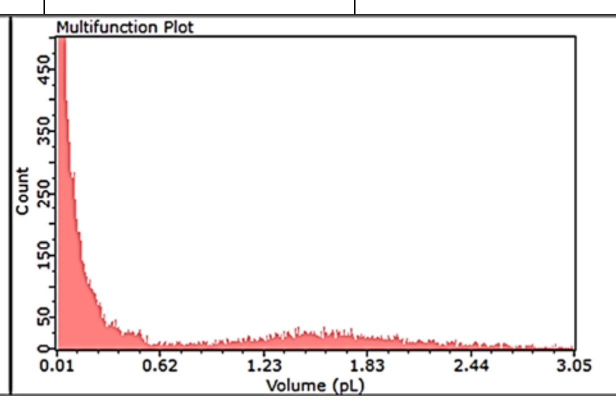

| C3 | Concentration | Diameter | Volume |
|---|---|---|---|
| 50µg/mL | 3.49e+05 | 7.43 | 0.21 |

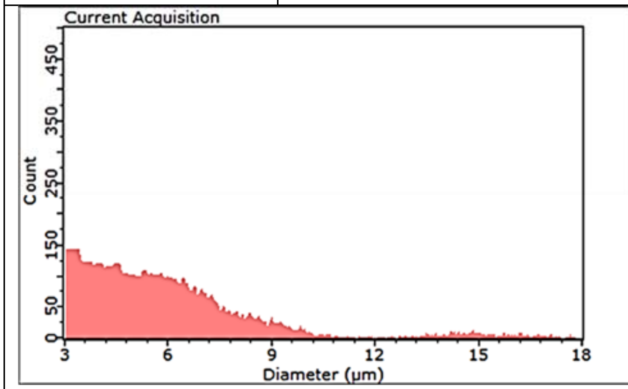


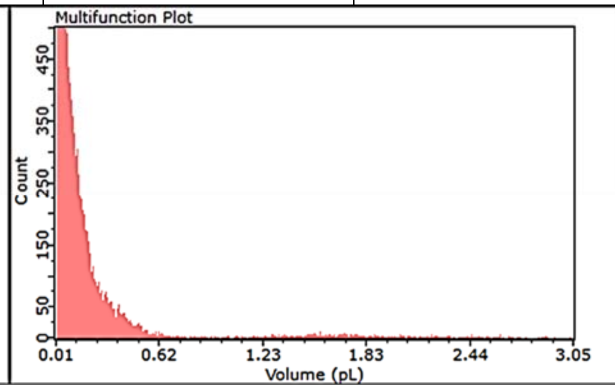


| C4 | Concentration | Diameter | Volume |
|---|---|---|---|
| 100µg/mL | 9.18e+04 | 4.36 | 0.04 |

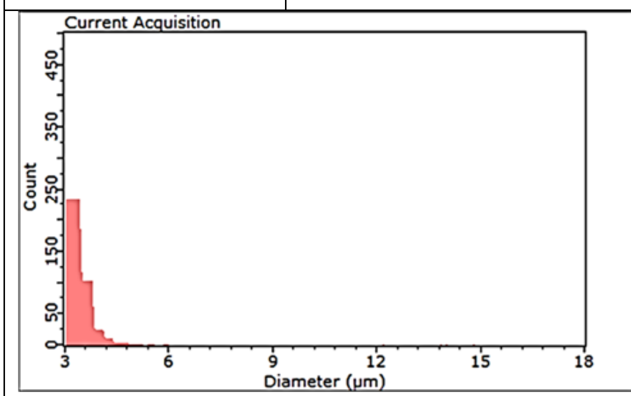


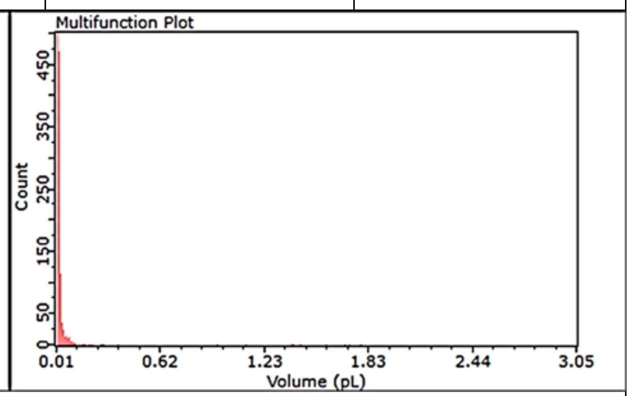


| C5 | Concentration | Diameter | Volume |
|---|---|---|---|
| 200µg/mL | 3.06e+04 | 4.33 | 0.04 |

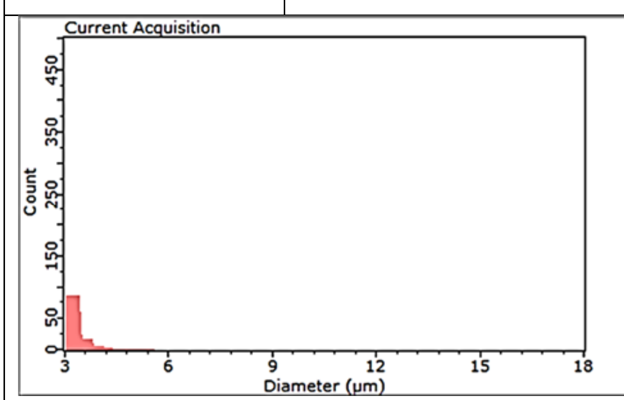


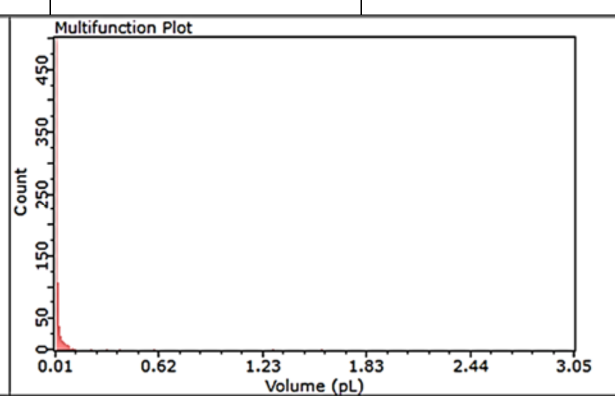

| C6 | Concentration | Diameter | Volume |
|---|---|---|---|
| 300µg/mL | 2.44e+04 | 5.54 | 0.09 |

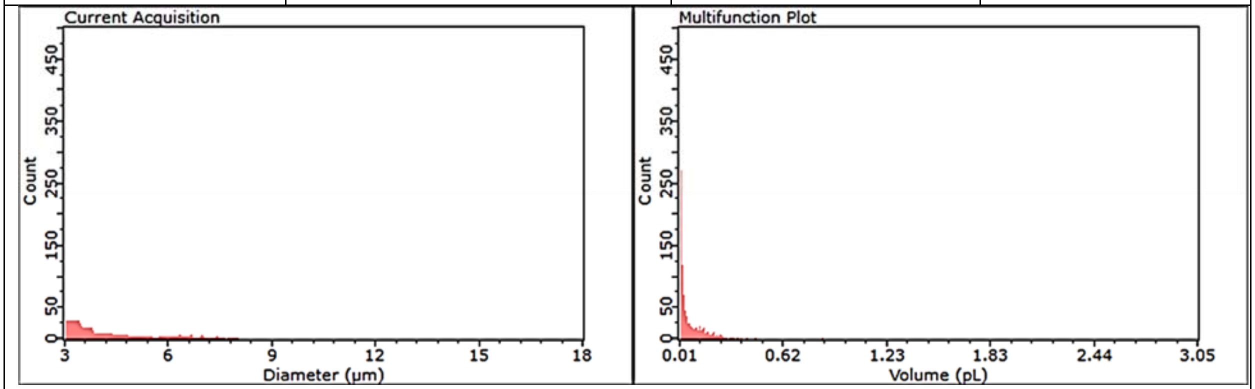


**G2**

| C1 | Concentration | Diameter | Volume |
|---|---|---|---|
| N2a | 4.25e+05 | 6.60 | 0.15 |

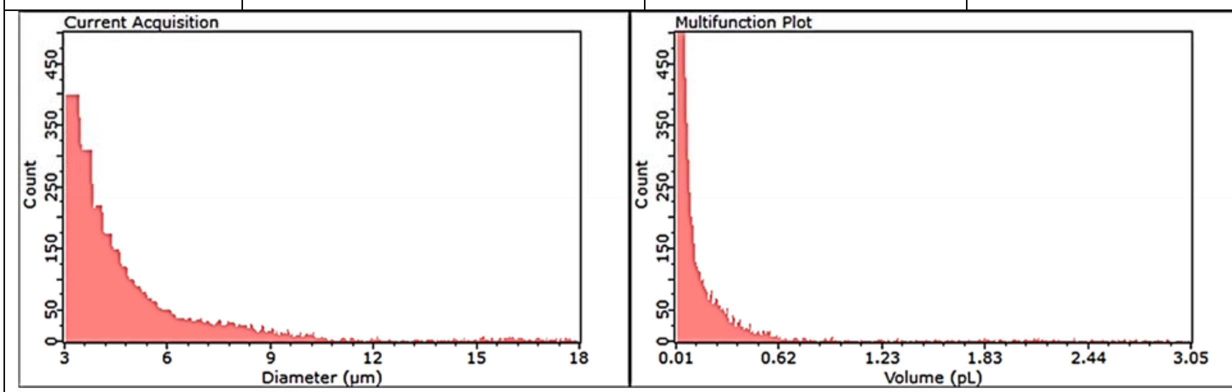


| C2 | Concentration | Diameter | Volume |
|---|---|---|---|
| 25 µg/mL | 3.58e+05 | 6.29 | 0.13 |

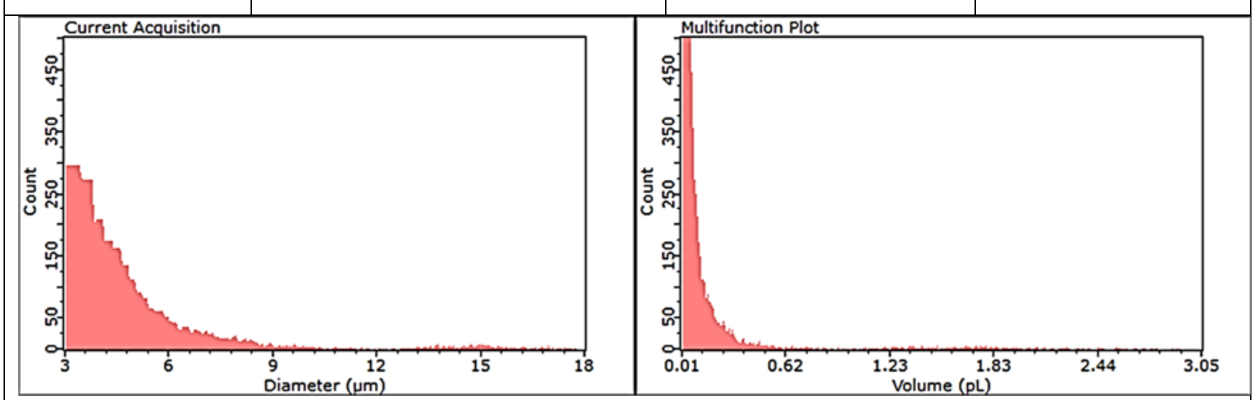

| C3 | Concentration | Diameter | Volume |
|---|---|---|---|
| 50µg/mL | 3.69e+05 | 5.99 | 0.11 |

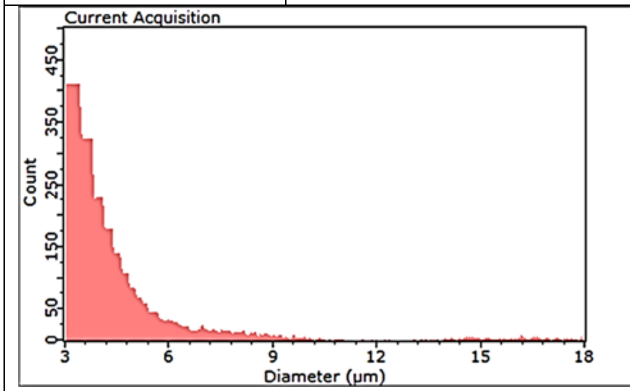


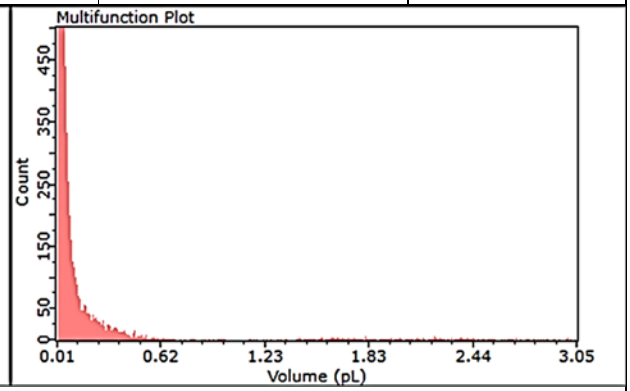


| C4 | Concentration | Diameter | Volume |
|---|---|---|---|
| 100µg/mL | 3.44e+05 | 6.95 | 0.18 |

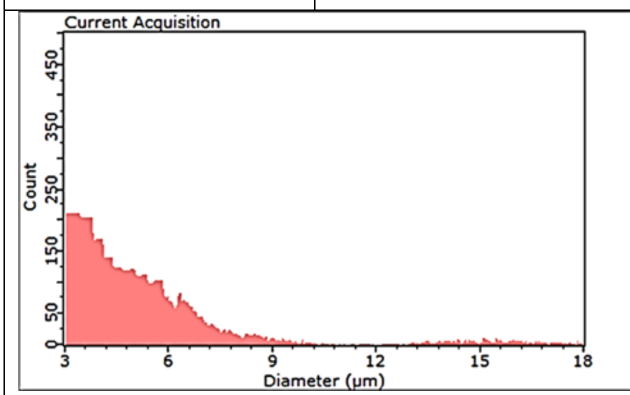


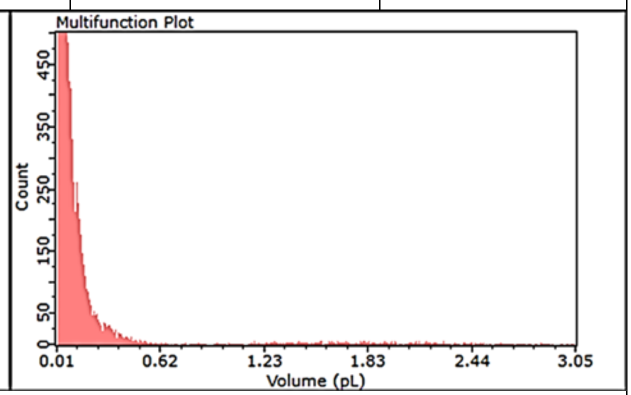


| C5 | Concentration | Diameter | Volume |
|---|---|---|---|
| 200µg/mL | 2.92e+05 | 6.21 | 0.13 |

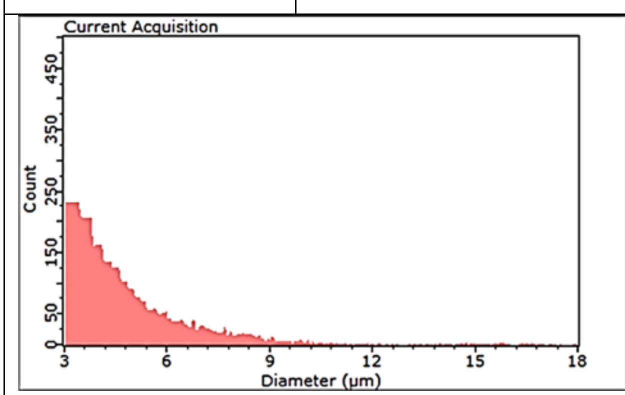


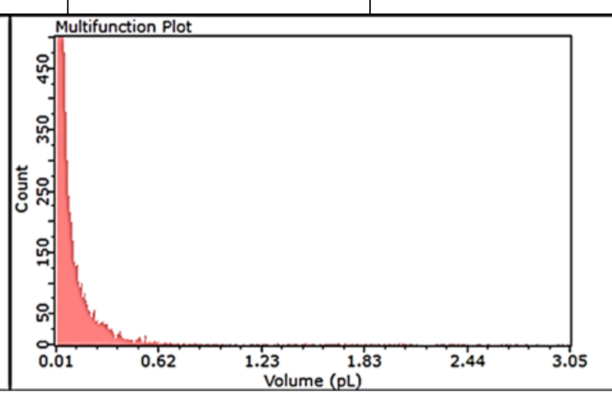

| C6 | Concentration | Diameter | Volume |
|---|---|---|---|
| 300µg/mL | 2.67e+05 | 6.18 | 0.12 |

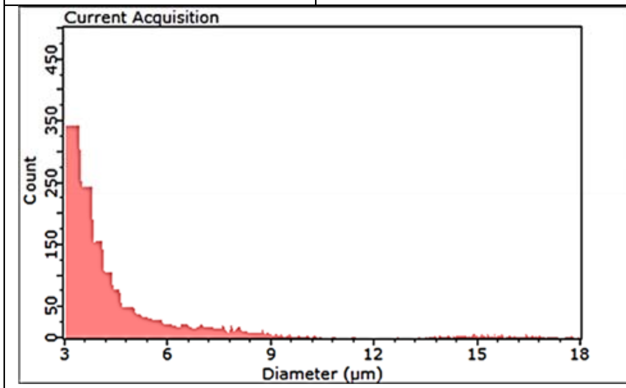


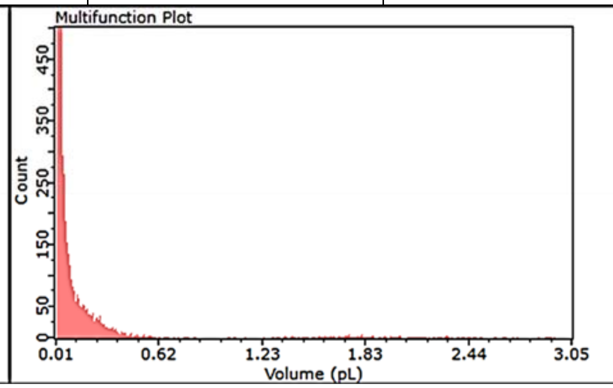


**G3**

| C1 | Concentration | Diameter | Volume |
|---|---|---|---|
| N2a | 2.71e+05 | 5.97 | 0.11 |

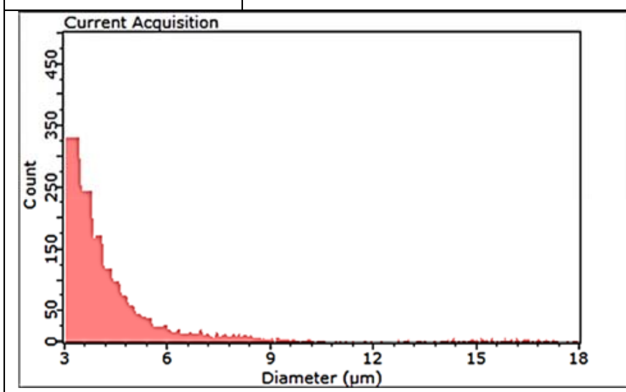


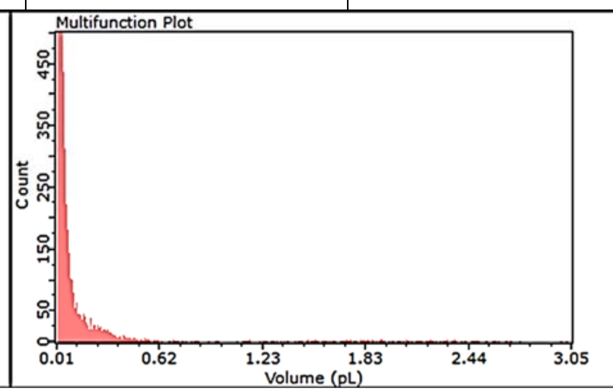


| C2 | Concentration | Diameter | Volume |
|---|---|---|---|
| 25 µg/mL | 2.92e+05 | 6.90 | 0.17 |

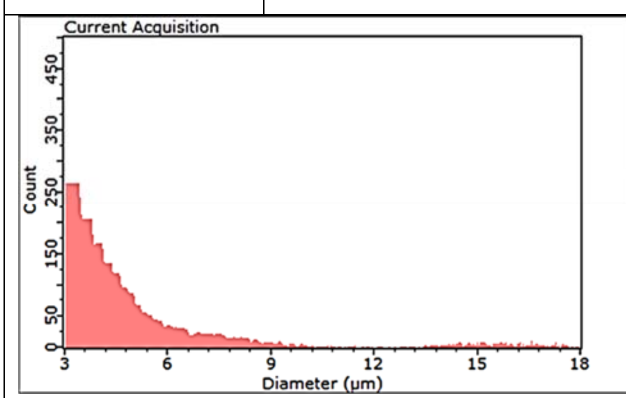


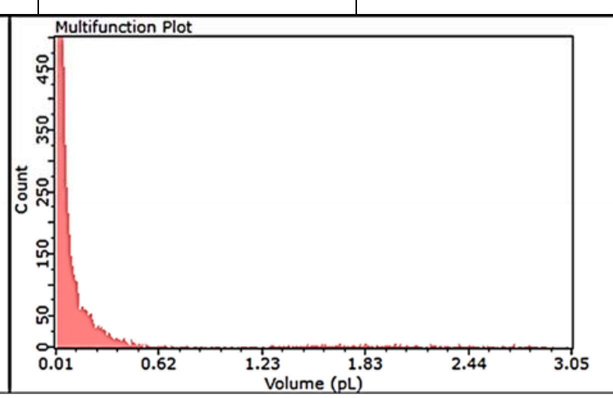

| C3 | Concentration | Diameter | Volume |
|---|---|---|---|
| 50µg/mL | 3.27e+05 | 5.93 | 0.11 |

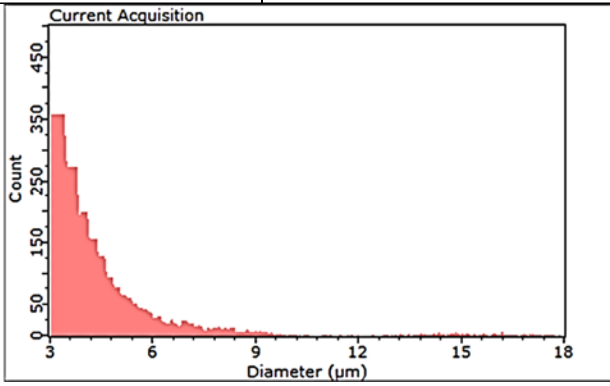


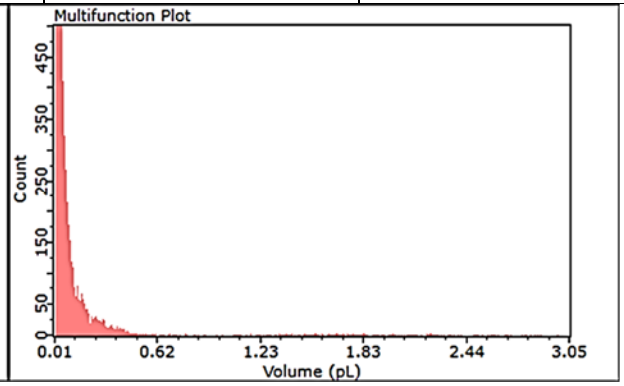


| C4 | Concentration | Diameter | Volume |
|---|---|---|---|
| 100µg/mL | 2.43e+05 | 6.05 | 0.12 |

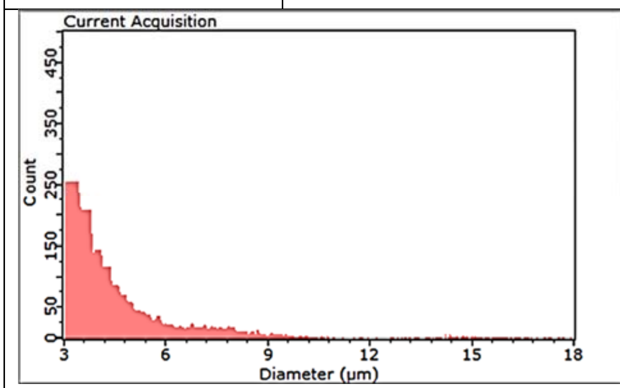


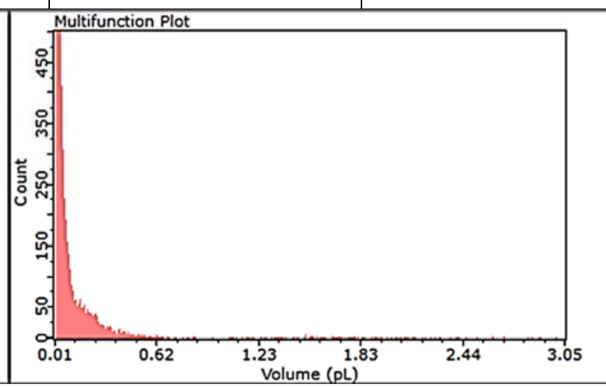


| C5 | Concentration | Diameter | Volume |
|---|---|---|---|
| 200µg/mL | 1.96e+05 | 5.29 | 0.08 |

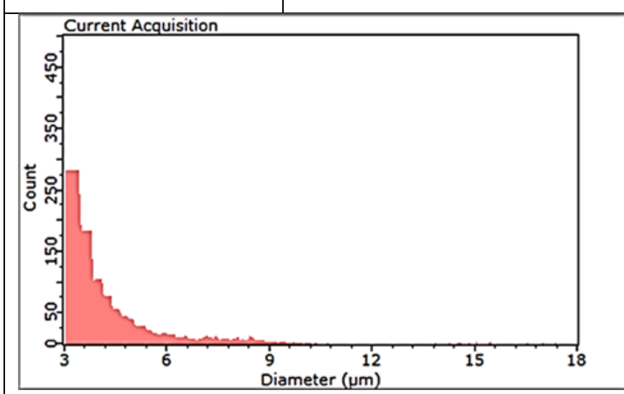


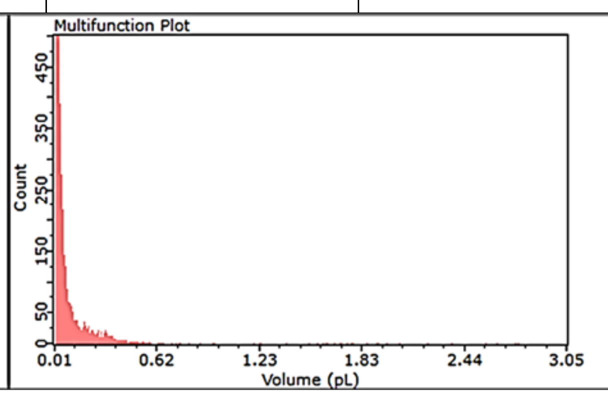

| C6 | Concentration | Diameter | Volume |
|---|---|---|---|
| 300µg/mL | 1.34e+05 | 6.59 | 0.15 |

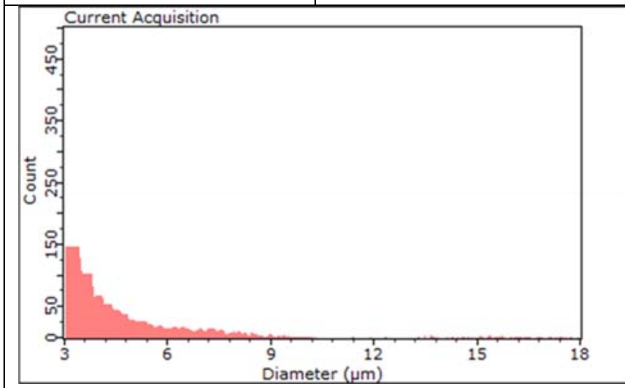


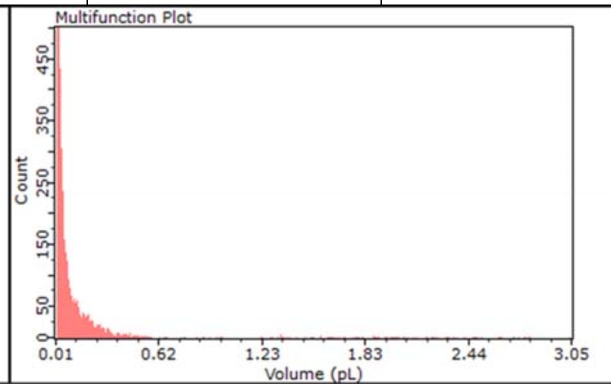


## C.2 PC Substrate

### G1

| C1 | Concentration | Diameter | Volume |
|---|---|---|---|
| N2a | 4.02e+05 | 7.04 | 0.18 |

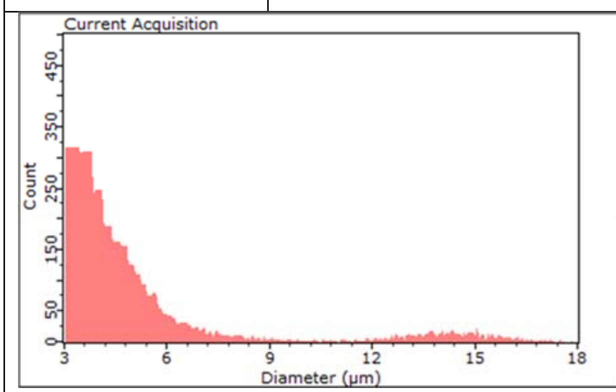


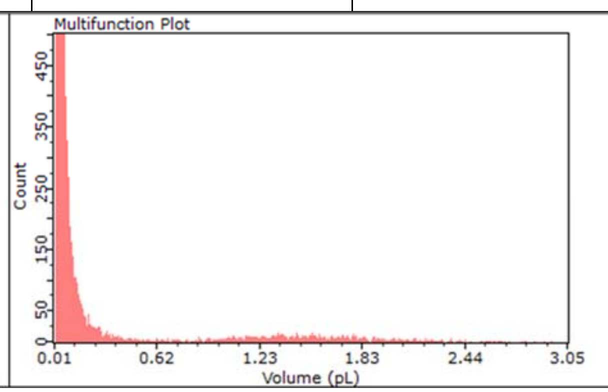

| C2 | Concentration | Diameter | Volume |
|---|---|---|---|
| 25 μg/mL | 3.43e+05 | 8.28 | 0.30 |

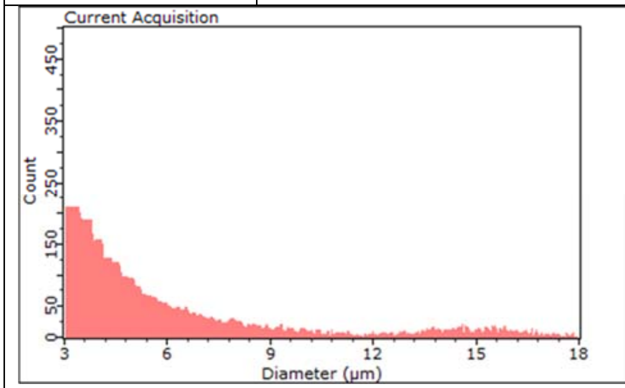


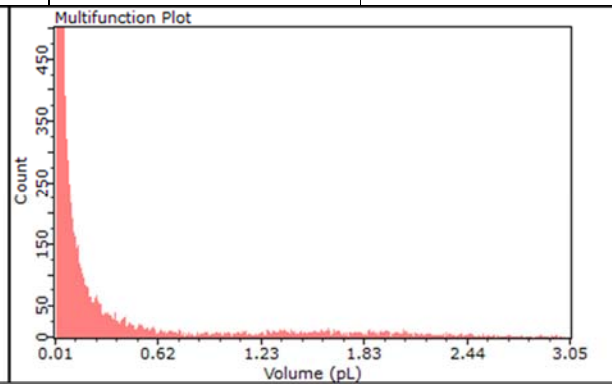


| C3 | Concentration | Diameter | Volume |
|---|---|---|---|
| 50 μg/mL | 5.47e+05 | 8.16 | 0.28 |

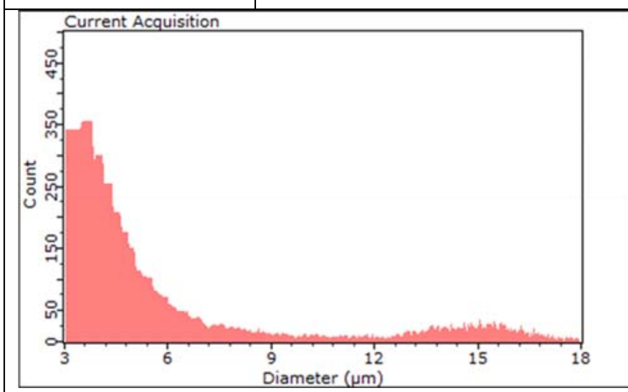


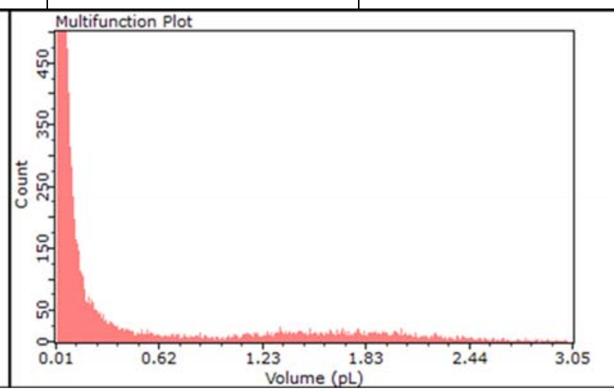


| C4 | Concentration | Diameter | Volume |
|---|---|---|---|
| 100 μg/mL | 3.77e+05 | 6.42 | 0.14 |

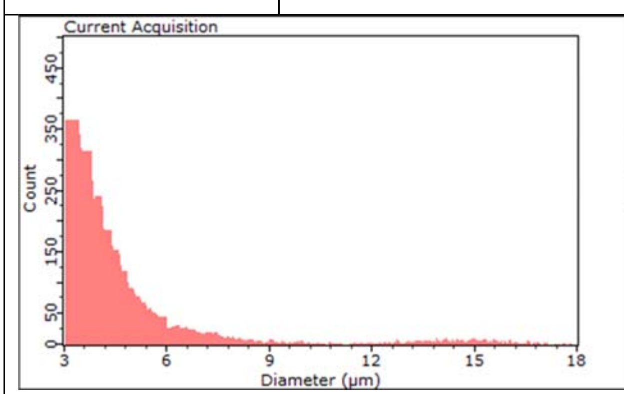


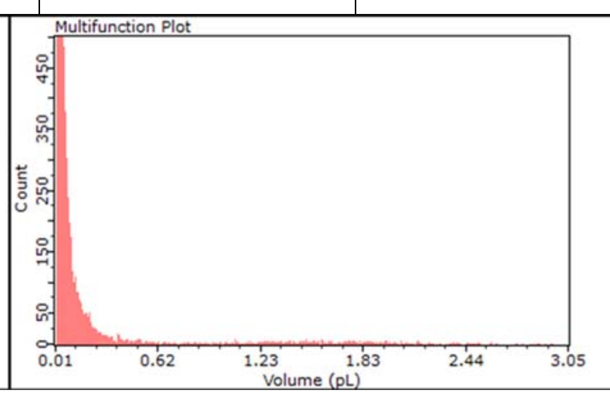

| C5 | Concentration | Diameter | Volume |
|---|---|---|---|
| 200 µg/mL | 3.09e+05 | 6.63 | 0.15 |

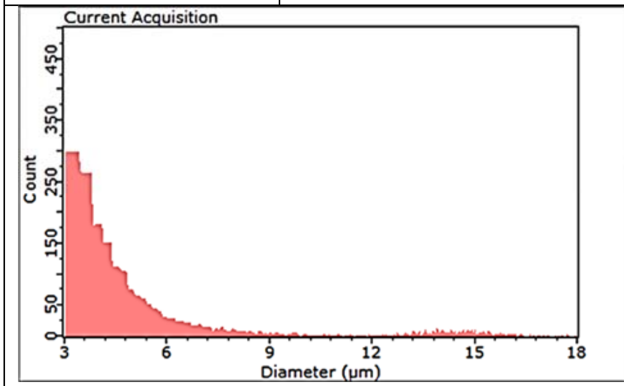


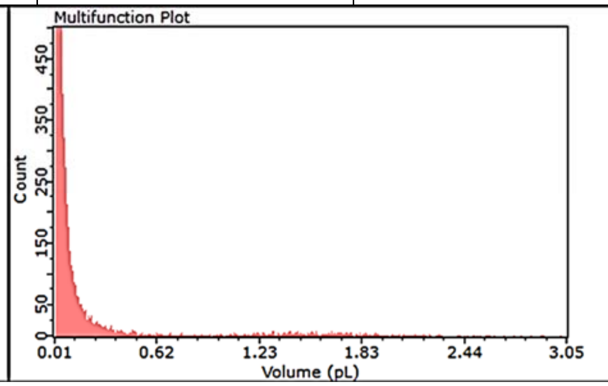


| C6 | Concentration | Diameter | Volume |
|---|---|---|---|
| 300 µg/mL | 2.79e+05 | 6.19 | 0.12 |

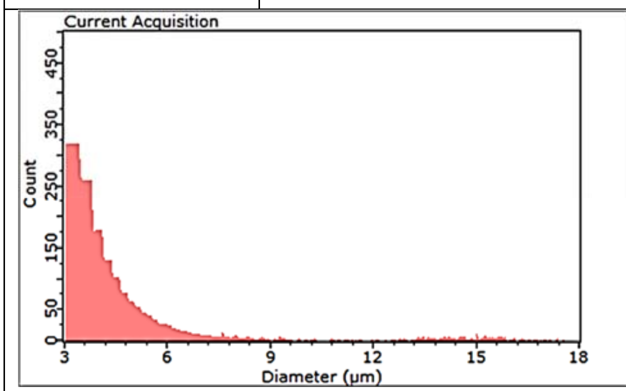


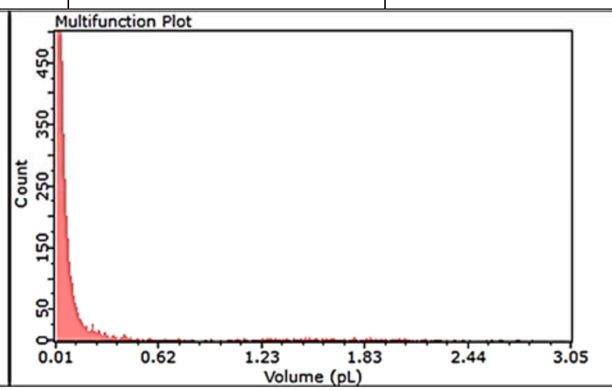


**G2**

| C1 | Concentration | Diameter | Volume |
|---|---|---|---|
| N2a | 4.12e+05 | 8.67 | 0.34 |

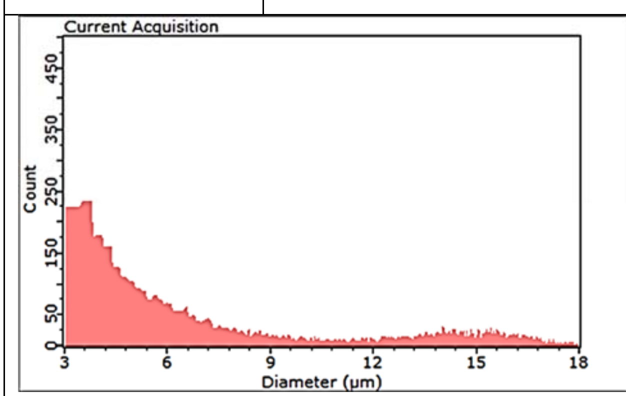


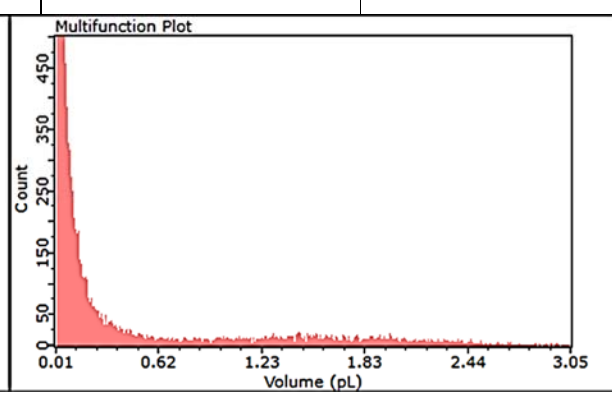

| C2 | Concentration | Diameter | Volume |
|---|---|---|---|
| 25 µg/mL | 3.86e+05 | 7.02 | 0.18 |

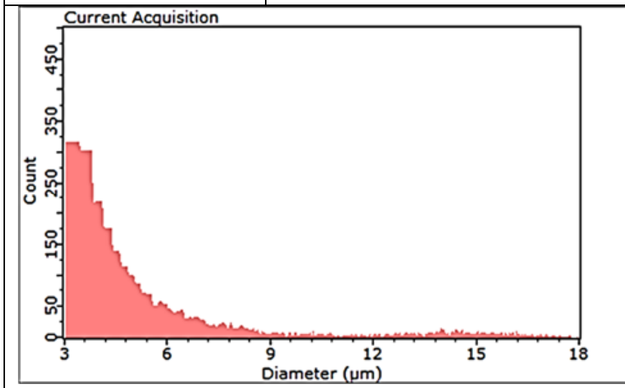


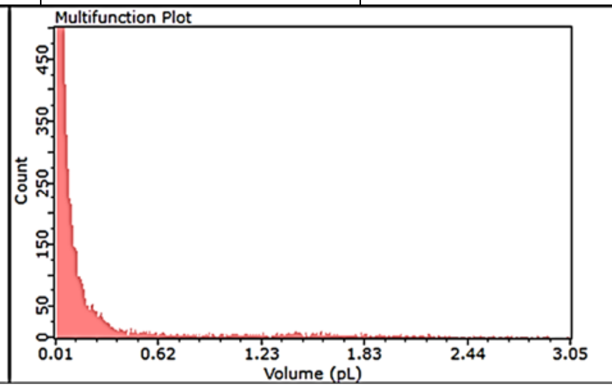


| C3 | Concentration | Diameter | Volume |
|---|---|---|---|
| 50 µg/mL | 3.68e+05 | 7.81 | 0.25 |

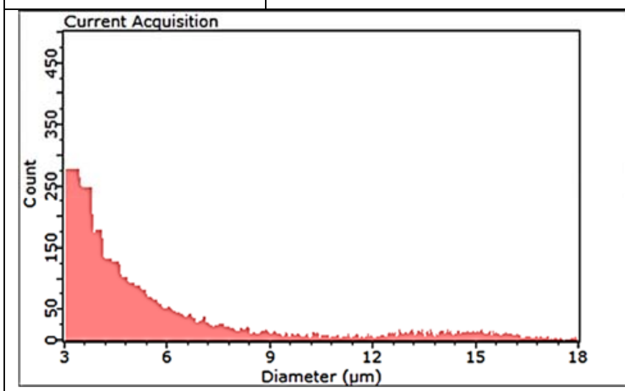


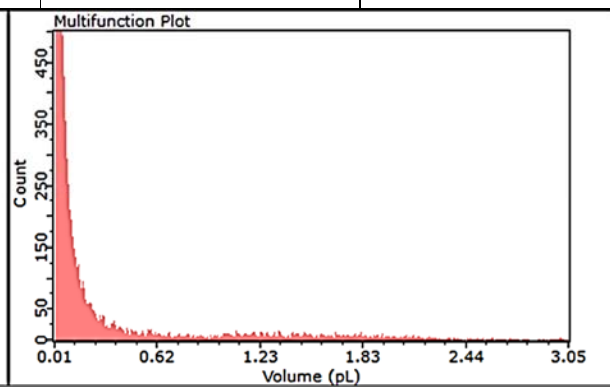


| C4 | Concentration | Diameter | Volume |
|---|---|---|---|
| 100 µg/mL | 2.44e+05 | 6.13 | 0.12 |

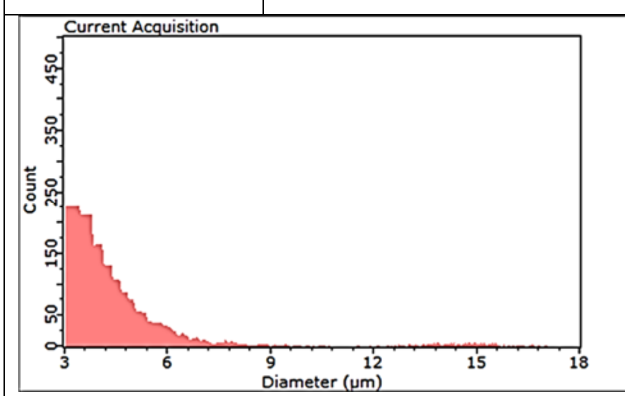


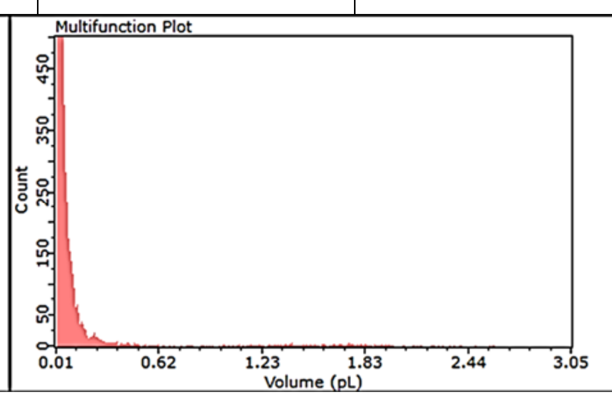

| C5 | Concentration | Diameter | Volume |
|---|---|---|---|
| 200 µg/mL | 2.47e+05 | 6.44 | 0.14 |

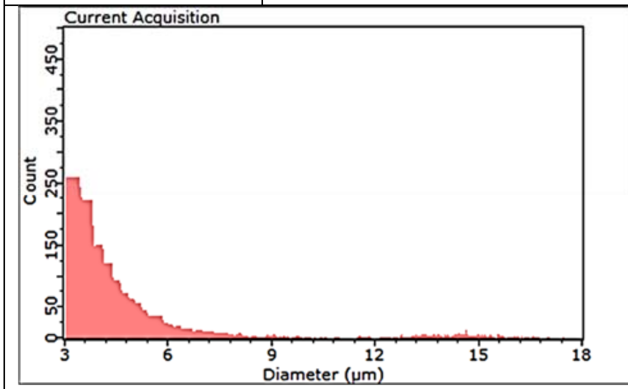


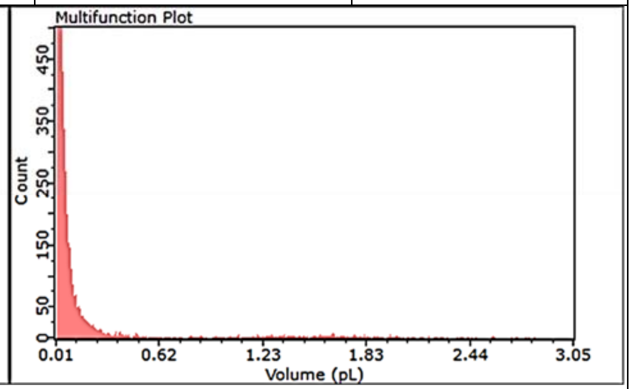


| C6 | Concentration | Diameter | Volume |
|---|---|---|---|
| 300 µg/mL | 2.15e+05 | 6.20 | 0.12 |

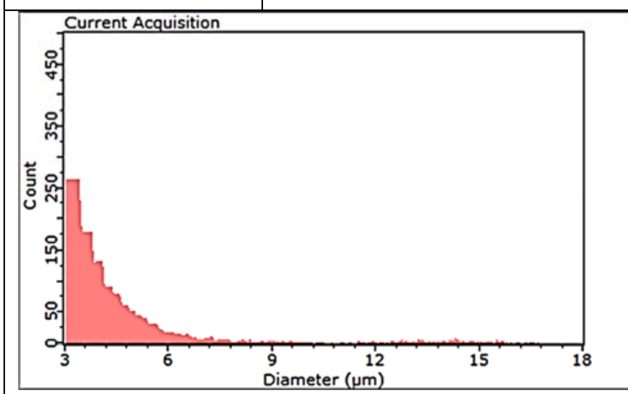


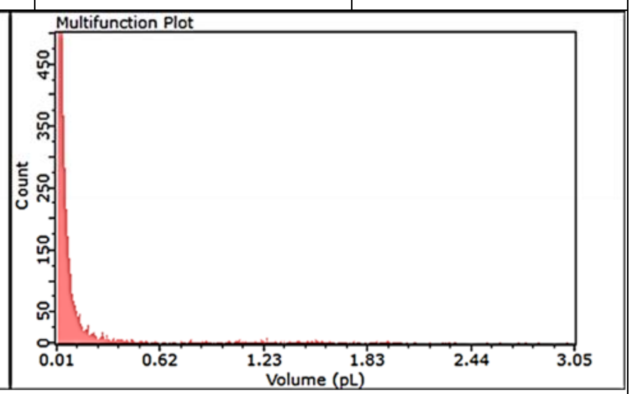


**G3**

| C1 | Concentration | Diameter | Volume |
|---|---|---|---|
| N2a | 5.38e+05 | 7.31 | 0.20 |

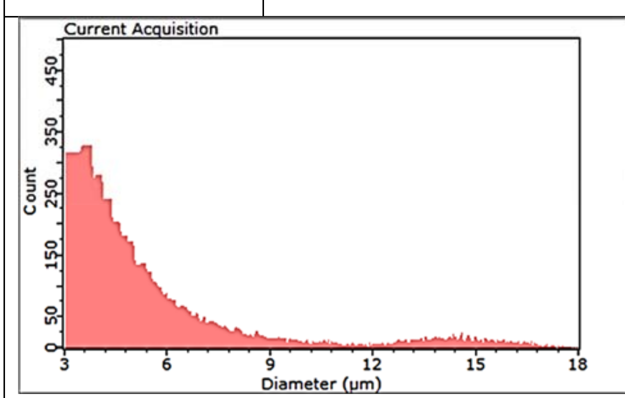


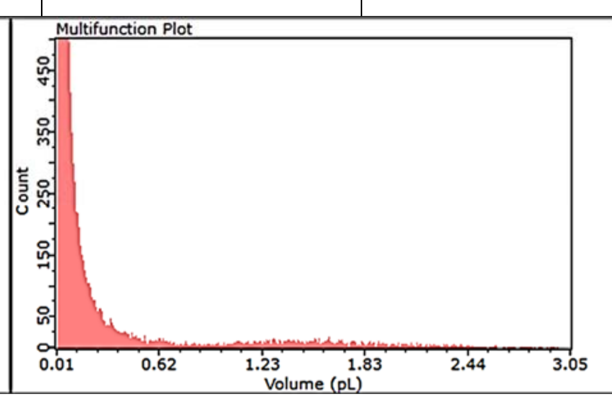

| C2 | Concentration | Diameter | Volume |
|---|---|---|---|
| 25 µg/mL | 5.79e+05 | 9.81 | 0.49 |

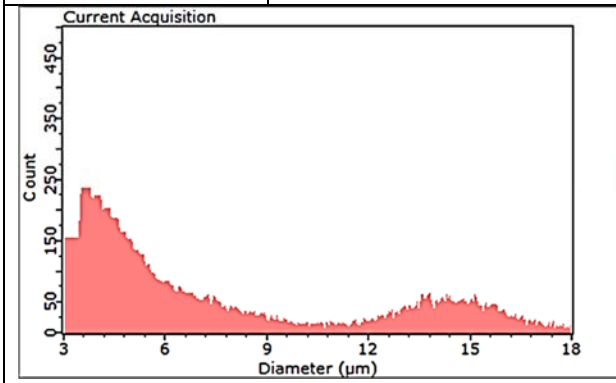


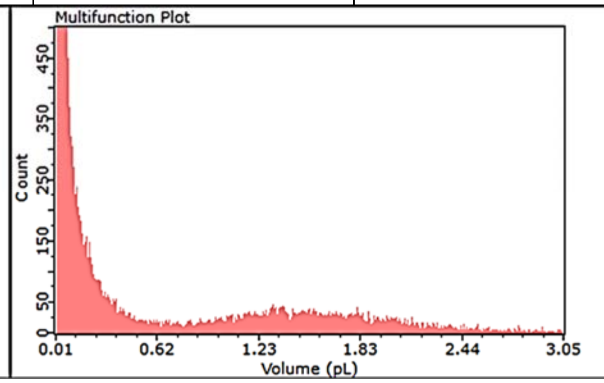


| C3 | Concentration | Diameter | Volume |
|---|---|---|---|
| 50 µg/mL | 4.40e+05 | 6.61 | 0.15 |

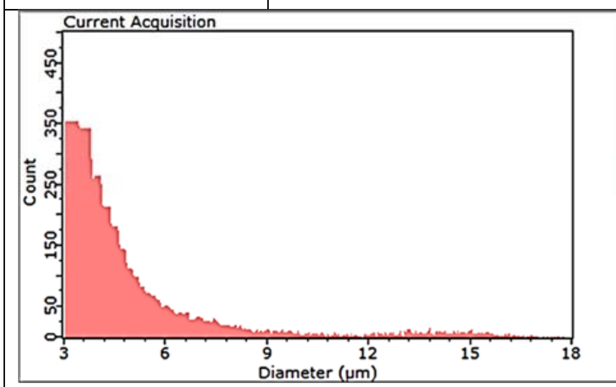


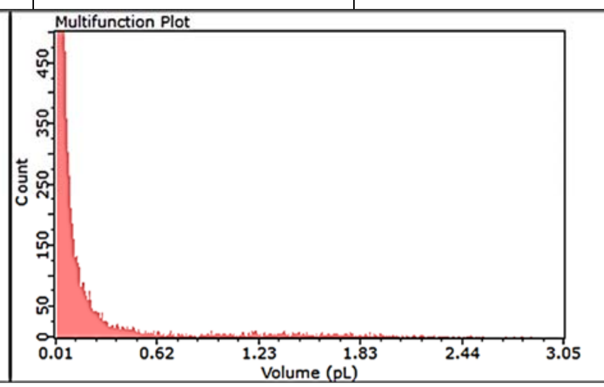


| C4 | Concentration | Diameter | Volume |
|---|---|---|---|
| 100 µg/mL | 6.02e+05 | 10.73 | 0.65 |

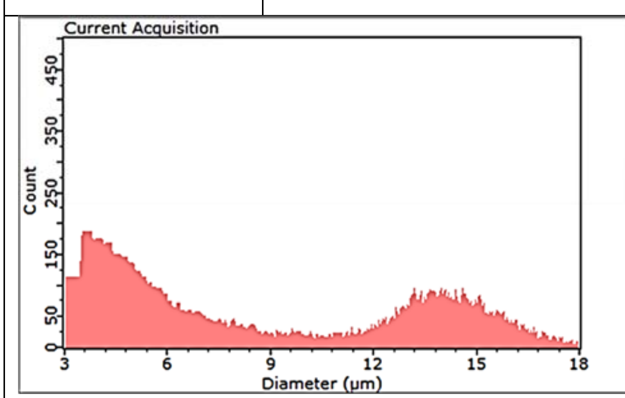


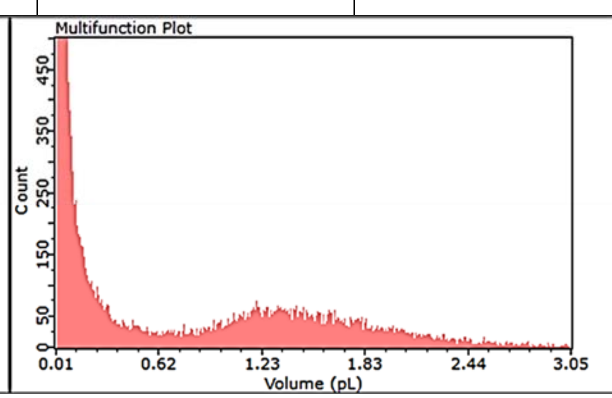

| C5 | Concentration | Diameter | Volume |
|---|---|---|---|
| 200 µg/mL | 5.69e+05 | 11.83 | 0.87 |

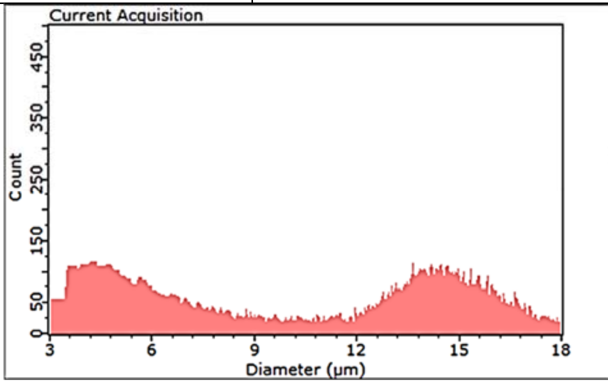


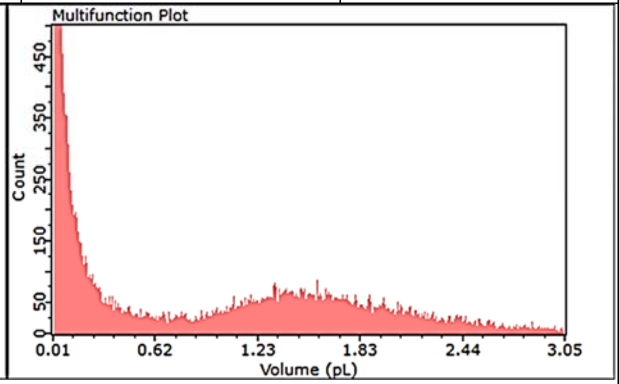


| C6 | Concentration | Diameter | Volume |
|---|---|---|---|
| 300 µg/mL | 4.91e+05 | 11.64 | 0.83 |

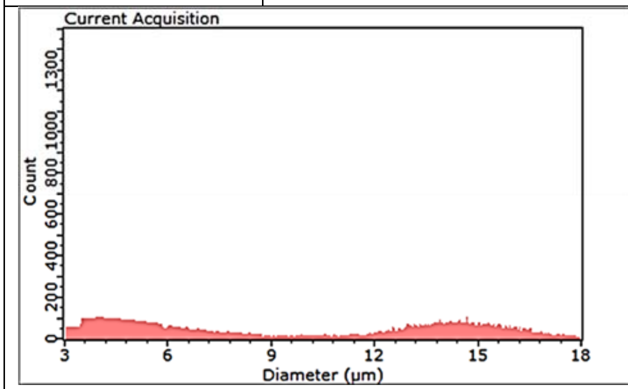


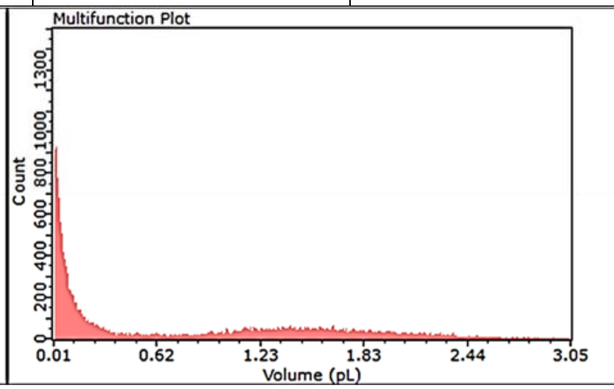

# Appendix D

## The Impedance Curves of the different concentrations of SPIONs in relation to the frequency

The following graphs show the curves of each of the impedance spectroscopy at different times T1=A, T2=B, T3=C, T4=D, T5=E, T6=F, T7=G and T8=H at different SPIONS concentrations (a) C1, (b)C2, (c) C3, (d) C4, (e)C5 and (f) C6

D. 1 TR 1 G1

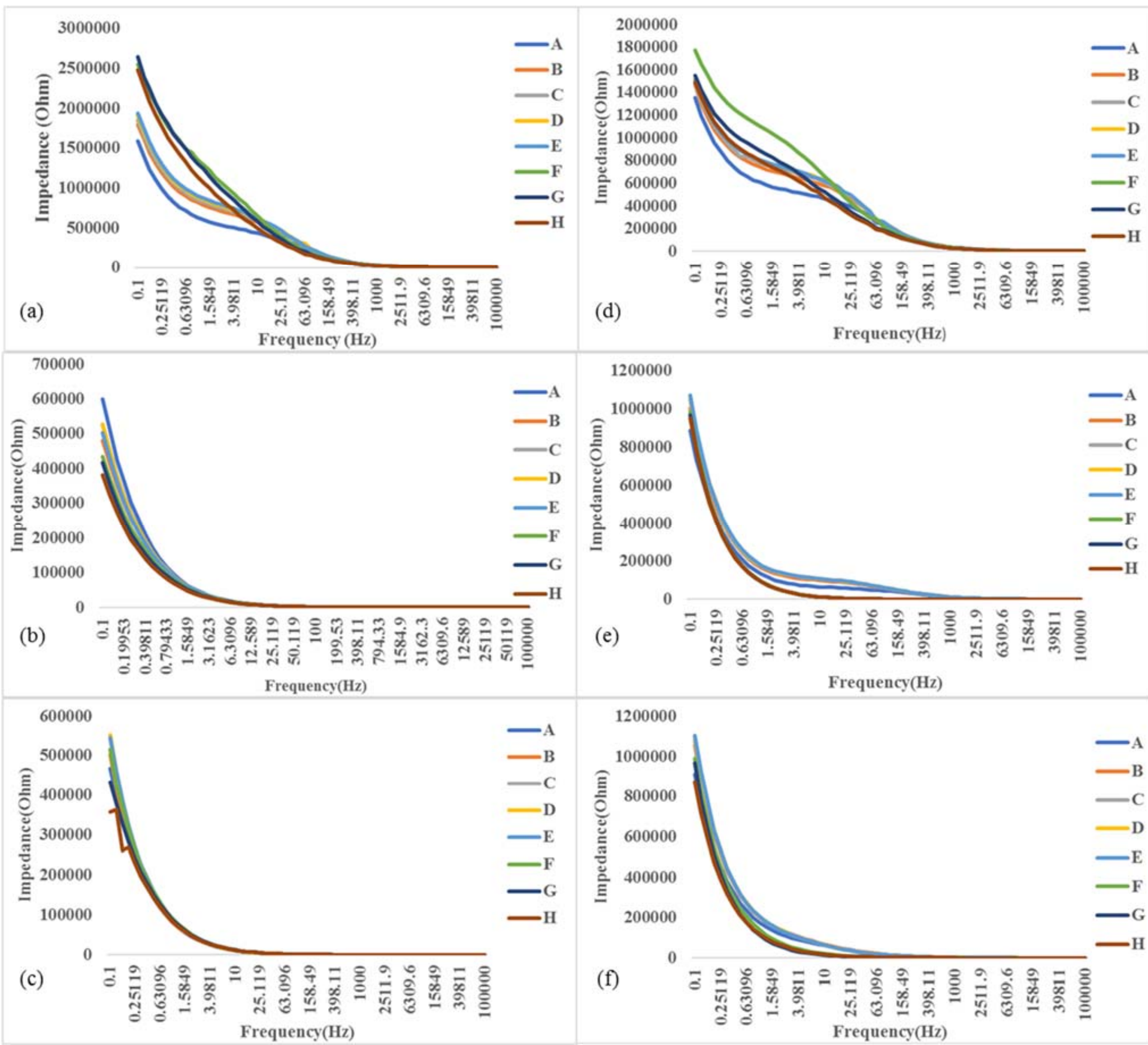

D. 2 TR 1 G2

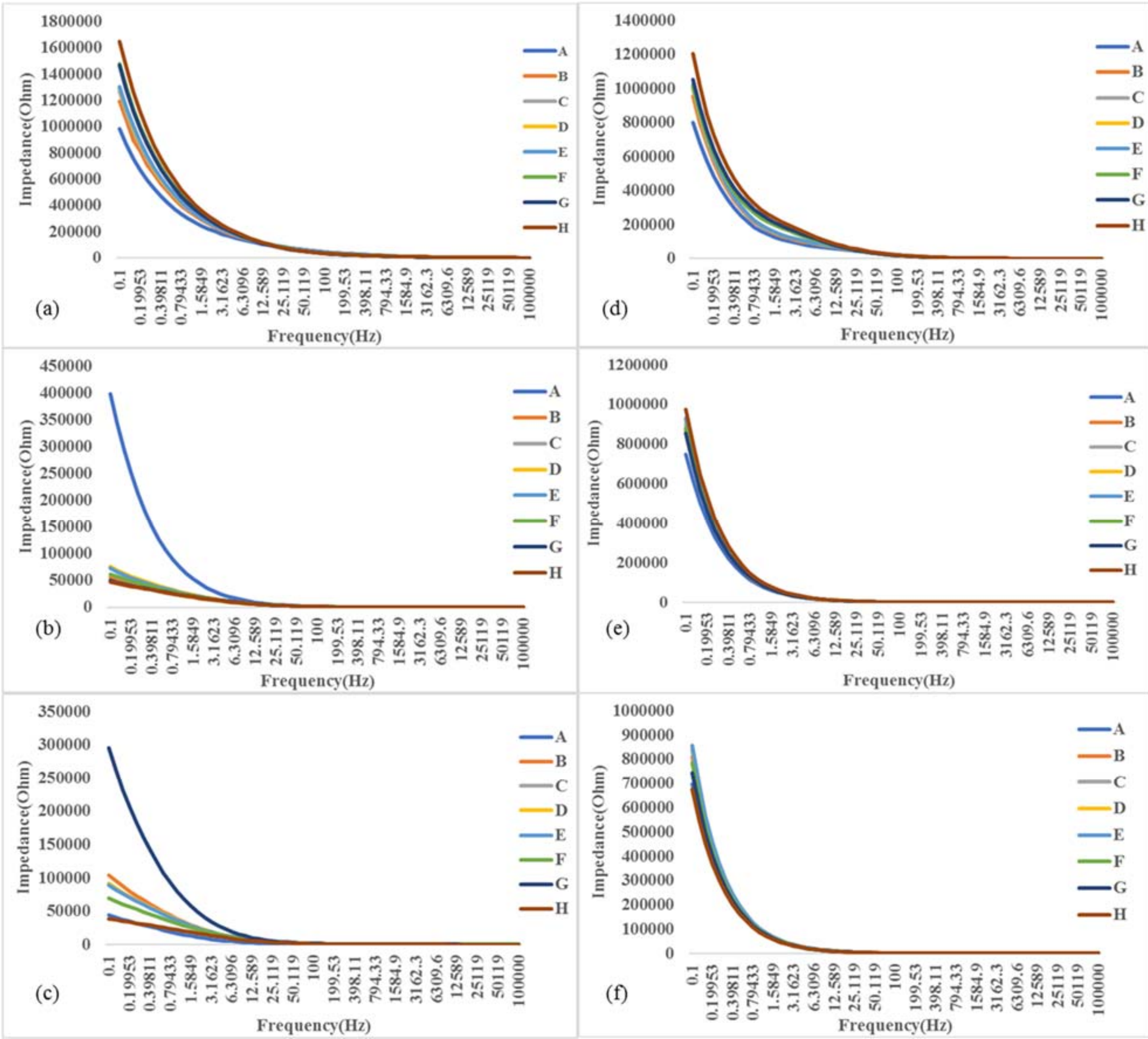

(a)
(b)
(c)
(d)
(e)
(f)
Impedance(Ohm)
Frequency(Hz)
A
B
C
D
E
F
G
H
0.1
0.19953
0.39811
0.79433
1.5849
3.1623
6.3096
12.589
25.119
50.119
100
199.53
398.11
794.33
1584.9
3162.3
6309.6
12589
25119
50119
100000

D. 3 TR 1 G3

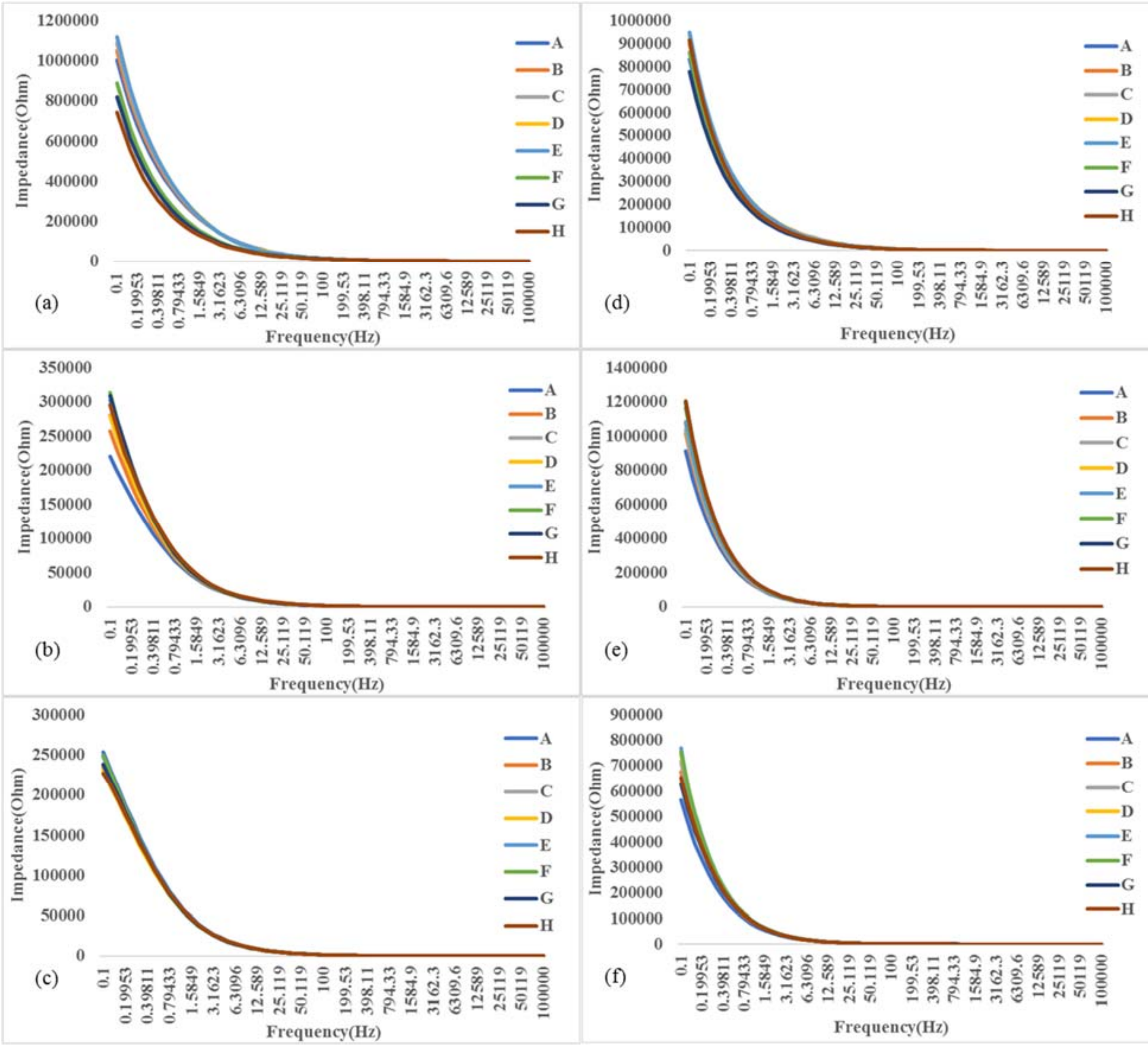

# Appendix E

## Integrated Impedance Spectroscopy results using equations

E.1. Impedance change ΔZ=Z(f)MAX-Z(f)MIN in different times and frequencies. The bar graphs show the AVG Z(f)MAX-Z(f)MIN for each group in all trials (a)TR1, (b) TR2, and (c) TR3. Bar graph in (d) shows the average of (a), (b) and (c) of C1-C6 with cells

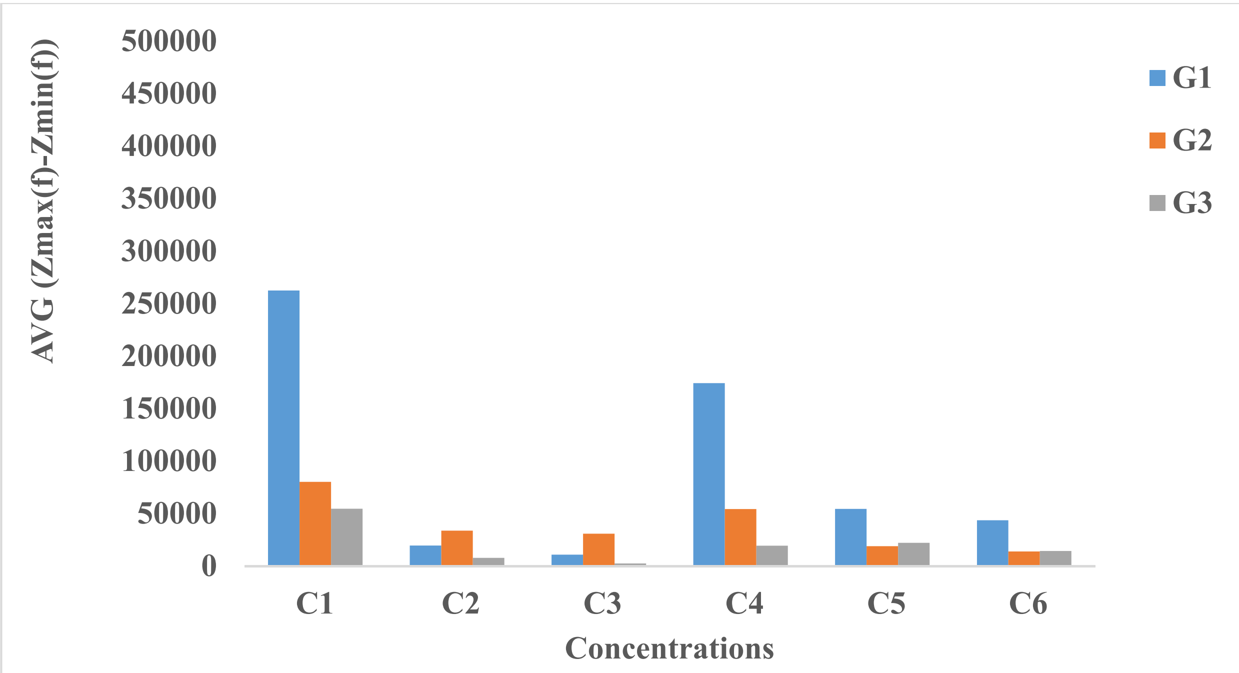


(a)

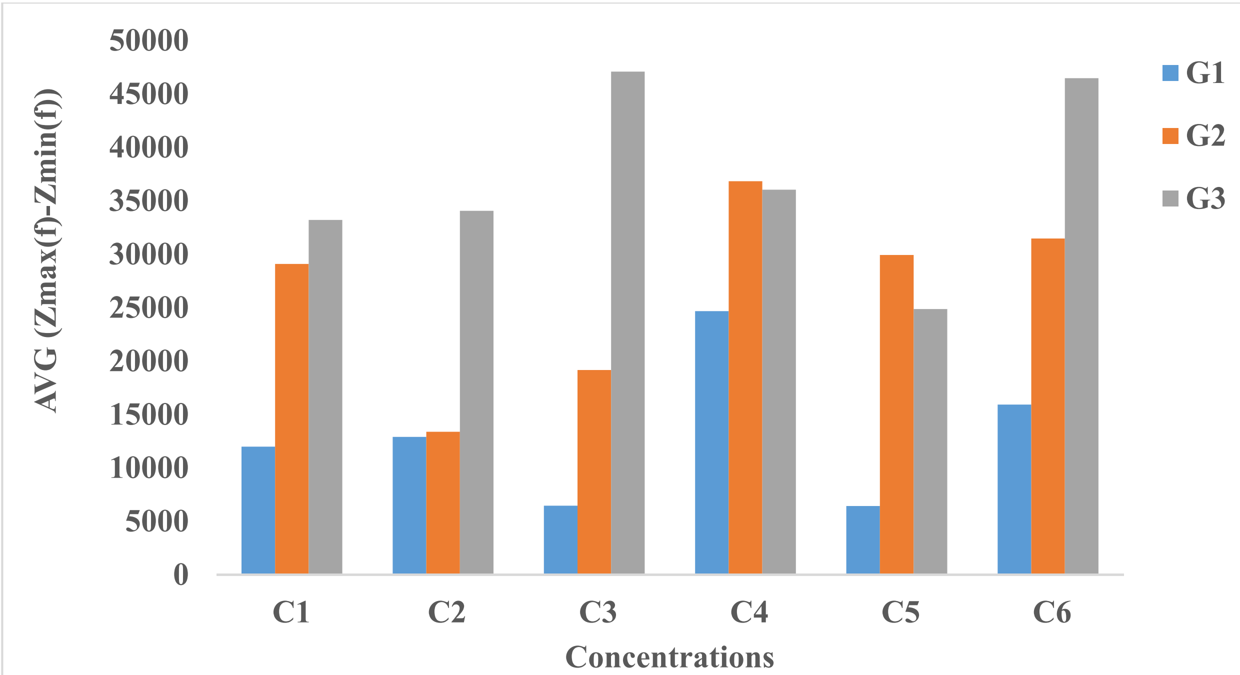
50000
45000
40000
35000
30000
25000
20000
15000
10000
5000
0
AVG (Zmax(f)-Zmin(f))
C1
C2
C3
C4
C5
C6
Concentrations
G1
G2
G3

(b)

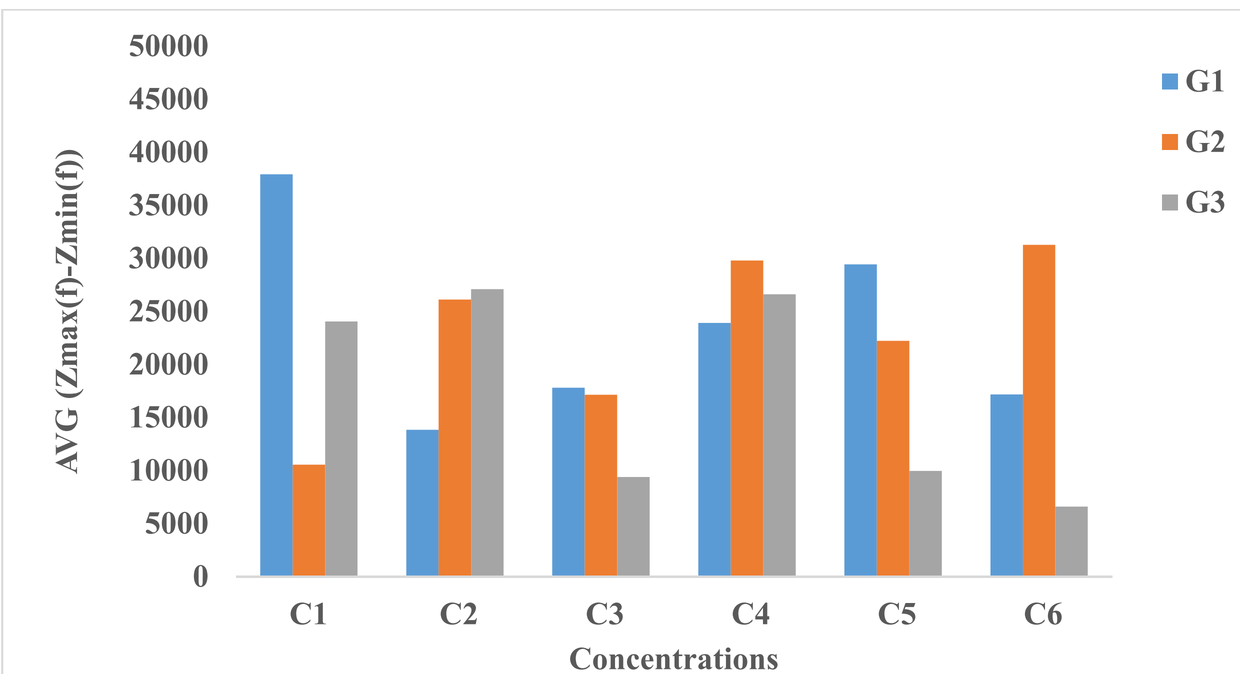
50000
45000
40000
35000
30000
25000
20000
15000
10000
5000
0
AVG (Zmax(f)-Zmin(f))
C1
C2
C3
C4
C5
C6
Concentrations
G1
G2
G3

(c)

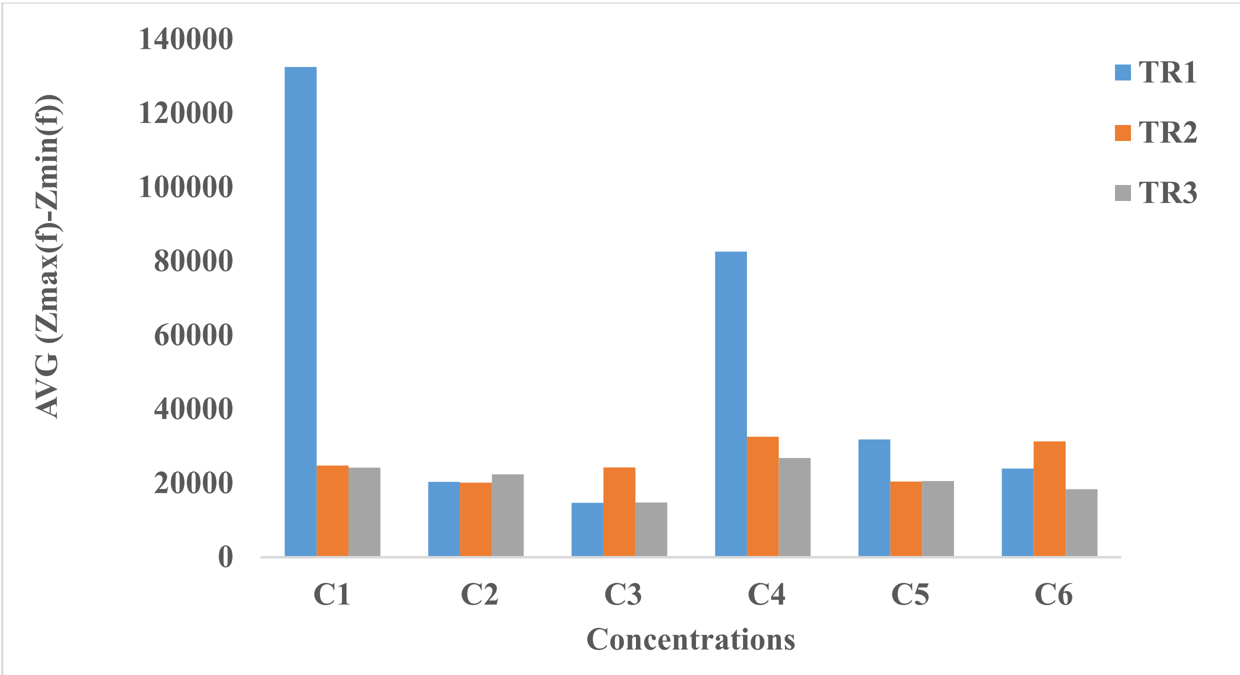


(d)

E.3 The bar graphs of (ZMAX-ZMIN(f) /AVG(f)) for each group in all trials (a)TR1, (b) TR2, and (c) TR3.

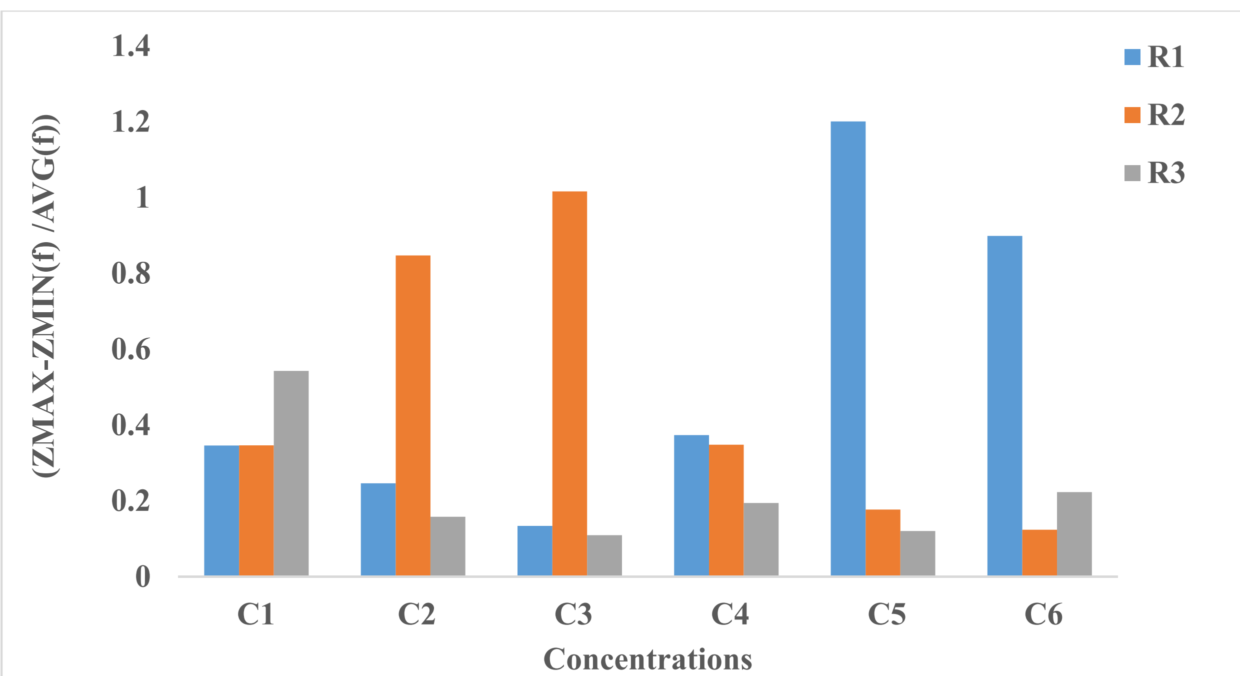


(a)

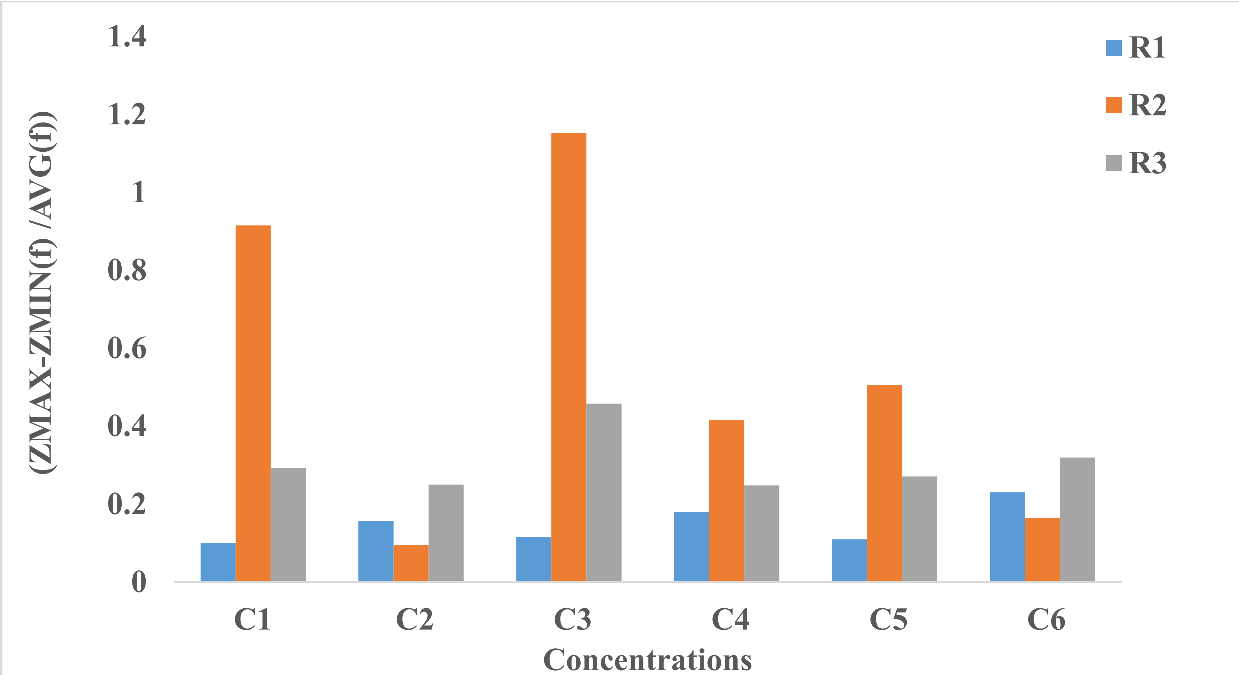
1.4
1.2
1
0.8
0.6
0.4
0.2
0
(ZMAX-ZMIN(f) /AVG(f))
R1
R2
R3
C1
C2
C3
C4
C5
C6
Concentrations

(b)

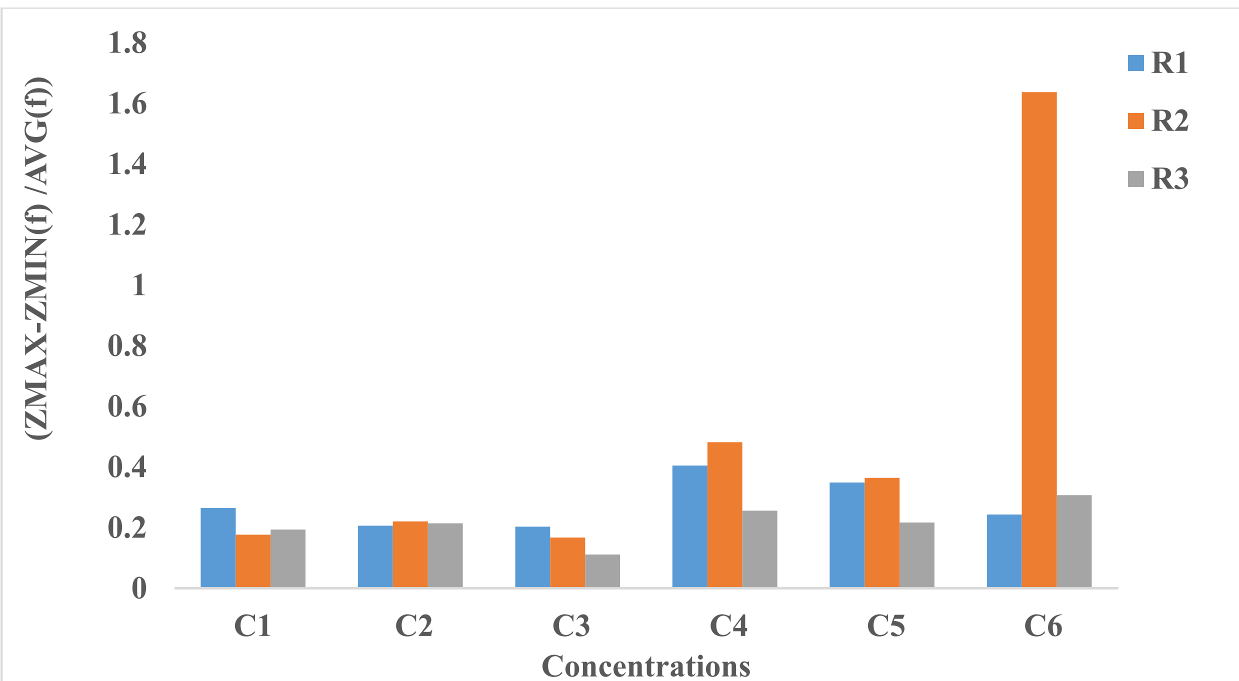
1.8
1.6
1.4
1.2
1
0.8
0.6
0.4
0.2
0
(ZMAX-ZMIN(f) /AVG(f))
R1
R2
R3
C1
C2
C3
C4
C5
C6
Concentrations

(c)

# REFERENCES


[1] J. S. Weinstein *et al.*, "Superparamagnetic iron oxide nanoparticles: Diagnostic magnetic resonance imaging and potential therapeutic applications in neurooncology and central nervous system inflammatory pathologies, a review," *Journal of Cerebral Blood Flow and Metabolism*. 2010.

[2] J. M. Poller *et al.*, "Selection of potential iron oxide nanoparticles for breast cancer treatment based on in vitro cytotoxicity and cellular uptake," *Int. J. Nanomedicine*, 2017.

[3] Y. S. Kang, S. Risbud, J. F. Rabolt, and P. Stroeve, "Synthesis and Characterization of Nanometer-Size Fe3O4 and γ-Fe2O3 Particles," *Chem. Mater.*, 1996.

[4] M. M. Cruz *et al.*, "Nanoparticles for magnetic hyperthermia," in *Nanostructures for Cancer Therapy*, 2017.

[5] R. D. Oude Engberink, S. M. A. van der Pol, E. L. A. Blezer, E. A. Döpp, and H. E. de Vries, "Comparison of SPIO and USPIO for in Vitro Labeling of Human Monocytes: MR Detection and Cell Function," *Radiology*, 2008.

[6] B. V. Zlokovic, "The Blood-Brain Barrier in Health and Chronic Neurodegenerative Disorders," *Neuron*. 2008.

[7] F. Re, M. Gregori, and M. Masserini, "Nanotechnology for neurodegenerative disorders," *Maturitas*. 2012.

[8] M. Masserini, "Nanoparticles for Brain Drug Delivery," *ISRN Biochem.*, 2013.

[9] L. B. Thomsen *et al.*, "Uptake and transport of superparamagnetic iron oxide nanoparticles through human brain capillary endothelial cells," *ACS Chem. Neurosci.*, 2013.

[10] M. Mahmoudi, S. Sant, B. Wang, S. Laurent, and T. Sen, "Superparamagnetic iron oxide nanoparticles (SPIONs): Development, surface modification and applications in chemotherapy," *Advanced Drug Delivery Reviews*. 2011.

[11] N. Singh, G. J. S. Jenkins, R. Asadi, and S. H. Doak, "Potential toxicity of superparamagnetic iron oxide nanoparticles (SPION)," *Nano Rev.*, 2010.

[12] T. Eustaquio and J. F. Leary, "Single-cell nanotoxicity assays of superparamagnetic iron oxide nanoparticles," *Methods Mol. Biol.*, 2012.

[13] M. R. Bashir, L. Bhatti, D. Marin, and R. C. Nelson, "Emerging applications for ferumoxytol as a contrast agent in MRI," *Journal of Magnetic Resonance Imaging*. 2015.

[14] C. Wang *et al.*, "Dual-purpose magnetic micelles for MRI and gene delivery," in *Journal of Controlled Release*, 2012, vol. 163, no. 1, pp. 82–92.

[15] P. Varallyay *et al.*, "Comparison of two superparamagnetic viral-sized iron oxide particles ferumoxides and ferumoxtran-10 with a gadolinium chelate in imaging intracranial tumors," *Am. J. Neuroradiol.*, 2002.

[16] M. Rausch, A. Sauter, J. Frohlich, U. Neubacher, E. W. Radu, and M. Rudin, "Dynamic patterns of USPIO enhancement can be observed in macrophages after ischemic brain damage," *Magn. Reson. Med.*, 2001.

[17] L. Yang *et al.*, "Development of receptor targeted magnetic iron oxide nanoparticles for efficient drug delivery and tumor imaging," *J. Biomed. Nanotechnol.*, 2008.

[18] H. H. Yang, S. Q. Zhang, X. L. Chen, Z. X. Zhuang, J. G. Xu, and X. R. Wang, "Magnetite-Containing Spherical Silica Nanoparticles for Biocatalysis and Bioseparations," *Anal. Chem.*, 2004.

[19] B. Steitz *et al.*, "Characterization of PEI-coated superparamagnetic iron oxide nanoparticles

for transfection: Size distribution, colloidal properties and DNA interaction," *J. Magn. Magn. Mater.*, 2007.
[20] J. Estelrich, E. Escribano, J. Queralt, and M. A. Busquets, "Iron oxide nanoparticles for magnetically-guided and magnetically-responsive drug delivery," *International Journal of Molecular Sciences*. 2015.
[21] S. J. Cheong *et al.*, "Superparamagnetic iron oxide nanoparticles-loaded chitosan-linoleic acid nanoparticles as an effective hepatocyte-targeted gene delivery system," *Int. J. Pharm.*, 2009.
[22] M. Pöttler *et al.*, "Impact of Superparamagnetic Iron Oxide Nanoparticles on Vocal Fold Fibroblasts: Cell Behavior and Cellular Iron Kinetics," *Nanoscale Res. Lett.*, 2017.
[23] H. Hong, Y. Yang, Y. Zhang, and W. Cai, "Non-Invasive Cell Tracking in Cancer and Cancer Therapy," *Curr. Top. Med. Chem.*, 2010.
[24] L. M. De Leõn-Rodríguez, A. F. Martins, M. C. Pinho, N. M. Rofsky, and A. D. Sherry, "Basic MR relaxation mechanisms and contrast agent design," *J. Magn. Reson. Imaging*, 2015.
[25] J. K. Kirsch, "Basic principles of magnetic resonance contrast agents," *Top. Magn. Reson. Imaging*, 2006.
[26] X. Yin *et al.*, "Large T1contrast enhancement using superparamagnetic nanoparticles in ultra-low field MRI," *Sci. Rep.*, 2018.
[27] M. H. Mendonca Dias and P. C. Lauterbur, "Ferromagnetic particles as contrast agents for magnetic resonance imaging of liver and spleen.," *Magn. Reson. Med.*, vol. 3, no. 2, pp. 328–30, 1986.
[28] A. K. Gupta and M. Gupta, "Cytotoxicity suppression and cellular uptake enhancement of surface modified magnetic nanoparticles," *Biomaterials*, 2005.
[29] A. Petri-Fink, M. Chastellain, L. Juillerat-Jeanneret, A. Ferrari, and H. Hofmann, "Development of functionalized superparamagnetic iron oxide nanoparticles for interaction with human cancer cells," *Biomaterials*, 2005.
[30] T. Fu, Q. Kong, H. Sheng, and L. Gao, "Value of Functionalized Superparamagnetic Iron Oxide Nanoparticles in the Diagnosis and Treatment of Acute Temporal Lobe Epilepsy on MRI," *Neural Plast.*, 2016.
[31] Y. Wang *et al.*, "The treatment value of IL-1β monoclonal antibody under the targeting location of alpha-methyl-l-tryptophan and superparamagnetic iron oxide nanoparticles in an acute temporal lobe epilepsy model 11 Medical and Health Sciences 1109 Neurosciences," *J. Transl. Med.*, 2018.
[32] J. L. Corchero and A. Villaverde, "Biomedical applications of distally controlled magnetic nanoparticles," *Trends in Biotechnology*. 2009.
[33] G. Phukan *et al.*, "Silica-coated magnetic nanoparticles impair proteasome activity and increase the formation of cytoplasmic inclusion bodies in vitro," *Sci. Rep.*, vol. 6, 2016.
[34] D. M. Wuest and K. H. Lee, "Optimization of endothelial cell growth in a murine in vitro blood-brain barrier model," *Biotechnol. J.*, 2012.
[35] H. C. Helms *et al.*, "In vitro models of the blood-brain barrier: An overview of commonly used brain endothelial cell culture models and guidelines for their use," *Journal of Cerebral Blood Flow and Metabolism*. 2015.
[36] D. Shi, G. J. Mi, S. Bhattacharya, S. Nayar, and T. J. Webster, "Optimizing superparamagnetic iron oxide nanoparticles as drug carriers using an in vitro blood-brain barrier model," *Int. J. Nanomedicine*, vol. 11, pp. 5371–5379, 2016.

[37] C. Jiang, S. Yang, N. Gan, H. Pan, and H. Liu, “A method for determination of [Fe3+]/[Fe2+] ratio in superparamagnetic iron oxide,” *J. Magn. Magn. Mater.*, 2017.
[38] D. L. Huber, “Synthesis, properties, and applications of iron nanoparticles,” *Small*. 2005.
[39] L. H. Li, J. Xiao, P. Liu, and G. W. Yang, “Super adsorption capability from amorphousization of metal oxide nanoparticles for dye removal,” *Sci. Rep.*, 2015.
[40] N. Singh, G. J. Jenkins, R. Asadi, and S. H. Doak, “Potential toxicity of superparamagnetic iron oxide nanoparticles (SPION),” *Nano Rev*, vol. 1, 2010.
[41] L. Maurizi, A. Claveau, and H. Hofmann, “Polymer adsorption on iron oxide nanoparticles for one-step amino-functionalized silica encapsulation,” *J. Nanomater.*, vol. 2015, 2015.
[42] E. A. Vermeij *et al.*, “The in-vivo use of superparamagnetic iron oxide nanoparticles to detect inflammation elicits a cytokine response but does not aggravate experimental arthritis,” *PLoS One*, 2015.
[43] L. D. Galuppo *et al.*, “Gene expression in synovial membrane cells after intraarticular delivery of plasmid-linked superparamagnetic iron oxide particles - A preliminary study in sheep,” *J. Nanosci. Nanotechnol.*, 2006.
[44] V. Polikov, M. Block, C. Zhang, W. M. Reichert, and J. S. Hong, “In Vitro Models for Neuroelectrodes: A Paradigm for Studying Tissue–Materials Interactions in the Brain,” *Neural Implant. Strateg. Contend. with Vivo Environ.*, 2008.
[45] S. Påhlman *et al.*, “Human neuroblastoma cells in culture: a model for neuronal cell differentiation and function.,” *Acta Physiol. Scand. Suppl.*, vol. 592, pp. 25–37, 1990.
[46] W. Rall, “Electrophysiology of a Dendritic Neuron Model,” *Biophys. J.*, vol. 2, no. 2, pp. 145–167, 1962.
[47] A. Petri-Fink, B. Steitz, A. Finka, J. Salaklang, and H. Hofmann, “Effect of cell media on polymer coated superparamagnetic iron oxide nanoparticles (SPIONs): Colloidal stability, cytotoxicity, and cellular uptake studies,” *Eur. J. Pharm. Biopharm.*, vol. 68, no. 1, pp. 129–137, 2008.
[48] M. Safi, J. Courtois, M. Seigneuret, H. Conjeaud, and J. F. Berret, “The effects of aggregation and protein corona on the cellular internalization of iron oxide nanoparticles,” *Biomaterials*, vol. 32, no. 35, pp. 9353–9363, 2011.
[49] A. K. Hauser, M. I. Mitov, E. F. Daley, R. C. McGarry, K. W. Anderson, and J. Z. Hilt, “Targeted iron oxide nanoparticles for the enhancement of radiation therapy,” *Biomaterials*, 2016.
[50] H. T. R. Wiogo, M. Lim, V. Bulmus, J. Yun, and R. Amal, “Stabilization of magnetic iron oxide nanoparticles in biological media by fetal bovine serum (FBS),” *Langmuir*, vol. 27, no. 2, pp. 843–850, 2011.
[51] A. Lesniak, A. Salvati, M. J. Santos-Martinez, M. W. Radomski, K. A. Dawson, and C. ??berg, “Nanoparticle adhesion to the cell membrane and its effect on nanoparticle uptake efficiency,” *J. Am. Chem. Soc.*, vol. 135, no. 4, pp. 1438–1444, 2013.
[52] P. Aggarwal, J. B. Hall, C. B. McLeland, M. A. Dobrovolskaia, and S. E. McNeil, “Nanoparticle interaction with plasma proteins as it relates to particle biodistribution, biocompatibility and therapeutic efficacy,” *Advanced Drug Delivery Reviews*, vol. 61, no. 6. pp. 428–437, 2009.
[53] A. Verma and F. Stellacci, “Effect of surface properties on nanoparticle-cell interactions,” *Small*. 2010.
[54] I. Schütz *et al.*, “Lysosomal dysfunction caused by cellular accumulation of silica nanoparticles,” *J. Biol. Chem.*, vol. 291, no. 27, pp. 14170–14184, 2016.

[55] Ö. F. Karataş, E. Sezgin, Ö. Aydin, and M. Çulha, “Interaction of gold nanoparticles with mitochondria,” *Colloids Surfaces B Biointerfaces*, vol. 71, no. 2, pp. 315–318, 2009.
[56] C. Xu, J. Xie, N. Kohler, E. G. Walsh, Y. E. Chin, and S. Sun, “Monodisperse magnetite nanoparticles coupled with nuclear localization signal peptide for cell-nucleus targeting,” *Chem. - An Asian J.*, vol. 3, no. 3, pp. 548–552, 2008.
[57] A. L. McNamara *et al.*, “Dose enhancement effects to the nucleus and mitochondria from gold nanoparticles in the cytosol,” *Phys. Med. Biol.*, vol. 61, no. 16, pp. 5993–6010, 2016.
[58] K. Baranes, M. Shevach, O. Shefi, and T. Dvir, “Gold Nanoparticle-Decorated Scaffolds Promote Neuronal Differentiation and Maturation,” *Nano Lett.*, vol. 16, no. 5, pp. 2916–2920, 2016.
[59] H. Chen *et al.*, “Magnetic Cell-Scaffold Interface Constructed by Superparamagnetic IONP Enhanced Osteogenesis of Adipose-Derived Stem Cells,” *ACS Appl. Mater. Interfaces*, 2018.
[60] M. Poot, M. Rosato, and P. S. Rabinovitch, “Analysis of Cell Proliferation and Cell Survival by Continuous BrdU Labeling and Multivariate Flow Cytometry,” in *Current Protocols in Cytometry*, 2004.
[61] K. Rothaeusler and N. Baumgarth, “Assessment of cell proliferation by 5-bromodeoxyuridine (BrdU) labeling for multicolor flow cytometry.,” *Curr. Protoc. Cytom.*, vol. Chapter 7, p. Unit7.31, 2007.
[62] CPI, “Trypan blue exclusion test of cell viability.,” *Curr. Protoc. Immunol.*, 2001.
[63] M. Fritzsche, J. M. Fredriksson, M. Carlsson, and C. F. Mandenius, “A cell-based sensor system for toxicity testing using multiwavelength fluorescence spectroscopy,” *Anal. Biochem.*, vol. 387, no. 2, pp. 271–275, 2009.
[64] E. Moczko, E. M. Mirkes, C. Cáceres, A. N. Gorban, and S. Piletsky, “Fluorescence-based assay as a new screening tool for toxic chemicals,” *Sci. Rep.*, 2016.
[65] L. Ceriotti, J. Ponti, P. Colpo, E. Sabbioni, and F. Rossi, “Assessment of cytotoxicity by impedance spectroscopy,” *Biosens. Bioelectron.*, vol. 22, no. 12, pp. 3057–3063, 2007.
[66] L. Ceriotti *et al.*, “Real-time assessment of cytotoxicity by impedance measurement on a 96-well plate,” *Sensors Actuators, B Chem.*, vol. 123, no. 2, pp. 769–778, 2007.
[67] X. Zhang, F. Li, A. N. Nordin, J. Tarbell, and I. Voiculescu, “Toxicity studies using mammalian cells and impedance spectroscopy method,” *Sens. Bio-Sensing Res.*, vol. 3, pp. 112–121, 2015.
[68] C. Newbold *et al.*, “Changes in biphasic electrode impedance with protein adsorption and cell growth,” *J. Neural Eng.*, vol. 7, no. 5, 2010.
[69] X. Zhu, E. Hondroulis, W. Liu, and C. Z. Li, “Biosensing approaches for rapid genotoxicity and cytotoxicity assays upon nanomaterial exposure,” *Small*, vol. 9, no. 9–10, pp. 1821–1830, 2013.
[70] O. A. Sadik, A. L. Zhou, S. Kikandi, N. Du, Q. Wang, and K. Varner, “Sensors as tools for quantitation, nanotoxicity and nanomonitoring assessment of engineered nanomaterials,” *J. Environ. Monit.*, vol. 11, no. 10, p. 1782, 2009.
[71] R. E. Özel, X. Liu, R. S. J. Alkasir, and S. Andreescu, “Electrochemical methods for nanotoxicity assessment,” *TrAC - Trends in Analytical Chemistry*, vol. 59. pp. 112–120, 2014.
[72] I. O. K’Owino and O. A. Sadik, “Impedance spectroscopy: A powerful tool for rapid biomolecular screening and cell culture monitoring,” *Electroanalysis*, vol. 17, no. 23. pp. 2101–2113, 2005.

[73] I. Giaever and C. R. Keese, "Monitoring fibroblast behavior in tissue culture with an applied electric field," *Proc. Natl. Acad. Sci. U. S. A.*, vol. 81, no. 12, pp. 3761–3764, 1984.
[74] A. R. A. Rahman, J. Register, G. Vuppala, and S. Bhansali, "Cell culture monitoring by impedance mapping using a multielectrode scanning impedance spectroscopy system (CellMap)," *Physiol. Meas.*, vol. 29, no. 6, pp. S227–S239, 2008.
[75] E. Sarr?? *et al.*, "Electrical impedance spectroscopy measurements using a four-electrode configuration improve on-line monitoring of cell concentration in adherent animal cell cultures," *Biosens. Bioelectron.*, vol. 31, no. 1, pp. 257–263, 2012.
[76] T. Valero, T. Jacobs, G. Moschopoulou, M. Naumann, P. Hauptmann, and S. Kintzios, "Electrical impedance analysis of N2a neuroblastoma cells in gel matrices after ACh-receptor triggering with an impedimetric biosensor," in *Procedia Chemistry*, 2009, vol. 1, no. 1, pp. 734–737.
[77] P. Seriburi, S. McGuire, A. Shastry, K. F. Böhringer, and D. R. Meldrum, "Measurement of the cell-substrate separation and the projected area of an individual adherent cell using electric cell-substrate impedance sensing," *Anal. Chem.*, vol. 80, no. 10, pp. 3677–3683, 2008.
[78] F. Witzel, R. Fritsche-Guenther, N. Lehmann, A. Sieber, and N. Blüthgen, "Analysis of impedance-based cellular growth assays," *Bioinformatics*, 2015.
[79] C. M. Lo, C. R. Keese, and I. Giaever, "Impedance analysis of MDCK cells measured by electric cell-substrate impedance sensing," *Biophys. J.*, 1995.
[80] W. Wang *et al.*, "Single cells and intracellular processes studied by a plasmonic-based electrochemical impedance microscopy," *Nat. Chem.*, 2011.
[81] P. Szymański, M. Markowicz, and E. Mikiciuk-Olasik, "Adaptation of high-throughput screening in drug discovery-toxicological screening tests," *International Journal of Molecular Sciences*. 2012.
[82] A. R. Collins *et al.*, "High throughput toxicity screening and intracellular detection of nanomaterials," *Wiley Interdisciplinary Reviews: Nanomedicine and Nanobiotechnology*, vol. 9, no. 1. 2017.
[83] B. Moe, S. Gabos, and X. F. Li, "Real-time cell-microelectronic sensing of nanoparticle-induced cytotoxic effects," *Anal. Chim. Acta*, vol. 789, pp. 83–90, 2013.
[84] E. Ghafar-Zadeh, M. Sawan, and V. P. Chodavarapu, "Micro-Organism-on-Chip: Emerging direct-write CMOS-Based platform for biological applications," in *IEEE Transactions on Biomedical Circuits and Systems*, 2009, vol. 3, no. 4, pp. 212–219.
[85] J. C. Williams, J. A. Hippensteel, J. Dilgen, W. Shain, and D. R. Kipke, "Complex impedance spectroscopy for monitoring tissue responses to inserted neural implants," *J. Neural Eng.*, 2007.
[86] R. Szulcek, H. J. Bogaard, and G. P. van Nieuw Amerongen, "Electric Cell-substrate Impedance Sensing for the Quantification of Endothelial Proliferation, Barrier Function, and Motility," *J. Vis. Exp.*, 2014.
[87] L. R. Arias, C. A. Perry, and L. Yang, "Real-time electrical impedance detection of cellular activities of oral cancer cells," *Biosens. Bioelectron.*, 2010.
[88] F. Asphahani *et al.*, "Single-cell bioelectrical impedance platform for monitoring cellular response to drug treatment," *Phys. Biol.*, 2011.
[89] M. F. Peters, S. D. Lamore, L. Guo, C. W. Scott, and K. L. Kolaja, "Human Stem Cell-Derived Cardiomyocytes in Cellular Impedance Assays: Bringing Cardiotoxicity Screening to the Front Line," *Cardiovasc. Toxicol.*, 2015.

[90] I. Kuzmanov, A. M. Herrmann, H.-J. Galla, S. G. Meuth, H. Wiendl, and L. Klotz, “An <em>In Vitro</em> Model of the Blood-brain Barrier Using Impedance Spectroscopy: A Focus on T Cell-endothelial Cell Interaction,” *J. Vis. Exp.*, 2016.

[91] M. Marcus *et al.*, “Iron oxide nanoparticles for neuronal cell applications: uptake study and magnetic manipulations,” *J. Nanobiotechnology*, vol. 14, no. 1, p. 37, 2016.

[92] M. Mahmoudi *et al.*, “A new approach for the in vitro identification of the cytotoxicity of superparamagnetic iron oxide nanoparticles,” *Colloids Surfaces B Biointerfaces*, vol. 75, no. 1, pp. 300–309, 2010.

[93] G. Jarockyte *et al.*, “Accumulation and toxicity of superparamagnetic iron oxide nanoparticles in cells and experimental animals,” *Int. J. Mol. Sci.*, vol. 17, no. 8, 2016.

[94] Z. Magdolenova *et al.*, “Coating-dependent induction of cytotoxicity and genotoxicity of iron oxide nanoparticles,” *Nanotoxicology*, vol. 9, no. S1, pp. 44–56, 2015.

[95] E. Ying and H. M. Hwang, “In vitro evaluation of the cytotoxicity of iron oxide nanoparticles with different coatings and different sizes in A3 human T lymphocytes,” *Sci. Total Environ.*, vol. 408, no. 20, pp. 4475–4481, 2010.

[96] Z. Sun *et al.*, “Characterization of cellular uptake and toxicity of aminosilane-coated iron oxide nanoparticles with different charges in central nervous system-relevant cell culture models,” *Int. J. Nanomedicine*, vol. 8, pp. 961–970, 2013.

[97] D. A. Mbeh *et al.*, “Human Alveolar Epithelial Cell Responses to Core-Shell Superparamagnetic Iron Oxide Nanoparticles (SPIONs).,” *Langmuir*, 2015.

[98] Invitrogen, “PrestoBlue Cell Viability Reagent Documentation,” *a13261*, 2010.

[99] S. J. H. Soenen, U. Himmelreich, N. Nuytten, and M. De Cuyper, “Cytotoxic effects of iron oxide nanoparticles and implications for safety in cell labelling,” *Biomaterials*, vol. 32, no. 1, pp. 195–205, 2011.

[100] C. Petters and R. Dringen, “Accumulation of iron oxide nanoparticles by cultured primary neurons,” *Neurochem. Int.*, vol. 81, pp. 1–9, 2015.

[101] E. Munnier *et al.*, “Doxorubicin delivered to MCF-7 cancer cells by superparamagnetic iron oxide nanoparticles: Effects on subcellular distribution and cytotoxicity,” *J. Nanoparticle Res.*, vol. 13, no. 3, pp. 959–971, 2011.

[102] M. Calero *et al.*, “Characterization of interaction of magnetic nanoparticles with breast cancer cells,” *J. Nanobiotechnology*, vol. 13, no. 1, 2015.

[103] Klebe and Ruddle, “Neuroblastoma: cell culture analysis of a differentiating stem cell system,” *J. Cell Biol*, 1969.

[104] S. Naqvi *et al.*, “Concentration-dependent toxicity of iron oxide nanoparticles mediated by increased oxidative stress,” *Int. J. Nanomedicine*, 2010.

[105] A. Lindemann, K. Lüdtke-Buzug, B. M. Fräderich, K. Gräfe, R. Pries, and B. Wollenberg, “Biological impact of superparamagnetic iron oxide nanoparticles for magnetic particle imaging of head and neck cancer cells,” *Int. J. Nanomedicine*, 2014.

[106] C. S. Chen, M. Mrksich, S. Huang, G. M. Whitesides, and D. E. Ingber, “Geometric control of cell life and death,” *Science (80-. ).*, 1997.